



HAL
open science

The numerics of hydrostatic structured-grid coastal ocean models: state of the art and future perspectives

Knut Klingbeil, Florian Lemarié, Laurent Debreu, Hans Burchard

► To cite this version:

Knut Klingbeil, Florian Lemarié, Laurent Debreu, Hans Burchard. The numerics of hydrostatic structured-grid coastal ocean models: state of the art and future perspectives. *Ocean Modelling*, 2018, 10.1016/j.ocemod.2018.01.007 . hal-01443357v1

HAL Id: hal-01443357

<https://inria.hal.science/hal-01443357v1>

Submitted on 23 Jan 2017 (v1), last revised 5 Feb 2018 (v3)

HAL is a multi-disciplinary open access archive for the deposit and dissemination of scientific research documents, whether they are published or not. The documents may come from teaching and research institutions in France or abroad, or from public or private research centers.

L'archive ouverte pluridisciplinaire **HAL**, est destinée au dépôt et à la diffusion de documents scientifiques de niveau recherche, publiés ou non, émanant des établissements d'enseignement et de recherche français ou étrangers, des laboratoires publics ou privés.

The numerics of hydrostatic structured-grid coastal ocean models: state of the art and future perspectives

Hans Burchard^a, Laurent Debreu^b, Knut Klingbeil^a, Florian Lemarié^b

^a*Leibniz Institute for Baltic Sea Research Warnemünde, Seestraße 15, D-18119 Rostock, Germany*

^b*Inria, Univ. Grenoble Alpes, CNRS, LJK, Grenoble F-38000, France*

Abstract

The state of the art of the numerics of hydrodynamic non-hydrostatic structured-grid coastal ocean models is reviewed here. First, some fundamental differences in the hydrodynamics of the coastal ocean, such as the large surface elevation variation compared to the mean water depth, are contrasted against large scale ocean dynamics. Then the hydrodynamic equations as they are used in coastal ocean models as well as in large scale ocean models are presented, including parameterisations for turbulent transports. As steps towards discretisation, coordinate transformations and vertical and horizontal discretisations based on a finite-volume approach are discussed with focus on the specific requirements for coastal ocean models. As in large scale ocean models, splitting of internal and external modes is essential also for coastal ocean models, but specific care is needed when wetting and drying of intertidal flats is included. As one obvious characteristic of coastal ocean models, open boundaries occur and need to be treated in a way that correct model forcing from outside is transmitted to the model domain without reflecting waves from the inside. Here, also new developments in two-way nesting are presented. Single processes such as internal inertia-gravity waves, advection and turbulence closure models are discussed with focus on the coastal scales. Some overview on existing hydrostatic structured-grid coastal ocean models is given, including their extensions towards non-hydrostatic models. Finally, an outlook on future perspectives is made.

Keywords: coastal ocean models, hydrostatic models, adaptive coordinates, mode splitting, wetting and drying, two-way nesting

1. Introduction

This review paper presents the state of the art of hydrodynamic coastal ocean modelling, with focus on structured-grid hydrostatic models. Here, we define the coastal ocean as ranging from estuaries and shallow coastal areas to the shelf break region. On the small scale end, near-shore and coastal engineering scales are not resolved, but parameterised, if needed. On the large scale end, the dynamics of the ocean basins will not be explicitly treated, since their effects are introduced by means of lateral boundary conditions.

The coastal ocean as defined here, is strongly affected by the superposition of direct human impacts and climate change and variability. Direct human impacts include for example eutrophication, fishery, large scale constructions (such as offshore wind farms), dredging and dumping of material, discharges (e.g., of cooling water) and pollution. Aspect of natural and anthropogenic climate change and variability impacting on the coastal ocean are relative sea level rise (global and local), global warming, changes of the water cycle (precipitation, evaporation, run-off), and changed wind forcing. These local, regional and global forcings may lead to severe changes in the coastal environment, such as regime shifts in biogeochemistry, coastal erosion, flooding of low-laying coastal regions, increase of oxygen minimum zones, invasion of alien species, and many more. Changes are strong in many coastal regions around the world, but specifically serious in the Arctic where the warming is strongly accelerated.

To understand the changing coastal oceans, numerical modelling is one of the most effective tools, allowing for reconstructions of historic states, hindcasts and analysis of the dynamics in the last decades, short term forecasts of coastal ocean states, as well as for coastal climate projections and possible future scenarios. One core requirement for the predictability of such model exercises is the way how basic hydrodynamic processes are reproduced.

Main aspects which need to be resolved are exchanges of matter (such as salt, heat, oxygen, nutrients and particulate matter) in vertical and lateral directions. In the lateral direction, the coast-to-ocean exchange is mediated by estuarine dynamics, tidal dispersion, tidal fronts, and meso-scale and submeso-scale dynamics. In the vertical, critical interfaces play a crucial role, such as the sediment-water interface, the *clines* (lutocline, halocline, thermocline, redoxcline), the surface and bottom wave-affected layers as well as the air-sea interface. Internal waves play a special role for linking horizontal and vertical scales. All these features need to be properly resolved.

38 In this paper, we discuss specific requirements for the hydrodynamic cores
39 of coastal ocean models in terms of driving biogeochemical and suspended
40 sediment models. This will include consequences for interfacing with models
41 for other compartments such as atmospheric models, surface wave models,
42 sea ice models, hydrological models and bottom sediment models, without
43 explicitly discussing such models itself. Also issues of data assimilation will
44 be excluded here. Scales where resolution of non-hydrostatic pressure con-
45 tributions become relevant will be parameterised such that we restrict the
46 discussions on hydrostatic models. Furthermore, we restrict ourselves to the
47 class of structured-grid models, since the numerical methods in unstructured-
48 grid modelling differ significantly from the structured-grid methods. Due to
49 their flexible grids, unstructured-grid models are known to be specifically
50 suitable for investigating multi-scale dynamics in the ocean. We will here
51 discuss how also structured-grid models combined with nesting strategies are
52 able to resolve multiple scales.

53 2. Characteristics of coastal ocean dynamics

54 The coastal ocean has a number of characteristics which discriminate it
55 from the global ocean in a way that specific physical and numerical treatment
56 is required. In the following, these characteristics are expressed in terms of
57 characteristic horizontal and vertical length scales H and L , respectively, and
58 the time scale T .

59 2.1. Relatively thick mixed layers

60 In temperate shelf seas, the surface and bottom mixed layers may occupy
61 a considerable fraction of the water depth. In summer, when stratification
62 shows a maximum, they may still cover 60%-80% of the water column, while
63 in autumn and winter they may completely merge into a vertically homoge-
64 neous water column (Bolding et al., 2002). In contrast to this, surface and
65 bottom mixed layers in ocean basins, which may have a comparable absolute
66 thickness to shelf seas may cover only a small portion of the total depth of
67 several thousands of metres (Martin (1985)).

68 With H being the local time-averaged water depth, and D_s and D_b de-
69 noting surface and bottom mixed layer thickness, respectively, this charac-
70 teristics of coastal seas can be expressed as

$$71 \quad \frac{D_s + D_b}{H} = \mathcal{O}(1) \quad (1)$$

72 The major consequence of this is that turbulence closure models are
73 needed which resolve the vertical structure of the mixed layers including the
74 interaction of vertical stratification and mixing. For the relatively thick bot-
75 tom boundary layers, another implication is that the bed friction generates
76 relatively strong dissipation of kinetic energy in the water column. The latter
77 may be enhanced in shallow water, when the surface wave length becomes
78 comparable to the water depth, such that the orbital wave motion adds to
79 the bed stress. Due to the dynamic importance of the bottom boundary layer
80 it is required that it is vertically well-resolved everywhere. This means for
81 the generally strongly variable bottom bathymetry of the coastal ocean that
82 *bottom-following vertical coordinates* are mandatory (see section 4.2).

83 *2.2. Relatively high surface elevation amplitude*

84 The sea surface elevation variability due to tides and storm surges is
85 strongly enhanced in the shallow coastal ocean, adding an important non-
86 linearity to the dynamics. When denoting the standard deviation of the
87 surface elevation as $\sigma(\eta)$, this characteristics of the coastal ocean could be
88 formulated as

$$89 \quad \frac{\sigma(\eta)}{H} = \mathcal{O}(1). \quad (2)$$

90 First of all, coastal ocean models need to predict the temporally and spatially
91 varying free surface elevation η , rather than applying the rigid-lid approxi-
92 mation which large scale ocean models originally used in order to allow for
93 large time steps (Bryan, 1969). Furthermore, the relatively high surface el-
94 evation variation requires the use of *surface-following vertical coordinates* to
95 ensure sufficient vertical resolution of the near surface region.

96 An extreme case occurs when the surface elevation variability is larger
97 than the mean water depth, such that the sea bed is falling dry at times:

$$98 \quad \frac{\sigma(\eta)}{H} > 1. \quad (3)$$

99 In such cases, wetting and drying algorithms must be implemented to prevent
100 unphysical negative water depths (see e.g., Burchard et al., 2004; Warner
101 et al., 2013, and section 5).

102 *2.3. Relatively strong horizontal and vertical gradients*

103 By definition, all global riverine input is discharged into coastal seas.
104 Since the exchange between the coasts and the interior of the adjacent shelf

105 seas is limited, strong gradients build up in the coastal ocean. Salinity may
 106 vary from river concentration (almost zero) to ocean concentration within
 107 a few kilometres in the horizontal. Strong stratification may be generated
 108 in the vicinity of freshwater discharge such that also vertical gradients may
 109 be strong. In addition to the salinity, also other tracers such a nutrients
 110 or suspended matter discharged by rivers may show strong gradients. Let c
 111 be a relevant tracer (e.g., salinity), then the fact that horizontal or vertical
 112 gradients may be relative strong in coastal seas can be expressed as

$$113 \quad \frac{\Delta c}{|\partial_{[x,y]}c|} \ll L, \quad \frac{\Delta c}{|\partial_z c|} \ll H, \quad (4)$$

114 with $\partial_{[x,y]}$ denoting horizontal gradients and ∂_z denoting vertical gradients.

115 *2.4. Relatively short time scale*

116 The relevant time scale T in the coastal ocean is typically much shorter
 117 than in the global ocean. The key time scales in the coastal ocean are tidal,
 118 inertial, diurnal or synoptic, i.e. $\mathcal{O}(1 \text{ day})$, whereas large scale ocean stud-
 119 ies generally concentrate on time scales reaching from seasonal to millennial
 120 or beyond. The latter can be achieved by parameterising effects of tides,
 121 inertial oscillations or storms (see, e.g., Eden et al. (2014)). In estuaries
 122 and coastal regions, complex dynamical changes will occur during a tidal
 123 cycle with strong tidal asymmetries in mixing and secondary circulation,
 124 and substantial impact on transport e.g. of salt and suspended matter (see,
 125 MacCready and Geyer (2010)). One example for this is the strain-induced
 126 periodic stratification (SIPS, see Simpson et al. (1990)) due to horizontal den-
 127 sity gradients as often observed in regions of freshwater influence (see, e.g.,
 128 Rippeth et al., 2001). Interior mixing in shelf seas is often caused by inertial
 129 shear caused by episodic storm events combined with coastal coupling (Craig
 130 (1989); van Haren et al. (1999); Knight et al. (2002)), a process which cannot
 131 be parameterised in the coastal ocean due to its complex bathymetry and
 132 coastline. Therefore, different model physics e.g. in terms of turbulence clo-
 133 sure models (see the discussion at the end of section 3.2.1) requiring different
 134 numerical schemes are needed for coastal ocean models.

135 *2.5. Relatively small spatial scales*

136 Probably the most obvious characteristics of the coastal ocean is its lim-
 137 ited spatial extent:

$$138 \quad L \ll r_{Earth}, \quad (5)$$

139 with the Earth's radius r_{Earth} . Even if the entire coastal ocean is considered
140 as one single global object (see concepts by Holt et al. (2009)), large scale
141 global or regional drivers need to be transferred to the coastal ocean. For
142 the remote meteorological forcing (weather systems) this is typically done
143 by one-way or two-way nesting to a regional atmospheric model which itself
144 is coupled to a global model. For the remote oceanic impact (tides, surges,
145 planetary waves, etc.) this has to be done via lateral boundary conditions
146 coming from external models. Therefore, the problem of *open boundary con-*
147 *ditions (OBCs) and model nesting* is characteristic for coastal ocean models
148 (as well as for the basin-scale ocean models), see the discussions in Section
149 6.

150 3. Basic equations

151 3.1. Momentum and tracer equations

152 Coastal and large scale ocean models typically use a common set of dy-
153 namic equations, which is based on the Reynolds-averaged primitive equa-
154 tions including hydrostatic and Boussinesq approximations. Detailed deriva-
155 tions of these equations are e.g. found in Griffies and Adcroft (2008).

156 These equations are derived from the Navier-Stokes equations on the ro-
157 tating Earth by first adopting the Boussinesq approximation which includes
158 the use of a constant reference density ρ_0 (instead of the potential density ρ)
159 in all terms except in the gravity term. This has the consequence that mass
160 conservation is replaced by volume conservation. In a next step, the effects
161 of small-scale turbulent fluctuations on the larger scales are considered in a
162 parameterised way without the necessity to numerically resolve them. This
163 procedure assumes an ensemble averaging of the Navier-Stokes equations re-
164 sulting in the Reynolds-averaged Navier-Stokes equations which now include
165 unknown turbulent stresses which need to be parameterised (see section 3.2).
166 Finally, a scaling analysis assuming a small aspect ratio (vertical scales are
167 much smaller than horizontal scales) results in the degeneration of the vertical
168 component of the momentum equation to the hydrostatic balance, neglect-
169 ing vertical acceleration, the non-linear and the stress divergence terms and
170 the effects of Earth rotation (see the discussion in Kanarska et al., 2007;
171 Klingbeil and Burchard, 2013). The hydrostatic approximation includes the
172 traditional approximation for the Coriolis terms, neglecting the horizontal
173 contributions of Earth rotation in the horizontal momentum equations. The

174 dynamic equations are here for simplicity expressed in local Cartesian co-
 175 ordinates (see section 4 for spherical and curvilinear coordinates). After
 176 inserting the Boussinesq approximation into the mass conservation equation,
 177 the incompressibility condition remains:

$$178 \quad \partial_x u + \partial_y v + \partial_z w = 0, \quad (6)$$

179 with the space coordinate vector (x, y, z) (eastwards, northwards, upwards),
 180 and the three-dimensional velocity vector (u, v, w) .

181 Applying the incompressibility condition (6) and the hydrostatic condi-
 182 tion (with pressure p and gravitational acceleration $g = 9.81 \text{ m s}^{-2}$),

$$183 \quad \partial_z p = -g\rho, \quad (7)$$

184 (remainder of the vertical component of the Navier-Stokes equations) into
 185 the horizontal momentum equations, the resulting dynamic equations are of
 186 the following form:

$$\begin{aligned} & \partial_t u + \partial_x (u^2) + \partial_y (uv) + \partial_z (uw) + \partial_{\tilde{x}} J_{\tilde{x}}^u + \partial_{\tilde{y}} J_{\tilde{y}}^u + \partial_z J_z^u - fv \\ & = -\frac{1}{\rho_0} \partial_x p_a - \frac{g}{\rho_0} \partial_x \int_z^\eta \rho \, d\xi \\ & = -\frac{1}{\rho_0} \partial_x p_a - g \partial_x \eta + \int_z^\eta \partial_x b \, d\xi \end{aligned} \quad (8)$$

188 and

$$\begin{aligned} & \partial_t v + \partial_x (vu) + \partial_y (v^2) + \partial_z (vw) + \partial_{\tilde{x}} J_{\tilde{x}}^v(u, v) + \partial_{\tilde{y}} J_{\tilde{y}}^v(u, v) + \partial_z J_z^v + fu \\ & = -\frac{1}{\rho_0} \partial_y p_a - \frac{g}{\rho_0} \partial_y \int_z^\eta \rho \, d\xi \\ & = -\frac{1}{\rho_0} \partial_y p_a - g \partial_y \eta + \int_z^\eta \partial_y b \, d\xi, \end{aligned} \quad (9)$$

189 with time t , the local Coriolis frequency $f = 2\Omega \sin(\phi)$ (with the angular
 190 speed of Earth rotation $\Omega = 7.29 \cdot 10^{-5} \text{ s}^{-1}$ and the latitude ϕ), the surface
 191 elevation η , and the surface pressure p_a . $J_{[\tilde{x}, \tilde{y}, z]}^u$ and $J_{[\tilde{x}, \tilde{y}, z]}^v$ are shear stress
 192 vectors along the local plain spanned by the vector (\tilde{x}, \tilde{y}) which might be
 193

194 along geopotentials ($\tilde{x} = x$, $\tilde{y} = y$), or along general vertical coordinates
195 or along isopycnals. This simplifying notation is used to avoid the intro-
196 duction of rotated diffusion tensors and to facilitate the practical numerical
197 implementation. The terms on the left hand sides of (8) and (9) are the
198 tendency term, the three components of the advection terms (written in so-
199 called integral form), the stress divergence terms, and the Coriolis term. The
200 terms on the right hand side form the horizontal pressure gradient compo-
201 nents $\partial_x p / \rho_0$ and $\partial_y p / \rho_0$. The formulation in the last line splits the pressure
202 gradient into the external pressure gradient (composed of the atmospheric
203 pressure gradient and the surface slope) and the internal pressure gradient,
204 where $b = -(g/\rho_0)(\rho - \rho_0)$ is the buoyancy. The last lines of (8) and (9)
205 result from assuming $\rho(\eta)/\rho_0 \approx 1$ which is consistent with the Boussinesq
206 approximation. In (8) and (9), the flux form for the advective terms is used,
207 which results for any quantity q from the incompressibility condition (6):

$$208 \quad u\partial_x q + v\partial_y q + w\partial_z q = \partial_x(uq) + \partial_y(vq) + \partial_z(wq), \quad (10)$$

209 which is the preferred form for coastal models in contrast to large-scale mod-
210 els sometimes based on the vector-invariant form for nonlinear terms, which
211 allow an integral conservation of potential enstrophy and/or total energy
212 (e.g. Arakawa and Lamb, 1977) (see section 7.1).

213 Equations (8) and (9) are valid for $-H(x, y) < z < \eta(x, y, t)$ (with the
214 bottom coordinate $z = -H$). Dynamic boundary conditions at the free
215 surface are

$$216 \quad J_z^{[u,v]} \Big|_{z=\eta} = \frac{\tau_{[x,y]}^s}{\rho_0}, \quad (11)$$

217 with the surface stress vector (τ_x^s, τ_y^s) , which is calculated from meteorological
218 data using bulk formulae (e.g., Kondo (1975); Fairall et al. (1996)). At the
219 bottom, the dynamic boundary conditions are the no-slip conditions

$$220 \quad [u, v] \Big|_{z=-H} = 0. \quad (12)$$

221 For numerical reasons, however, generally an equivalent flux boundary con-
222 dition is applied,

$$223 \quad J_z^{[u,v]} \Big|_{z=-H} = \frac{\tau_{[x,y]}^b}{\rho_0}, \quad (13)$$

224 with the bed stress vector (τ_x^b, τ_y^b) reconstructed from a logarithmic velocity
225 profile (see Section 7.5).

226 Kinematic surface and bottom boundary conditions are:

$$227 \quad w|_{z=\eta} = \partial_t \eta + u|_{z=\eta} \partial_x \eta + v|_{z=\eta} \partial_y \eta + (E - P), \quad (14a)$$

$$228 \quad w|_{z=-H} = -u|_{z=-H} \partial_x H - v|_{z=-H} \partial_y H, \quad (14b)$$

230 with the evaporation rate E and the precipitation rate P . River run-off can
231 be treated in various ways, e.g. as lateral boundary condition.

232 There is a large variety of lateral boundary conditions, which will be
233 further discussed in section 6.

234 Within the Boussinesq approximation, the budget equation for internal
235 energy reduces to a conservation equation for potential temperature θ :

$$236 \quad \partial_t \theta + \partial_x (u\theta) + \partial_y (v\theta) + \partial_z (w\theta) + \partial_{\bar{x}} J_{\bar{x}}^{\theta} + \partial_{\bar{y}} J_{\bar{y}}^{\theta} + \partial_z J_z^{\theta} = \frac{1}{C_p \rho_0} \partial_z I, \quad (15)$$

237 with the horizontal and vertical turbulent fluxes of θ given by $J_{[\bar{x}, \bar{y}, z]}^{\theta}$, the
238 specific heat capacity of water at constant pressure, C_p , and irradiance in
239 water, I . The positive vertical gradient of irradiance depends on the light
240 absorption model applied. A classical model would be the model by Paulson
241 and Simpson (1977), but often more complex models taking into account
242 water colour, suspended matter and biogeochemical components are used.
243 In (15), the heating due to viscous dissipation of turbulent kinetic energy is
244 neglected, since in comparison to other terms in the local heat budget of the
245 ocean this is a very small term (in contrast to conditions in the higher atmo-
246 sphere). The surface boundary condition for the turbulent flux of potential
247 temperature is formulated as

$$248 \quad J_z^{\theta}|_{z=\eta} = \frac{Q_s + Q_l + Q_b}{C_p \rho_0}, \quad (16)$$

249 with the sensitive heat flux Q_s (due to the air-sea temperature difference), the
250 latent heat flux Q_l (due to evaporation), and the long-wave back radiation
251 Q_b . Note that upward (positive) fluxes of potential temperature lead to
252 cooling at the surface. For the parameterisation of these heat fluxes various
253 models are available, with the bulk formulae by Kondo (1975) and Fairall
254 et al. (1996) being the most common ones for coastal applications.

255 The conservation equation for the salinity S is of similar form as the
256 temperature conservation equation, but without source term:

$$257 \quad \partial_t S + \partial_x (uS) + \partial_y (vS) + \partial_z (wS) + \partial_{\bar{x}} J_{\bar{x}}^S + \partial_{\bar{y}} J_{\bar{y}}^S + \partial_z J_z^S = 0. \quad (17)$$

258 The diffusive salinity flux at the surface is given as

$$259 \quad J_z^S|_{z=\eta} = -(E - P)S, \quad (18)$$

260 see Beron-Vera et al. (1999) for details. The salinity unit which should be
 261 used in all ocean models is the absolute salinity which indicates the mass
 262 fraction of salt in seawater in [g/kg], defined according to the TEOS-10 stan-
 263 dard (IOC, SCOR and IAPSO (2010)). The potential density is calculated by
 264 means of an empirical equation of state as function of potential temperature
 265 θ , absolute salinity S and pressure p :

$$266 \quad \rho = \rho(\theta, S, p). \quad (19)$$

267 A recent and accurate formulation for Boussinesq models has been provided
 268 by Roquet et al. (2015).

269 *3.2. Turbulence closure modelling*

270 Turbulence closure modelling involves complex theories which cannot be
 271 discussed here. For an overview, the reader is referred to text books (Kantha
 272 and Clayson, 2000b; Griffies, 2004; Cushman-Roisin and Beckers, 2011;
 273 Olbers et al., 2012). In most ocean models, vertical and horizontal turbulent
 274 fluxes of scalars are parameterised by a down-gradient approximation of the
 275 form

$$276 \quad J_{[\tilde{x}, \tilde{y}]}^c = -A_c \partial_{[\tilde{x}, \tilde{y}]} c, \quad (20)$$

$$277 \quad J_z^c = -K_c \partial_z c, \quad (21)$$

279 using horizontal and vertical eddy diffusivities A_c and K_c for any scalar c .
 280 With this, the turbulent fluxes are directed towards the lower concentrations,
 281 as postulated for molecular fluxes in ideal gases.

282 For the vertical turbulent momentum fluxes, an equivalent formulation is
 283 generally used:

$$284 \quad J_z^{[u, v]} = -K_M \partial_z [u, v], \quad (22)$$

285 with the vertical eddy viscosity K_M . For the parameterisation of the hori-
 286 zontal turbulent momentum fluxes, additional invariance to vector rotation

287 needs to be taken into account (Blumberg and Mellor, 1987):

$$\begin{aligned}
 J_{\bar{x}}^u(u) &= -2A_M \partial_{\bar{x}} u, \\
 J_{\bar{y}}^u(u, v) &= -A_M (\partial_{\bar{y}} u + \partial_{\bar{x}} v), \\
 J_{\bar{x}}^v(u, v) &= -A_M (\partial_{\bar{y}} u + \partial_{\bar{x}} v), \\
 J_{\bar{y}}^v(v) &= -2A_M \partial_{\bar{y}} v,
 \end{aligned}
 \tag{23}$$

288
289 with the horizontal eddy viscosity A_M .

290 3.2.1. Small-scale closure models

291 For the parameterisation of vertical eddy viscosity and diffusivity, two
292 basic approaches are commonly used in ocean models.

293 One of them is based on direct algebraic computation of the eddy param-
294 eters from bulk properties (boundary fluxes, mixed layer depth, bulk Richard-
295 son number) of the surface and bottom mixed layers, the so-called K-profile
296 parameterisation (KPP) which has been originally proposed for large-scale
297 ocean models by Large et al. (1994). In addition to the down-gradient fluxes,
298 also counter-gradient flux components (for example for convectively unstable
299 boundary layers) are included in the KPP model. Many extensions of the
300 original KPP model have been proposed (see, e.g., Smyth et al., 2002; Durski
301 et al., 2004; Uchiyama et al., 2010) to extend its applicability also to coastal
302 ocean applications (see, e.g., Blaas et al., 2007). The KPP model assumes
303 that the boundary layer turbulence is in equilibrium with the surface or bot-
304 tom fluxes, respectively. For large scale ocean models, this might often be
305 an adequate approximation. In many coastal model applications however,
306 the deviation from this equilibrium is a first-order process which cannot be
307 neglected.

308 The other closure approach, which in contrast to the KPP model consid-
309 ers high temporal and spatial variability in boundary layers, is based on a
310 dynamic equation for the turbulent kinetic energy (TKE), k , which can be
311 derived from the Navier-Stokes equations by means of Reynolds-averaging
312 (Wilcox, 1998; Burchard, 2002a):

$$\partial_t k + \partial_x (uk) + \partial_y (vk) + \partial_z (wk) - \partial_z \left(\frac{K_M}{Sc_k} \frac{\partial k}{\partial z} \right) = P + B - \varepsilon, \tag{24}$$

314 with the shear production, $P = K_M M^2$ including the vertical shear squared,
 315 M^2 , and the buoyancy production, $B = -K_c N^2$, with the buoyancy fre-
 316 quency (or Brunt-Väisälä frequency) squared, N^2 , and the dissipation rate,
 317 ε . The shear production P transfers kinetic energy lost from the mean flow
 318 due to vertical stress divergence to the turbulent kinetic energy, whereas the
 319 buoyancy production B exchanges energy between the mean potential en-
 320 ergy to the turbulent kinetic energy. Note, that in (24) the down-gradient
 321 approximation has been adopted with the turbulent Schmidt number Sc_k ,
 322 which is of order unity. Horizontal turbulent fluxes are generally neglected
 323 for the TKE budget (Delhez et al., 1999). This may also be the case for the
 324 advective terms, but in tidally energetic regimes, such a neglect might lead
 325 to significant errors or instabilities. In addition to the TKE, also the length
 326 scale of the energy containing eddies, l , needs to be approximated to obtain
 327 an estimate for the vertical eddy viscosity and eddy diffusivity. Once k and
 328 l are known, the vertical eddy coefficients can be calculated as

$$329 \quad K_M = S_M k^{1/2} l, \quad K_c = S_c k^{1/2} l, \quad (25)$$

330 with the non-dimensional stability functions S_M and S_c . These stability
 331 functions can be parameterised by means of second-moment closures based on
 332 Reynolds-averaging the Navier-Stokes equations (Mellor and Yamada, 1982;
 333 Canuto et al., 2001) or based on simpler empirical relations (Rodi, 1987;
 334 Burchard and Baumert, 1995). The dissipation rate ε can be calculated from
 335 l via the cascading relation

$$336 \quad \varepsilon = c_\varepsilon \frac{k^{3/2}}{l} \quad (26)$$

337 with the empirical constant c_ε .

338 Surface and bottom boundary conditions are typically derived from the
 339 law of the wall, resulting in k being proportional to the surface or bed stress,
 340 respectively, and the length scale to be proportional to the respective rough-
 341 ness length. Equivalent flux conditions, which proved to be numerically more
 342 stable have been proposed (Burchard and Petersen, 1999). To parameterise
 343 effects of breaking surface waves, injection of TKE at the surface is applied
 344 (Burchard, 2001). Effects of Langmuir Circulation on the dynamics of the
 345 surface mixed layer may be parameterised as well (see, e.g., Harcourt, 2014).
 346 Additional frictional effects of surface waves on wave drag in shallow water
 347 can also be considered in the bottom boundary condition (Mellor, 2002).

348 Various methods are used in ocean modelling to calculate the length scale
 349 l . In one-equation turbulence closure models (the one equation is for the

350 computation of the TKE), l is calculated from combinations of geometric
351 length scales (such as the distance from the surface or the bottom) or from
352 hydrodynamic length scales (such as the Ozmidov scale), see e.g., Mellor and
353 Yamada (1982); Gaspar et al. (1990). More common in coastal ocean models
354 are however two-equation turbulence closure models which in addition to the
355 TKE equation calculate a budget equation for a length-scale related quantity
356 such as for the dissipation rate ε (k - ε models, see Rodi, 1987; Burchard
357 and Baumert, 1995), for the turbulent frequency $\omega = \varepsilon/k$ (k - ω models, see
358 Wilcox, 1998; Umlauf et al., 2003), the quantity kl (k - kl models, see Mellor
359 and Yamada, 1982), or the generic length-scale related property $k^m l^n$ with
360 real numbers m and n (the generalised length-scale model, see Umlauf and
361 Burchard, 2003). When properly calibrated, all these two-equation models
362 perform similarly (Burchard et al., 1998; Umlauf and Burchard, 2003; Warner
363 et al., 2005).

364 Two-equation turbulence closure models including algebraic second-mo-
365 ment closures as outlined here (see also the review by Umlauf and Burchard,
366 2005) have proven in many applications as a good compromise between com-
367 putational efficiency and realistic representation of relevant processes in the
368 coastal ocean.

369 There is a number of reasons, why such second-moment turbulence closure
370 models are a necessary feature of coastal ocean models. First of all, as
371 discussed in section 2.1, a large portion of water columns in the coastal
372 ocean (if not the entire water column) are covered by surface or bottom
373 boundary layers. These boundary layers have a vertical structure which
374 locally influences the mixing coefficients. Therefore, boundary layer models
375 reacting on local forcing instead of surface or bottom fluxes only are required.
376 Secondly, relevant times scale in the coastal ocean are much shorter than in
377 the global ocean (see section 2.4). Therefore, the turbulence closure models
378 need to react on correct time scales to rapid time changes in surface or bottom
379 stress instead of instantaneously adjusting the eddy coefficients in the entire
380 mixed layers such as in the KPP model. Such requirements are only fulfilled
381 by carefully calibrated second-moment turbulence closure models.

382 There are a few global ocean models using low-level second-moment clo-
383 sures (see, e.g., Oschlies (2002); Danabasoglu et al. (2014)), which typically
384 are based on the Gaspar et al. (1990) one-equation model, where the tur-
385 bulent length scale l is algebraically computed. Two-equation turbulence
386 closure models are generally too complex for global ocean models. This is
387 mainly due to the large baroclinic time steps of global models (about 1 hour)

388 and the coarse resolution in boundary layers. Increasing spatial and tempo-
 389 ral resolution of large-scale ocean models in order to allow for the inclusion
 390 of two-equation turbulence closure models would result in additionally high
 391 computational costs which probably might not pay off on the temporal and
 392 spatial scales relevant for global ocean simulations. Therefore, in large-scale
 393 ocean models, the KPP model (see above) or other models with reduced
 394 dynamics (see, e.g., Jackson et al. (2008)) are used.

395 3.2.2. Meso-scale and submeso-scale closure models

396 Whereas in ocean models a consistent theoretical framework for the ver-
 397 tical turbulent fluxes exists, such a rigorous closure for the horizontal tur-
 398 bulent fluxes due to meso-scale and submeso-scale eddies is still missing. In
 399 the stratified ocean, the physically most relevant direction of horizontal mix-
 400 ing is along isopycnal surfaces. Since this is however numerically demanding
 401 in non-isopycnal models (see the discussion by Griffies et al., 1998; Beckers
 402 et al., 1998), in many model applications horizontal mixing is simply carried
 403 out along coordinate surfaces.

404 Two simplistic common approaches used in the coastal ocean modelling
 405 community are to either neglect horizontal turbulent fluxes (and then rely on
 406 the numerical fluxes due to monotone, upstream-biased advection schemes,
 407 see section 7) or to set A_M and A_c to constant values. In the latter case, the
 408 proper choice of the horizontal exchange coefficients is then determined by
 409 sensitivity studies. A physically more sound, resolution-dependent parame-
 410 terisation of horizontal momentum fluxes has been proposed by Smagorinsky
 411 (1963). For incompressible fluids under the (quasi)hydrostatic pressure ap-
 412 proximation the horizontal eddy viscosity can be derived as

$$413 \quad A_M = C_M(\Delta x \Delta y) \sqrt{(\partial_x u)^2 + \frac{1}{2}(\partial_y u + \partial_x v)^2 + (\partial_y v)^2}, \quad (27)$$

414 with the horizontal grid sizes Δx and Δy , and with the empirical parameter
 415 C_M . The latter has been estimated by Holt and James (2006) in a shelf sea
 416 application as $C_M \approx 0.2$. The same approach as (27) can also be applied for
 417 horizontal tracer diffusivities (see, e.g., Gräwe et al., 2015), using a different
 418 value for the empirical parameter.

419 For large scale ocean models which do not resolve meso-scale eddies, other
 420 closures have been proposed, such as the Gent and McWilliams (1990) closure
 421 for isopycnal mixing or the dynamic meso-scale eddy closure by Eden and
 422 Greatbatch (2008). However, in coastal ocean models eddies are at least

423 partially resolved, such that these closures cannot directly be used in such
424 models. On the other hand, theories for submeso-scale dynamics are not yet
425 mature and general enough to derive applicable eddy closures.

426 **4. Coordinate transformations and spatial discretisation**

427 The set of governing equations, consisting of the continuity equation (6),
428 the hydrostatic momentum equations (8) and (9), and the prognostic equa-
429 tions for temperature (15) and salinity (17), so far has been formulated in a
430 local Cartesian reference frame at the Earth surface for simplicity. However,
431 the transformation to coordinate systems that align with the geometry of the
432 domain is often advantageous.

433 Most coastal ocean models support orthogonal curvilinear coordinates in
434 the horizontal to offer to some extent the alignment with coastlines and an
435 increased horizontal resolution towards the coast as required by the typically
436 strong near-coastal horizontal gradients, see (4). The corresponding basis
437 transformation introduces additional metric coefficients and terms that also
438 offer the formulation in spherical coordinates, see Sec. 4.3 for details. For
439 clarity, the governing equations in the remainder of this review will be kept
440 in horizontal Cartesian coordinates.

441 In the vertical the alignment with the boundaries (free surface and bottom
442 topography) and proper resolution (of e.g. the boundary layers and pycno-
443 clones) is even more critical than in the horizontal. A general description that
444 supports various types of vertical coordinates is given by the s -coordinates
445 of Kasahara (1974). The general vertical coordinate $s(x, y, z, t)$ must be
446 strictly monotone in z in order to guarantee a unique inverse transformation
447 $z(x, y, s, t)$ and a well-defined Jacobian $\partial_s z = (\partial_z s)^{-1}$ for the transformation
448 of the governing equations. For isopycnal coordinates $s = \rho$ this precludes
449 the representation of unstable stratification. The horizontal coordinates and
450 time do not change under the transformation and, if necessary for the purpose
451 of clarity, derivatives with respect to constant s and z will be distinguished
452 by $(\cdot)_s$ and $(\cdot)_z$, respectively. With the Lagrangian derivative D/Dt it can
453 easily be shown, that the grid-related vertical velocity, defined as the differ-
454 ence of the fluid's vertical velocity and the vertical velocity of the coordinate

455 surfaces w^{grid} , is given by

456 $w^{\text{s}} = w - w^{\text{grid}}$
457 $= \left[\frac{\text{D}}{\text{D}t} - \left(\frac{\text{D}}{\text{D}t} \right)_s \right] z(x, y, s, t) = \partial_s z \left[\frac{\text{D}}{\text{D}t} - \left(\frac{\text{D}}{\text{D}t} \right)_s \right] s = \partial_s z \frac{\text{D}s}{\text{D}t}. \quad (28)$
458

459 4.1. Layer-integrated equations

460 The vertical discretisation of the transformed space into k_{max} layers with
461 interfaces at fixed levels $s_{k+1/2}$ (independent of x, y, t and with $k \in [0, k_{\text{max}}]$)
462 is equivalent to a discretisation of the physical space into k_{max} layers with
463 interfaces at variable levels $z_{k+1/2}(x, y, t) = z(x, y, s_{k+1/2}, t)$ and $z_{k+1/2} >$
464 $z_{k-1/2}$, see Burchard and Petersen (1997).

465 With layer heights $h_k(x, y, t) = \int_{s_{k-1/2}}^{s_{k+1/2}} \partial_s z ds = z_{k+1/2} - z_{k-1/2}$, layer-
466 averaged prognostic quantities $\varphi_k(x, y, t) = h_k^{-1} \int_{z_{k-1/2}}^{z_{k+1/2}} \varphi dz$, for $k \in [1, k_{\text{max}}]$
467 and $\varphi \in \{u, v, \theta, S\}$, and $w_{k+1/2}^{\text{s}}(x, y, t) = w^{\text{s}}(x, y, z_{k+1/2}, t)$, the layer-integration
468 of (6), (8), (9), (15) and (17) yields:

469 $\partial_t h_k + \partial_x (h_k u_k) + \partial_y (h_k v_k) + (w_{k+1/2}^{\text{s}} - w_{k-1/2}^{\text{s}}) = 0, \quad (29)$
470

$$\begin{aligned} & \partial_t (h_k u_k) + \partial_x (h_k u_k u_k) + \partial_y (h_k v_k u_k) + \left(w_{k+1/2}^{\text{s}} \tilde{u}_{k+1/2} - w_{k-1/2}^{\text{s}} \tilde{u}_{k-1/2} \right) \\ & = f h_k v_k - g h_k \partial_x \eta - h_k \frac{1}{\rho_0} \partial_x p_a + (\tau_{x,k+1/2} - \tau_{x,k-1/2}) \\ & \quad + h_k \tilde{F}_x^{\text{h}}(h_k, u_k, v_k) + h_k F_{x,k}^{\text{IP}}, \end{aligned} \quad (30)$$

472 $\partial_t (h_k v_k) + \partial_x (h_k u_k v_k) + \partial_y (h_k v_k v_k) + \left(w_{k+1/2}^{\text{s}} \tilde{v}_{k+1/2} - w_{k-1/2}^{\text{s}} \tilde{v}_{k-1/2} \right)$

473 $= -f h_k u_k - g h_k \partial_y \eta - h_k \frac{1}{\rho_0} \partial_y p_a + (\tau_{y,k+1/2} - \tau_{y,k-1/2}) \quad (31)$

474 $+ h_k \tilde{F}_y^{\text{h}}(h_k, u_k, v_k) + h_k F_{y,k}^{\text{IP}},$

475 $\partial_t (h_k \theta_k) + \partial_x (h_k u_k \theta_k) + \partial_y (h_k v_k \theta_k) + \left(w_{k+1/2}^{\text{s}} \tilde{\theta}_{k+1/2} - w_{k-1/2}^{\text{s}} \tilde{\theta}_{k-1/2} \right)$
 $= -\partial_x (h_k J_{\tilde{x},k}^{\theta}) - \partial_y (h_k J_{\tilde{y},k}^{\theta}) - (J_{z,k+1/2}^{\theta} - J_{z,k-1/2}^{\theta}) \quad (32)$

$$+ \frac{1}{C_p \rho_0} (I_{k+1/2} - I_{k-1/2}),$$

476

$$\begin{aligned}
& \partial_t (h_k S_k) + \partial_x (h_k u_k S_k) + \partial_y (h_k v_k S_k) + \left(w_{k+1/2}^s \tilde{S}_{k+1/2} - w_{k-1/2}^s \tilde{S}_{k-1/2} \right) \\
& = -\partial_x (h_k J_{\tilde{x},k}^S) - \partial_y (h_k J_{\tilde{y},k}^S) - (J_{z,k+1/2}^S - J_{z,k-1/2}^S).
\end{aligned} \tag{33}$$

477

478 In (29)-(33) the interfacial values $\tilde{\varphi}_{k+1/2}$ with $\varphi \in \{u, v, \theta, S\}$ are ap-
479 proximated by the vertical advection scheme, see Sec. 7.1. The salinity of
480 freshwater fluxes is zero, i.e. $\tilde{S}_{k_{\max}+1/2} = \tilde{S}_{1/2} = 0$. According to (28) the kine-
481 matic boundary conditions (14a) and (14b) transform to $w_{k_{\max}+1/2}^s = E - P$
482 and $w_{1/2}^s = 0$.

483 In (30) and (31) the internal pressure gradient force is given by

$$F_{[x,y],k}^{\text{IP}} = \frac{1}{h_k} \int_{z_{k-1/2}}^{z_{k+1/2}} (\partial_{[x,y]})_z \int_z^\eta b d\xi dz, \tag{34}$$

484

485

486 and is approximated in terms of the layer-averaged buoyancies b_k (see, e.g.
487 Shchepetkin and McWilliams, 2003 and Sec. 7.2).

488 Considering the dynamic boundary conditions (11) and (13), the vertical
489 shear stresses are defined as

$$\tau_{[x,y],k+1/2} = \begin{cases} \tau_{[x,y]}^s(u_{k_{\max}}, v_{k_{\max}}), & k = k_{\max} \\ K_{M,k+1/2} \frac{[u, v]_{k+1} - [u, v]_k}{z_{k+1} - z_k}, & k \in [1, k_{\max} - 1], \\ \tau_{[x,y]}^b(h_1, u_1, v_1), & k = 0 \end{cases} \tag{35}$$

490

491

492 with centre positions $z_k = \frac{1}{2} (z_{k-1/2} + z_{k+1/2})$.

493 The lateral contributions of the stress tensor are approximated according
494 to Mellor and Blumberg (1985) and Kantha and Clayson (2000a):

$$\tilde{F}_{[x,y]}^h(h, u, v) = -\frac{1}{h} \left(\partial_x \left(h J_{\tilde{x}}^{[u,v]}(u, v) \right) + \partial_y \left(h J_{\tilde{y}}^{[u,v]}(u, v) \right) \right), \tag{36}$$

495

496

497 with the diffusive fluxes $J_{[\tilde{x},\tilde{y}]}^{[u,v]}$ given by (23) and all gradients calculated along
498 layer k . In case of diffusion along directions not aligned with constant s ,
499 additional terms due to non-diagonal elements of the diffusion tensor would
500 occur (Griffies (2004)).

501 In (32) and (33) $J_{[\tilde{x},\tilde{y}],k}^c$ denotes the lateral turbulent fluxes (again with
502 all gradients calculated along layer k), $J_{z,k\pm 1/2}^c$ the vertical turbulent fluxes at
503 the layer interfaces, with $J_{k_{\max}+1/2}^S = 0$ and $I_{k\pm 1/2}$ the interfacial irradiance.

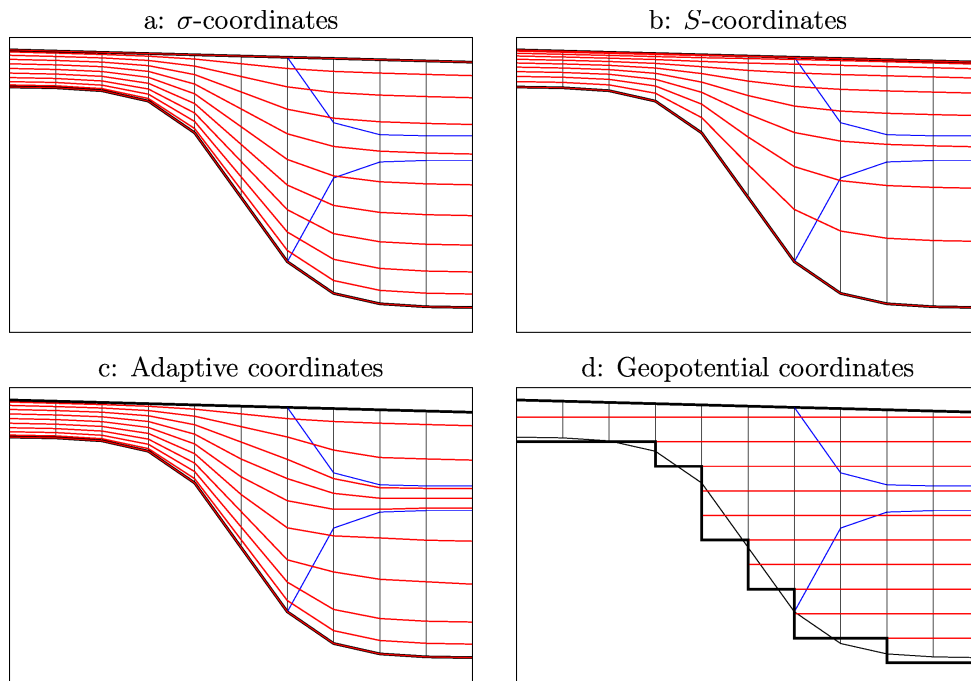


Figure 1: Sketch showing a vertical transect through a coastal ocean model domain including four different vertical coordinates. The blue lines indicate two selected isopycnals representing a tidal front with a stratified shelf sea region to the right and a well-mixed coastal region to the left. The vertical black lines indicate the horizontal discretisation, the red lines show the vertical coordinate surfaces and the bold black lines show the bottom and surface representation of the coordinates. a: σ -coordinates with zooming towards the surface and the bottom; b: S -coordinates with high near-surface resolution; c: Adaptive coordinates with increased resolution in the stratified region; d: Geopotential coordinates without partial cells at the bottom.

504 *4.2. Examples for vertical coordinates*

505 The almost arbitrary choice of the transformation function $s = s(x, y, z, t)$
506 or equivalently of the moving layer interfaces $z_{k+1/2}(x, y, t)$ allows for a high
507 degree of freedom for the vertical layout which can be exploited to improve
508 the model performance.

509 *4.2.1. Geopotential coordinates*

510 Geopotential (or z -) coordinates (see Figure 1d) are based on globally
511 defined z -levels $z_{k+1/2}$ which do not depend on location or time, except for
512 the uppermost coordinate level $z_{k_{\max}+1/2} = \eta$ which is identical to the free
513 surface. Vertical resolution is typically increased near the surface to properly
514 reproduce the dynamics of the surface mixed layer. Since for too fine near-
515 surface vertical resolution the moving and sloping free surface might intersect
516 with one or more coordinate levels, the uppermost geopotential coordinate
517 level $z_{k_{\max}-1/2}$ is chosen such that it is below the minimum surface elevation.
518 For models of shelf seas with a large maximum tidal range (see Sec. 2.2)
519 this would result in a large mean thickness of the upper layer of $\mathcal{O}(10\text{m})$,
520 such that near-surface processes are not well-resolved (see, e.g., Mathis et al.
521 (2015)). For simulations of shallow coastal regions including drying and
522 flooding this would mean that all areas with intertidal flats are not vertically
523 resolved. One solution to this problem has been proposed by Casulli and
524 Cheng (1992) and Burchard and Baumert (1998): Layers at the surface are
525 locally added or removed when the surface layer becomes too thick or too
526 thin, respectively. This problem can also be solved by applying so-called z^* -
527 coordinates (Adcroft and Campin (2004)), where geopotential coordinates
528 are obtained for $\eta = 0$ everywhere, and all layer thicknesses are then locally
529 multiplied by $(\eta + H)/H$, such that the layers are squeezed or expanded with
530 the changing water depth. Another disadvantage of geopotential models near
531 the surface (which is not solved by the above mentioned treatment) is that
532 the tidal elevation triggers a large oscillating vertical velocity relative to the
533 fixed coordinate levels which generates strong numerical mixing due to the
534 vertical advection schemes, see Sec. 7.1.

535 At the bottom geopotential layers will be intersecting with the sloping
536 bottom. This leads to a stair-case type of discretisation of bottom slopes
537 which leads to low accuracy in resolving bottom parallel currents such as
538 dense bottom currents (Ezer and Mellor (2004)). A partial solution to this
539 problem has been proposed by Beckmann and Döscher (1997) by coupling an
540 empirical terrain-following bottom boundary layer model to the geopotential

541 model grid, allowing for bottom-parallel down-slope flow. Another approach
 542 to improve representation of along-bottom flow has been proposed by Ad-
 543 croft et al. (1997): to introduce *shaved cells* at the bottom to better fit the
 544 bottom topography. Geopotential coordinates over sloping topography have
 545 one other inherent problem: they do not allow a high vertical resolution near
 546 the bottom. A resolution of the bottom layer of 1 m would require equidis-
 547 tant geopotential coordinates over the entire water column, which is often
 548 computationally not affordable.

549 Given all these disadvantages of geopotential coordinates they can gener-
 550 ally not be recommended for coastal ocean simulations. There is however one
 551 potential problem of vertical coordinates which is not relevant for geopoten-
 552 tial coordinates: the internal pressure gradient problem, see Sec. 7.2. There-
 553 fore, models with geopotential coordinates are still applied for problems with
 554 strong stratification such as the Baltic Sea (Wang et al. (2015)).

555 The numerical treatment of geopotential coordinates fits into the concept
 556 of general vertical coordinates by formally allowing layers of zero thickness at
 557 the bottom and, in the case of removable surface layers, also at the surface.

558 4.2.2. Terrain-following coordinates

559 A transformation function of the form $z(s) - \eta = S(x, y, s, t)D(x, y, t)$
 560 with the local water depth $D = \eta + H$, the stretching function S being
 561 strictly monotone in s , $S(s_{1/2}) = -1$ and $S(s_{k_{\max}+1/2}) = 0$ generates terrain-
 562 following coordinates with $z_{1/2} = -H$ and $z_{k_{\max}+1/2} = \eta$. In addition to the
 563 free surface being a coordinate surface (as for the z^* -coordinates), also the
 564 bottom is a coordinate surface. Thus, in every watercolumn k_{\max} layers are
 565 active and masking of layers is not necessary. A classical option for coastal
 566 ocean model simulations are σ -coordinates defined by $S = s = \sigma$ (Nihoul
 567 et al. (1986); Blumberg and Mellor (1987)), see Figure 1a. They result in
 568 layer thicknesses proportional only to the local water depth, which is a dis-
 569 advantage especially in deeper waters (where layers may become too thick
 570 and thus resolution in critical parts of the water column too coarse) or above
 571 steep bottom slopes (where coordinate slopes are relatively steep throughout
 572 the water column, see Deleersnijder and Beckers (1992)). One other prob-
 573 lem of terrain-following coordinates is the intersection of sloping coordinate
 574 surfaces with isopycnals. For the calculation of the internal pressure gradi-
 575 ent, this results in a balance of two large terms which typically results in
 576 large truncation errors and thus artificial currents (see Sec. 7.2 for a detailed
 577 discussion.

578 Some of these problems can be reduced by using non-equidistant σ -
579 levels $\sigma_{k+1/2}$ (equivalent to non-linear stretching functions $S(s)$) and modified
580 stretching functions $S(x, y, s)$ that rescale the near-surface layer heights pro-
581 portional to a fixed critical water depth instead of to the local water depth
582 (Song and Haidvogel, 1994; Shchepetkin and McWilliams, 2009), see Figure
583 1b.

584 An alternative transformation function that maintains high resolution at
585 the surface or at the bottom independently of the local water depth has
586 been developed by Burchard and Petersen (1997) and Burchard and Bolding
587 (2002).

588 On order to obtain higher accuracy, hybridisations between s - and z -
589 coordinates have been proposed, leading to less steep coordinate slopes than
590 for s coordinates and smaller bottom steps than for z -coordinates, see Gerdes
591 (1993); Burchard and Petersen (1997) for details.

592 4.2.3. Arbitrary Lagrangian-Eulerian (ALE) coordinates

593 For geopotential and terrain-following coordinates the transformation func-
594 tion $z(s)$ is explicitly prescribed. The temporal evolution of the correspond-
595 ing interface positions $z_{k+1/2}(x, y, t)$ and layer heights $h_k(x, y, t)$ is fully deter-
596 mined by a prognostic equation for the sea surface elevation $\eta(x, y, t)$ (see Sec.
597 5.1). In this case the continuity equation (29) does not serve as a prognos-
598 tic equation for h_k , but as a diagnostic equation for the grid-related vertical
599 velocity $w_{k+1/2}^s$. Following Adcroft and Hallberg (2006), this is the Eulerian
600 treatment of the vertical direction (EVD).

601 In contrast, the Lagrangian treatment of the vertical direction (LVD) is
602 based on a Lagrangian vertical coordinate, formally defined by $\frac{Ds}{Dt} = 0$ (Starr,
603 1945). In this case the grid-related vertical velocity vanishes $w^s = 0$, see (28),
604 and the continuity equation (29) serves as a prognostic equation for the layer
605 heights h_k .

606 Numerical mixing (induced by truncation errors of discrete advective
607 fluxes; see e.g. Klingbeil et al., 2014) is significantly reduced in Lagrangian
608 vertical coordinates because of the missing advective transport through the
609 coordinate surfaces. However, a pure Lagrangian movement of the layers is
610 prone to grid distortion and possibly vanishing layers, which complicates the
611 numerical treatment.

612 Therefore, a combination of LVD and EVD gains increasingly popular-
613 ity. Originally Hirt et al. (1974) defined the Arbitrary Lagrangian-Eulerian
614 (ALE) method by a Lagrangian mesh movement (LVD step) followed by

615 an optional readjustment of the mesh associated with grid-related advective
616 transports (EVD step). The advection during the EVD step can be replaced
617 by instantaneous "remapping" (monotone and conservative interpolation, see
618 e.g. White and Adcroft, 2008) which relaxes the strict CFL constraint to a
619 less severe Lipschitz condition.

620 Another approach is to consider Lagrangian tendencies in the calcu-
621 lation of the layer heights used in EVD algorithms. Separable terrain-
622 following coordinates of the form $z - \eta = S(s)D(x, y, t)$ inherently im-
623 ply a Lagrangian treatment of merely barotropic motions (Shchepetkin and
624 McWilliams, 2009). Non-separable terrain-following coordinates with time-
625 independent stretching functions $S(x, y, s)$ do not exactly treat barotropic
626 motions in a Lagrangian way, but also significantly reduce the correspond-
627 ing grid-related vertical transports by scaling the layer heights according to
628 $h_k = \frac{D}{H} h_k^{(\eta=0)}$. The same holds for the z^* -coordinates of Adcroft and Campin
629 (2004).

630 Recently, Leclair and Madec (2011) proposed to also treat fast oscillat-
631 ing baroclinic currents in a Lagrangian way by introducing the so-called
632 \tilde{z} -coordinate.

633 4.2.4. Adaptive coordinates

634 In order to further optimise the vertical grid layout in 3D models, Hofmeis-
635 ter et al. (2010) presented adaptive coordinates, see Figure 1c. These do not
636 only consider Lagrangian tendencies, but also a zooming of layers towards
637 boundaries, stratification and shear. This zooming is based on a vertical
638 diffusion equation for the interface positions,

$$639 \quad \partial_t z_{k+1/2} - \left(D_{k+1}^{\text{grid}}(z_{k+3/2} - z_{k+1/2}) - D_k^{\text{grid}}(z_{k+1/2} - z_{k-1/2}) \right) = 0, \quad (37)$$

641 with boundary conditions $z_{1/2} = -H$ and $z_{k_{\text{max}}+1/2} = \eta$ (Burchard and Beck-
642 ers, 2004). A vertically constant layer "diffusion" coefficient D^{grid} (unit s^{-1})
643 tends to generate equidistant layers, whereas locally increased coefficients
644 (e.g. proportional to stratification and shear) increase the local concentra-
645 tion of layer interfaces and thus the vertical resolution. Improved vertical
646 resolution decreases the truncation errors of vertical advective fluxes and
647 thus reduces vertical numerical mixing. The layer distribution in adjacent
648 water columns is coupled by lateral adjustment of layer heights and inter-
649 face positions. In addition, an optional isopycnal tendency aligns the layers
650 with isopycnals and thus avoids the spurious diapycnal mixing of tracers due

651 to explicit and numerical along-layer mixing in the model. Furthermore, an
652 isopycnal alignment of the layers reduces internal pressure gradient errors (see
653 Sec. 7.2). It should be noted, that pure isopycnal coordinates are not appropri-
654 ate for coastal ocean models, because of the relatively large mixed layers
655 according to (1). Gräwe et al. (2015) demonstrated the clear advantages
656 of adaptive coordinates compared to σ -coordinates in a realistic state-of-
657 the-art model application with different dynamical regimes (tidal/non-tidal
658 parts, seasonal thermocline / permanent halocline).

659 *4.3. Horizontal discretisation*

660 The layer-integrated equations (29) - (33) include horizontal divergence
661 terms for advection and diffusion which still need to be discretised. Inde-
662 pendently from the vertical coordinate specification, a horizontal coordinate
663 transformation is carried out. For the simplest case, no coordinate transfor-
664 mation is needed, such that horizontal coordinates remain Cartesian, with
665 typically x denoting the coordinate to the right and y denoting the coordinate
666 orthogonally to it in a right-hand system. Such Cartesian coordinates are
667 consistent with UTM coordinates. This however limits model applications
668 to domains being very small compared to the Earth's radius, since the model
669 domain is assumed to be planar. For larger domains (such as shelf seas), a
670 transformation into spherical coordinates is carried out, with coordinates λ
671 (pointing eastwards) and ϕ (pointing northwards), which is consistent with
672 geographical coordinates. The transformation to spherical coordinates re-
673 sults in geometric coefficients by which terms in the dynamic equations are
674 weighted (see, e.g., the text book by Kantha and Clayson (2000a)). To sup-
675 port multi-scale applications also with regular coordinates (and not only with
676 unstructured-grid models), orthogonal curvi-linear coordinates have been in-
677 troduced (Haidvogel et al. (1991)), having enough flexibility to focus into
678 certain parts of the domain such as estuaries or coastal regions. Curvi-linear
679 coordinates may be referenced to Cartesian or to spherical coordinates, de-
680 pending on the scale of the problem, but the resulting grids (after discretisa-
681 tion) are of the same type. It should be noted that Cartesian and spherical
682 coordinates can be regarded as special cases of orthogonal curvi-linear coor-
683 dinates, such that models which include the latter do automatically offer the
684 numerics for the other two types. Note that also non-orthogonal curvilinear
685 coordinates are in use, to further increase flexibility in spatial resolution,
686 but those have not become common in coastal ocean modelling (Kantha and
687 Clayson (2000a)).

688 After the horizontal transformation, a horizontal discretisation is carried
689 out, by dividing the two coordinates of the Cartesian, spherical or orthogonal
690 curvi-linear coordinates into not necessarily equidistant spatial increments.
691 This leads to a tiling of the horizontal model domain by grid cells which may
692 be rectangles (Cartesian coordinates), trapezoids (spherical coordinates) or
693 general quadruples (orthogonal curvi-linear coordinates). Note that angles
694 between edges are orthogonal only for Cartesian coordinates. Each grid cell
695 has thus four corners and four edges. Grid cells which include mainly land
696 areas are then masked out.

697 The layer-integrated equations (29) - (33) are then area-integrated over
698 these cells, such that in combination with the vertical layer-integration an
699 integration over so-called finite volumes is obtained. By means of this vol-
700 ume integration, divergence terms are transformed to differences of interface-
701 integrated advective and diffusive fluxes, such that advection and diffusion
702 are discretised in a conservative way. Non-conservative source and sink terms
703 appear as volume-integrals. These finite volumes have 8 corners, 12 edges and
704 6 interfaces, see Fig. 2. With $\Delta x_{i,j}$ and $\Delta y_{i,j}$ denoting mean length and width
705 of the volumes and $h_{i,j,k}$ denoting the mean height, these volumes are defined
706 as $\mathcal{V}_{i,j,k} = \Delta x_{i,j} \Delta y_{i,j} h_{i,j,k}$. With $\Delta x_{i,j\pm 1/2}$ and $\Delta y_{i\pm 1/2,j}$ denoting the length
707 and width at the lateral edges, the vertical interfaces of the finite volume
708 have the areas $A_{i\pm 1/2,j,k} = \Delta y_{i\pm 1/2,j} h_{i\pm 1/2,j,k}$ and $A_{i,j\pm 1/2,k} = \Delta x_{i,j\pm 1/2} h_{i,j\pm 1/2,k}$.
709 With these notations, the volume-integral of the layer height equation (29)
710 reads as

$$\begin{aligned}
& \Delta x_{i,j} \Delta y_{i,j} \partial_t h_{i,j,k} \\
& + \left(\Delta y_{i+1/2,j} h_{i+1/2,j,k} u_{i+1/2,j,k} - \Delta y_{i-1/2,j} h_{i-1/2,j,k} u_{i-1/2,j,k} \right) \\
& + \left(\Delta x_{i,j+1/2} h_{i,j+1/2,k} v_{i,j+1/2,k} - \Delta x_{i,j-1/2} h_{i,j-1/2,k} v_{i,j-1/2,k} \right) \\
& + \Delta x_{i,j} \Delta y_{i,j} \left(w_{i,j,k+1/2}^s - w_{i,j,k-1/2}^s \right) = 0,
\end{aligned} \tag{38}$$

712 with $u_{i\pm 1/2,j,k}$, $v_{i,j\pm 1/2,k}$, and $w_{i,j,k\pm 1/2}^s$, denoting area-averaged velocities at the
713 respective interfaces. Tracer mass conservation requires the finite-volume

714 discretisation of e.g. the salinity equation of the following form:

$$\begin{aligned}
& \Delta x_{i,j} \Delta y_{i,j} \partial_t h_{i,j,k} S_{i,j,k} \\
& + \left(\Delta y_{i+1/2,j} h_{i+1/2,j,k} u_{i+1/2,j,k} \tilde{S}_{i+1/2,j,k} \right. \\
& \quad \left. - \Delta y_{i-1/2,j} h_{i-1/2,j,k} u_{i-1/2,j,k} \tilde{S}_{i-1/2,j,k} \right) \\
& + \left(\Delta x_{i,j+1/2} h_{i,j+1/2,k} v_{i,j+1/2,k} \tilde{S}_{i,j+1/2,k} \right. \\
& \quad \left. - \Delta x_{i,j-1/2} h_{i,j-1/2,k} v_{i,j-1/2,k} \tilde{S}_{i,j-1/2,k} \right) \\
715 & + \Delta x_{i,j} \Delta y_{i,j} \left(w_{i,j,k+1/2}^s \tilde{S}_{i,j,k+1/2} - w_{i,j,k-1/2}^s \tilde{S}_{i,j,k-1/2} \right) = \\
& - \Delta y_{i+1/2,j} \left(h_{i+1/2,j,k} J_{\bar{x},i+1/2,j,k}^S \right) + \Delta y_{i-1/2,j} \left(h_{i-1/2,j,k} J_{\bar{x},i-1/2,j,k}^S \right) \\
& - \Delta x_{i,j+1/2} \left(h_{i,j+1/2,k} J_{\bar{y},i,j+1/2,k}^S \right) + \Delta x_{i,j-1/2} \left(h_{i,j-1/2,k} J_{\bar{y},i,j-1/2,k}^S \right) \\
& - \Delta x_{i,j} \Delta y_{i,j} \left(J_{z,i,j,k+1/2}^S - J_{z,i,j,k-1/2}^S \right), \\
\end{aligned} \tag{39}$$

716 with the interfacial salinity values $\tilde{S}_{i\pm 1/2,j,k}$, $\tilde{S}_{i,j\pm 1/2,k}$ and $\tilde{S}_{i,j,k\pm 1/2}$ and the
717 volume averaged salinity $S_{i,j,k}$. For constant tracers and zero turbulent tracer
718 fluxes the tracer equation must recover (38).

719 The natural spatial discretisation which results from the volume-inte-
720 gration carried out in (38) and (39) suggests to locate the discrete velocity
721 points $u_{i\pm 1/2,j,k}$, $v_{i,j\pm 1/2,k}$, and $w_{i,j,k\pm 1/2}^s$ at the centres of the 6 interfaces of the
722 finite volume. The natural location for the volume-averaged salinity $S_{i,j,k}$
723 (and consequently also of the potential temperature $\theta_{i,j,k}$ and the buoyancy
724 $b_{i,j,k}$) would then be the centre of the finite volume, see Fig. 2. This would
725 be in accordance with the classical Arakawa C-grid (Arakawa and Lamb
726 (1977)), where velocity points and *pressure points* (salinity, potential tem-
727 perature, buoyancy, and thus also pressure) are staggered in space. Such a
728 grid layout guarantees that (38) and (39) can be discretised at second order
729 in space without any interpolations of velocity components. For the volume-
730 integrated u - and v -velocity equations (not shown here; note that for the
731 w -velocity no dynamic equation has to be integrated) separate (staggered)

732 finite volumes have to be constructed for which transport velocities have to
733 be interpolated to the respective interfaces (which has to be done for any
734 staggered or non-staggered grid layout). Turbulent quantities (such as verti-
735 cal eddy viscosity/diffusivity and turbulent kinetic energy) are best located
736 at the w -points, such that also for the turbulence equations specific finite
737 volumes centred around the w -points need to be constructed. There is one
738 disadvantage of the fully staggered grid layout: The respectively other hori-
739 zontal velocity component for the calculation of the Coriolis terms needs to be
740 interpolated from four adjacent velocity points in order to be second-order in
741 space. A grid layout which avoids this by collocating u - and v -components at
742 the corners of the finite volume is given by the B-grid (which still is staggered
743 with respect to vertical velocity and pressure points). Therefore large scale
744 ocean models for which an accurate spatial discretisation is essential typi-
745 cally use the B-grid, whereas coastal ocean models have traditionally been
746 written as C-grid models (see also Sec. 8.1). An excellent overview over the
747 discretisation of the linearised shallow water equations and its accuracies in
748 A- (all discrete points collocated), B- (only horizontal velocity points collo-
749 cated), C- (all staggered), and D-grids (as C-grid, but with u - and v -velocity
750 locations exchanged) is given by Beckers and Deleersnijder (1993).

751 5. Choices for mode splitting and wetting & drying

752 An essential feature of coastal ocean models is the consideration of a
753 temporally and spatially variable free surface, see (2) in section 2.2. Due
754 to the presence of a free surface, fast surface gravity waves are part of the
755 numerical solution, and drying and flooding in shallow areas of the domain
756 is possible. Both issues require special numerical techniques that will be
757 outlined in the following two subsections.

758 5.1. Mode splitting

759 Within the EVD-treatment (see Section 4.2.3) the layer-integrated conti-
760 nuity equation (29) serves as a diagnostic equation for the grid-related verti-
761 cal velocities $w_{k+1/2}^s$, and the layer heights h_k are determined in terms of the
762 total water depth D and the free surface elevation η . In this case a prognos-
763 tic equation for the free surface elevation must be derived from the vertical
764 sum of the layer-integrated continuity equation (29) and consideration of the
765 kinematic boundary conditions (14a) and (14b):

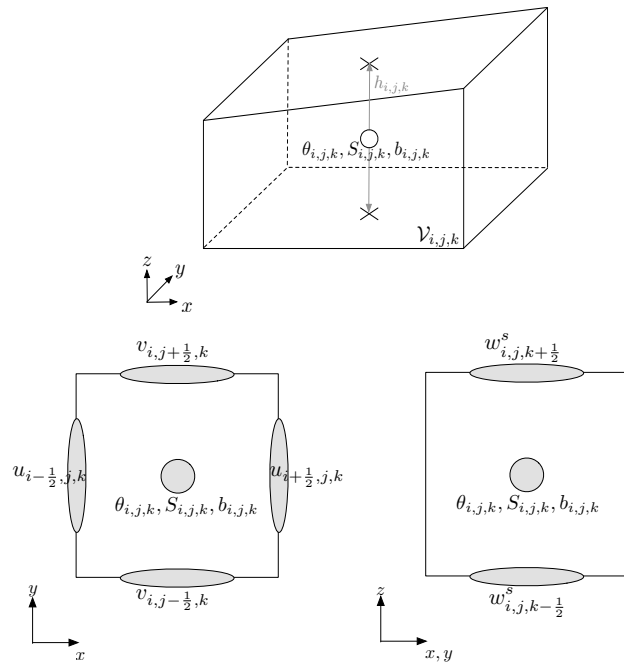


Figure 2: Control volume for cell-centered variables (top), C-grid staggering showing the location of the dependent variables in the horizontal (bottom, left) and in the vertical (bottom, right).

$$\partial_t(\eta+H) = \partial_t D = \partial_t \left(\sum_{k=1}^{k_{\max}} h_k \right) = -\partial_x \left(\sum_{k=1}^{k_{\max}} h_k u_k \right) - \partial_y \left(\sum_{k=1}^{k_{\max}} h_k v_k \right) - (E-P). \quad (40)$$

766

767 The direct numerical integration of the set (40) and (29)–(33) is possible.
 768 However, within an explicit temporal discretisation the time step is strongly
 769 constrained by the celerity of the fastest surface gravity waves. Alternatively,
 770 an implicit discretisation offers larger time steps (Casulli and Cheng, 1992),
 771 but also requires the inversion of a penta-diagonal system for the free surface
 772 elevation.

773

774 Since surface gravity waves are solely represented by the barotropic mode,
 775 the computational costs can be significantly reduced by splitting the govern-
 776 ing equations into the barotropic and remaining baroclinic mode. Usually
 777 the slightly depth-dependent barotropic mode is approximated by the depth-
 778 integrated equations (also called external mode), given by (40) and the ver-
 tical sum of the layer-integrated momentum equations (30) and (31):

$$\partial_t D + \partial_x (D\bar{u}) + \partial_y (D\bar{v}) = -(E - P), \quad (41a)$$

780

781

$$\begin{aligned} & \partial_t (D\bar{u}) + \partial_x (D\bar{u}\bar{u}) + \partial_y (D\bar{v}\bar{u}) \\ & = fD\bar{v} - gD\partial_x \eta - D \frac{1}{\rho_0} \partial_x p_a + \tau_x^s(\bar{u}, \bar{v}) - \tau_x^b(D, \bar{u}, \bar{v}) + D\tilde{F}_x^h(D, \bar{u}, \bar{v}) + S_x, \end{aligned} \quad (41b)$$

784

785

786

$$\begin{aligned} & \partial_t (D\bar{v}) + \partial_x (D\bar{u}\bar{v}) + \partial_y (D\bar{v}\bar{v}) \\ & = -fD\bar{u} - gD\partial_y \eta - D \frac{1}{\rho_0} \partial_y p_a + \tau_y^s(\bar{u}, \bar{v}) - \tau_y^b(D, \bar{u}, \bar{v}) + D\tilde{F}_y^h(D, \bar{u}, \bar{v}) + S_y, \end{aligned} \quad (41c)$$

789

790 with the water depth,

$$D \equiv \sum_{k=1}^{k_{\max}} h_k, \quad (42)$$

791

792 the barotropic transports,

$$[D\bar{u}, D\bar{v}] \equiv \sum_{k=1}^{k_{\max}} [h_k u_k, h_k v_k], \quad (43)$$

793

794 and the barotropic-baroclinic interaction terms:

$$\begin{aligned}
795 \quad S_{[x,y]} = & \quad \partial_x (D\bar{u}[\bar{u}, \bar{v}]) & - \sum_{k=1}^{k_{\max}} \partial_x (h_k u_k [u_k, v_k]) \\
796 & + \partial_y (D\bar{u}[\bar{u}, \bar{v}]) & - \sum_{k=1}^{k_{\max}} \partial_y (h_k u_k [u_k, v_k]) \\
797 & - D\tilde{F}_{[x,y]}^h(D, \bar{u}, \bar{v}) & + \sum_{k=1}^{k_{\max}} h_k \tilde{F}_{[x,y]}^h(h_k, u_k, v_k) \\
798 & - \tau_{[x,y]}^s(\bar{u}, \bar{v}) & + \tau_{[x,y]}^s(u_{k_{\max}}, v_{k_{\max}}) \\
799 & + \tau_{[x,y]}^b(D, \bar{u}, \bar{v}) & - \tau_{[x,y]}^b(h_1, u_1, v_1) \\
800 & & + \sum_{k=1}^{k_{\max}} h_k F_{[x,y],k}^{\text{IP}}. \quad (44) \\
801 & &
\end{aligned}$$

802 The remaining 3D equations (30)–(33), as well as the turbulence closure
803 equations (section 3.2) and other tracer equations such as biogeochemical
804 model equations represent the internal (baroclinic) mode. With (42), (43)
805 and (44) the splitting into external and internal mode equations is exact.
806 But, as mentioned above, it does not exactly separate the slightly depth-
807 dependent fast barotropic dynamics from the slow baroclinic ones. Therefore,
808 the time-stepping of the internal mode might still be constrained by some
809 fast dynamics.

810 A careful stability analysis of the linearised (flat-bottom) version of the
811 external mode (41a)–(41c),

$$812 \quad \partial_t \eta = -H (\partial_x \bar{u} + \partial_y \bar{v}); \quad \partial_t \bar{u} = -g \partial_x \eta + f \bar{v}; \quad \partial_t \bar{v} = -g \partial_y \eta - f \bar{u}, \quad (45)$$

813 has been carried out by Beckers and Deleersnijder (1993). For an explicit
814 discretisation on an equidistant C-grid, the stability criterion would be $\Delta t \leq$
815 $\Delta x / (2gH)^{1/2}$, which means for $\Delta x = 1000\text{m}$ and a depth of $H = 200\text{m}$ a
816 maximum timestep of $\Delta t \approx 5\text{s}$. Compared to that, the stability criterion
817 for discretising the internal mode is typically given by the advection terms.
818 For an explicit one-stage two-level discretisation (Durrant, 2013) of the linear
819 advection equation the stability criterion is $\Delta t \leq \Delta x / u_{\max}$, which would for
820 a typical maximum velocity of $u_{\max} = 1\text{m s}^{-1}$ give a maximum timestep of
821 $\Delta t = 200\text{s}$, which is a factor of about 40 larger. Non-linear systems retaining
822 all terms tend to have comparable timestep criteria.

823 If the surface elevation and the barotropic transports are not integrated
824 prognostically as part of the internal mode, but provided by the external
825 mode, an explicit temporal discretisation of the internal mode is not con-
826 strained by the celerity of the fastest surface gravity waves anymore, but
827 only by the much slower internal motions. In this case the internal mode can
828 be integrated explicitly with a timestep which, for coastal oceans, is $\mathcal{O}(10^1)$
829 times larger than that constrained by the celerity of shallow water surface
830 gravity waves. Since this increased timestep is usually already almost re-
831 quired to resolve the dynamical processes in e.g. tidally dominated coastal
832 oceans, the overhead of an implicit treatment of the 3D internal mode equa-
833 tions would be by far not balanced by the possible slight further increase of
834 the timestep. Therefore, the prognostic integration of the internal mode is
835 usually performed explicitly.

836 The prognostic integration of the external mode can be either carried out
837 implicitly with the same timestep as used for the explicit integration of the
838 internal mode, or explicitly within a series of smaller timesteps constrained
839 by the celerity shallow water surface gravity waves. Both methods have their
840 own merits and complications. Such a different numerical treatment of the
841 two modes is called mode splitting and has first been introduced by Madala
842 and Piacsek (1977).

843 5.1.1. *Semi-implicit external mode computation*

844 Let (41a)–(41c) being solved simultaneously, with the transports $D\bar{u}$ and
845 $D\bar{v}$ in (41a) being temporally weighted such that they are between the levels
846 of the old and the new surface elevation, and equivalently, with η in (41b) and
847 (41c) being temporally between the old and new transports. then, a semi-
848 implicit time stepping scheme for the external mode results. With the weight-
849 ing parameter $0 \leq \gamma \leq 1$, this can be expressed as $X^{n+\gamma} = (1-\gamma)X^n + \gamma X^{n+1}$
850 for any quantity X which is treated semi-implicitly (with superscripts de-
851 noting the number of time step). For $\gamma = 0$, the scheme would be fully
852 explicit, for $\gamma = 1$ the scheme would be fully implicit and for $\gamma = 0.5$, the
853 Crank-Nicolson scheme is obtained. The schemes are more stable (and more
854 implicit) the more the bias is towards the new time step, i.e., the larger γ is.
855 This procedure gives a linear system of equations with a matrix of dimension
856 $N \times N$ with N denoting the number of free-surface grid boxes. Depending
857 on the treatment of the Coriolis terms (explicit or semi-implicit), and when
858 calculating non-linear terms explicitly, each row of the matrix has 5 or 9
859 non-zero entries, such that the matrix is very sparse. One of the challenges

860 for solving these large systems of equations is to find accurate (typically iter-
861 ative) solvers which are efficient also on massively parallel high-performance
862 computers. An early example for a semi-implicit coastal ocean model in-
863 cluding semi-implicit treatment of the Coriolis term has been presented by
864 Backhaus (1985). This semi-implicit scheme is unconditionally stable for
865 $\gamma \geq 0.5$.

866 To avoid the requirement of solving large linear systems of equations
867 due to the semi-implicit treatment of the external mode, a directional-split
868 method had been introduced by Peaceman and Rachford (1955), in which
869 in an alternating manner the external mode is solved along one and then
870 along the other coordinate direction. This method is called Alternating Di-
871 rections Implicit (ADI). Many models in coastal engineering had adopted
872 this approach (see, e.g., Pietrzak et al., 2002). While ADI is easier to handle
873 computationally than a semi-implicit treatment without directional splitting,
874 additional errors due to the splitting have to be considered.

875 The advantage of the semi-implicit treatment is the relatively easy cou-
876 pling between the external and the internal mode, since both are computed
877 with the same time step. A disadvantage of implicit schemes is the demand-
878 ing computation of large and sparse linear system on parallel computers.
879 While the Crank-Nicolson scheme is energy-conserving (but still sensitive to
880 instabilities arising from the discretisation of other terms), a larger degree
881 of implicitness ($\gamma \rightarrow 1$) stabilises the scheme, a procedure which however
882 for larger time steps might become too dissipative (Walters et al. (2009)).
883 In tidal or tsunami simulations this sets a practical limitation to the overall
884 model time step.

885 *5.1.2. Explicit external mode computation*

886 In order to provide a reasonable free surface elevation and barotropic
887 transports for updating the internal mode from stage n to stage $n+1$, the ex-
888 ternal mode is integrated explicitly within a subcycle of M_{\max} timesteps from
889 stage $n,0$ to stage n,M_{\max} . The timestep of the external mode Δt_{2D} is con-
890 strained by the celerity of shallow water surface gravity waves, whereas the
891 internal mode is integrated with a larger internal timestep $\Delta t_{3D} = M\Delta t_{2D}$
892 with $M \leq M_{\max}$.

893 It is easy and accurate to discretise the external mode with an explicit-in-
894 time solver. In the following a time-staggered two-level scheme is outlined.
895 Staggering in time between the surface elevations and the barotropic trans-
896 ports would still guarantee second-order in time accuracy. This would be

897 achieved by subsequently calculating the surface elevation and the barotropic
 898 transports with using the newly updated transports and elevations on the
 899 right hand sides, see section 7.3. In the following the focus will be on volume
 900 and tracer mass conservation. Therefore, the discretisation of the momentum
 901 equations will be not presented in detail. A time-staggered discretisation of
 902 the free-surface equation (41a) is given by:

$$903 \frac{\eta^{n,m+1} - \eta^{n,m}}{\Delta t_{2D}} + \partial_x (D\bar{u})^{n,m+1/2} + \partial_y (D\bar{v})^{n,m+1/2} \\ 904 = - (E - P)^{n,m+1/2} \quad (46)$$

905
 906 Following Shchepetkin and McWilliams (2005) a filtered surface elevation is
 907 provided to the internal mode,
 908

$$909 \langle \eta \rangle^{n+1} \equiv \sum_{m=0}^{M_{\max}} a_m \eta^{n,m}, \quad (47)$$

910
 911 with normalised filter weights $\sum_{m=0}^{M_{\max}} a_m = 1$. If the initial surface elevation
 912 of each external mode cycle is reset to $\eta^{n,0} \equiv \langle \eta \rangle^n$, the compatible surface
 913 elevation equation resolved by the internal mode can be derived from (46) as
 914

$$915 \frac{\langle \eta \rangle^{n+1} - \langle \eta \rangle^n}{\Delta t_{3D}} + \partial_x \langle \langle D\bar{u} \rangle \rangle^{n+1/2} + \partial_y \langle \langle D\bar{v} \rangle \rangle^{n+1/2} \\ 916 = - \langle \langle E - P \rangle \rangle^{n+1/2} \quad (48)$$

917
 918 with

$$919 \langle \langle \psi \rangle \rangle^{n+1/2} \equiv \sum_{m=0}^{M_{\max}-1} b_m \psi^{n,m+1/2} \quad (49)$$

920
 921 and $b_m \equiv \frac{1}{M} \sum_{m'=m+1}^{M_{\max}} a_{m'}$. The general filter applied in (47) offers different
 922 types of filtering. Deleersnijder (1993) proposed to provide the instantane-
 923 ous surface elevation $\langle \eta \rangle^{n+1} = \eta^{n,M}$ and averaged barotropic transports
 924 $\langle \langle [D\bar{u}, D\bar{v}] \rangle \rangle^{n+1/2} = \sum_{m=0}^{M-1} [D\bar{u}, D\bar{v}]^{n,m+1/2}$ to the internal mode. This treat-
 925 ment corresponds to $M_{\max} = M$, $a_m = \delta_{mM}$, $b_m = 1$ and involves no re-
 926 set of the external quantities, i.e. $\eta^{n+1,0} = \eta^{n,M}$ and $[D\bar{u}, D\bar{v}]^{n+1,0-1/2} =$
 927 $[D\bar{u}, D\bar{v}]^{n,M-1/2}$. In order to stabilise the retained fast dynamics within the

928 internal mode and to prevent aliasing errors Griffies (2007) suggested to pro-
 929 vide an averaged surface elevation $\langle \eta \rangle^{n+1} = \frac{1}{2M+1} \sum_{m=0}^{2M} \eta^{n,m}$ to the internal
 930 mode, obtained by $M_{\max} = 2M$, $a_m = \frac{1}{2M+1}$ and $b_m = \frac{2M-m}{M(2M+1)}$. Non-uniform
 931 filter weights, centered around $m = M < M_{\max}$, were presented by Shchep-
 932 etkin and McWilliams (2005) to offer more frequency-selective filtering.

933 Volume conservation requires that the layer-integrated continuity equa-
 934 tion (29) in the internal mode,

$$935 \quad \frac{h_k^{n+1} - h_k^n}{\Delta t_{3D}} + \partial_x (h_k u_k)^{n+1/2} + \partial_y (h_k v_k)^{n+1/2} + \left(w_{k+1/2}^{s,n+1/2} - w_{k-1/2}^{s,n+1/2} \right) = 0, \quad (50)$$

936

937 recovers (48) when vertically summed. Thus

$$938 \quad \sum_{k=1}^{k_{\max}} h_k^{n+1} \equiv \langle \eta \rangle^{n+1} + \langle H \rangle^{n+1} = \langle D \rangle^{n+1}, \quad (51a)$$

$$939 \quad \sum_{k=1}^{k_{\max}} [h_k u_k, h_k v_k]^{n+1/2} \equiv \langle \langle [D\bar{u}, D\bar{v}] \rangle \rangle^{n+1/2} \quad (51b)$$

$$940 \quad w_{k_{\max}+1/2}^{s,n+1/2} \equiv \langle \langle E - P \rangle \rangle^{n+1/2}. \quad (51c)$$

941

942 Compatibility condition (51b) can be obtained by shifting the velocity pro-
 943 files obtained from the baroclinic momentum equations (30) and (31). It
 944 should be noted again, that for tracer mass conservation the discrete tracer
 945 equations must recover (50) for constant tracers. Therefore, the shifting
 946 of velocity profiles must be done before the grid-related vertical velocity is
 947 diagnosed from (50) and the tracer equations are integrated. At the end of
 948 each internal timestep, the interaction-terms (44) can be updated in terms of
 949 $\langle \langle [D\bar{u}, D\bar{v}] \rangle \rangle^{n+1/2}$, $[h_k u_k, h_k v_k]^{n+1/2}$ and $F_{[x,y],k}^{\text{IP},n+1}$. Since these interaction-terms
 950 are held constant over the next external subcycle, integrating the barotropic
 951 transports from $(D\bar{u})^{n+1,0-1/2}$ to $(D\bar{u})^{n+1,M_{\max}-1/2}$, a time lag is introduced.

952 5.2. Drying and flooding

953 In many coastal areas intertidal flats are an important topographic fea-
 954 ture. During high water those areas are inundated and during ebb tide they
 955 may fall dry, approaching zero water depth $D \rightarrow 0$, but never becoming nega-
 956 tive. To understand how this is reflected in the mathematical formulations for

957 coastal ocean dynamics, it is instructive to reformulate the depth-integrated
 958 continuity equation (41a) into an advection equation for the water depth:

$$959 \quad \partial_t D + \bar{u} \partial_x D + \bar{v} \partial_y D = -(\partial_x \bar{u} + \partial_y \bar{v}) D - (E - P). \quad (52)$$

960 The conservative form (41a) shows that total water volume is conserved. The
 961 advective form (52) demonstrates positivity of the water depth, because its
 962 total derivative depends on a sink term which vanishes for decaying water
 963 depth. The divergence stays bounded, because for frictionally dominated
 964 regimes the depth-integrated momentum equations (41b) and (41c), and the
 965 quadratic bed friction (77) guarantee bounded depth-mean velocities. The
 966 evaporation E which reduces the water depth must be numerically treated
 967 such that it vanishes for vanishing water depth.

968 Various ways have been proposed in coastal ocean models to guarantee
 969 the two major properties (i) volume conservation (for incompressible flow)
 970 according to (41a) and (ii) positivity according to (52), also numerically.

971 It should be straight-forward to directly discretise one of the equations.
 972 Usually (41a) is used as a basis. In contrast, for a vertically integrated
 973 model, Stelling and Duinmeijer (2003) successfully applied a first-order up-
 974 stream scheme to discretise the advection equation (52), and later Zijlema
 975 et al. (2011) postulated that positivity could also be achieved using a Total
 976 Variation Diminishing (TVD) scheme with the MUSCL limiter (van Leer
 977 (1979)).

978 Given that the spatial discretisation is for a C-grid (section 4.3), and in
 979 order to conserve volume locally and globally, the transports $\bar{u}D$ and $\bar{v}D$ need
 980 to be identical to the sum of the layer-integrated transports used in (29).
 981 This consistency of local and global volume conservation is also essential
 982 for the conservation of momentum and tracers. Therefore, a numerical re-
 983 calculation of $\bar{u}D$ and $\bar{v}D$ in (41a) would require a correction to the layer-
 984 integrated transports calculated prognostically in (30) and (31). This is
 985 the general principle of conservative drying and flooding: to manipulate the
 986 layer-integrated momentum equations in a physically sound and reasonable
 987 way, and to use the same transports in (41a).

988 There are various approaches to this, all of them leaving a thin film
 989 of water in dry cells, where the dynamics is manipulated in some way to
 990 avoid zero or negative water depth. In early coastal ocean models (Flather
 991 and Heaps, 1975; Backhaus, 1976, 1985; Jungclaus and Backhaus, 1994), a
 992 number of rules were defined on how to reduce fluxes out of a grid cell when

993 the application of these fluxes would lead to negative water depth (or the
 994 undercut of a prescribed minimum water depth). Also the wetting and drying
 995 schemes of Oey (2005) and Warner et al. (2013) are based on this principle.
 996 The method works reliably, but to guarantee positive water depth, it has to
 997 be taken into account that reduction or shut-off of fluxes around one grid cell
 998 would change the net fluxes into the neighboring cells, such that an iterative
 999 procedure might become necessary. This problem has been partially solved
 1000 by Warner et al. (2013), by shutting off all transports around a cell when the
 1001 water depth at the old time step is below the critical depth, see also Defne and
 1002 Ganju (2015) who simulated a large lagoonal back-barrier estuary at the US
 1003 east coast including extensive intertidal flats. Moreover, the direct correction
 1004 of fluxes might in some models lead to spatially and temporally oscillating
 1005 patterns of dry and wet cells. Furthermore, shutting on and off transports
 1006 instantaneously could lead to complications in turbulence closure models,
 1007 since the bed stress which largely determines the eddy viscosity profiles (via
 1008 the turbulent kinetic energy and the macro length scale of turbulence, see
 1009 section 3.2.1) would be suddenly switched on or shut off regularly.

1010 In some models (e.g., Casulli and Cattani, 1994) the water depth at the
 1011 transport points of a C-grid is chosen as the minimum depth between the
 1012 adjacent pressure points, with the consequence that velocities feel the shallow
 1013 water and bed friction strongly reduces the volume transport. This however
 1014 might lead to significantly delayed drying and flooding processes (Burchard
 1015 and Bolding, 2002).

1016 In order to avoid explicit switching on or off of transports in drying cells,
 1017 Burchard et al. (2004) (see also Burchard and Bolding, 2002) proposed the
 1018 following measures when calculating the layer-integrated momentum equa-
 1019 tions:

- 1020 • A critical water depth D_{crit} , and a minimum water depth, D_{min} are
 1021 defined with $D_{\text{crit}} > D_{\text{min}}$ (see fig. 3). Typical values would be $D_{\text{crit}} =$
 1022 0.2 m and $D_{\text{min}} = 0.05 \text{ m}$. To simplify the dynamics in very shallow
 1023 water with $D < D_{\text{crit}}$, many terms in the layer-integrated momentum
 1024 equations are reduced by a factor linearly decreasing between 1 (for
 1025 $D = D_{\text{crit}}$) and 0 (for $D = D_{\text{min}}$), which basically reduces the local
 1026 dynamics to an external pressure gradient - friction balance. Such a
 1027 balance supports reduction of local transports, since the friction coeffi-
 1028 cient calculated from the law of the wall in the lowest grid box increases
 1029 towards infinity for the water depth converging towards zero, see equa-

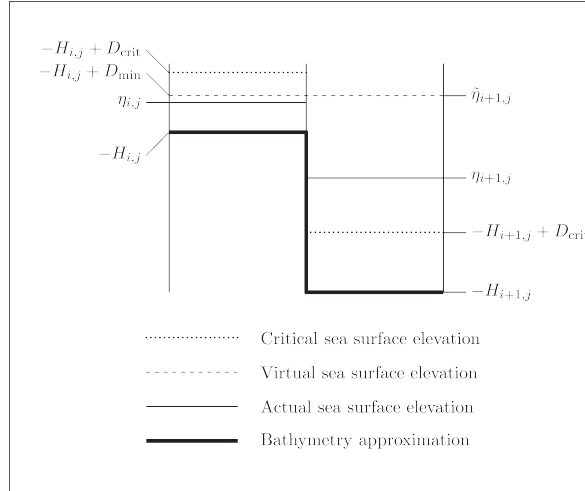


Figure 3: Sketch explaining the geometry of bathymetry and surface elevation approximations as it is defined in GETM. This figure has been modified from Burchard et al. (2004).

1030 tion (76).

- 1031 • Additionally, when the surface elevation in one grid box is below the
- 1032 bottom coordinate plus the minimum depth in any adjacent cell (which
- 1033 often happens at steep bathymetry in shallow water and relatively
- 1034 coarse horizontal resolution, see fig. 3, where $\eta_{i+1,j} < -H_{i,j} + D_{\min}$), a
- 1035 virtual surface elevation is defined from which the external pressure gra-
- 1036 dient ($\partial_x \eta, \partial_y \eta$) is calculated. In that case, $\tilde{\eta}_{i+1,j} = \max\{\eta_{i+1,j}, -H_{i,j} +$
- 1037 $D_{\min}\}$, and the surface elevation gradient is calculated as $(\tilde{\eta}_{i+1,j} -$
- 1038 $\eta_{i,j})/\Delta x$. In the extreme case shown in fig. 3 water volume would ac-
- 1039 tually flow against the elevation gradient, because $\eta_{i,j} < -H_{i,j} + D_{\min}$.

- 1040 • Despite the above measures, direct reduction or shut-off of transports
- 1041 surrounding a grid cell may still be necessary at singular locations. To
- 1042 stabilise the drying and flooding algorithm, increasing the minimum
- 1043 and critical water depth is often a preferred option.

1044 Using these algorithms Gräwe et al. (2016) could carry out a stable and multi-

1045 annual simulation of the entire Wadden Sea of the South-Eastern North Sea

1046 at a horizontal resolution of 200 m.

1047 6. Treatment of open boundary conditions and model nesting

1048 Coastal ocean models focus on limited areas of interest and thus data are
1049 needed to force the models at open boundaries, see Section 2.5. The data can
1050 typically come from an external source (e.g. climatology, coarser resolution
1051 run on a wider domain) following a one-way (coarse \rightarrow fine) approach. In
1052 comparison, in a two-way approach, the external data (a numerical model)
1053 feel the local coastal solution through a feedback term. Local and external
1054 models generally differ on several key points among them grid resolution (in
1055 space and time) and physics. Across the interface, inflow and outflow can
1056 occur. In the case of inflow conditions, the quality of the local solution is
1057 strongly dependent on the quality of external data while in the case of out-
1058 flow, the main issue is to prevent wave reflection at the interface. A two-way
1059 approach helps in maintaining some consistency between local and external
1060 solutions, at least when the physics of the two models are close. In both one-
1061 way and two-way approaches, the design of the boundary conditions must be
1062 carefully done. Due to the complexity of the physics, the scale heterogene-
1063 ity in space and time, ideal boundary conditions are not achievable and a
1064 reasonable choice relies on a compromise between accuracy and robustness.
1065 Section (6.1) briefly introduces the general framework. Section (6.2) treats
1066 the problem of model forcing in a one-way approach (open boundary condi-
1067 tions). Section (6.3) introduces two-way approaches. Some considerations
1068 on discrete approximations are given in Section (6.4).

1069 6.1. General framework

1070 We consider a domain Ω_{loc} embedded in a domain Ω_{ext} as shown in Figure
1071 4. The local and external solutions, ϕ_{loc} and ϕ_{ext} , are integrated according
1072 to

$$\partial_t \phi_{\text{loc}} + L_{\text{loc}}(\phi_{\text{loc}}) = f_{\text{loc}} \text{ in } \Omega_{\text{loc}}, \quad \partial_t \phi_{\text{ext}} + L_{\text{ext}}(\phi_{\text{ext}}) = f_{\text{ext}} \text{ in } \Omega_{\text{ext}}.$$

1073 L_{loc} and L_{ext} are spatial differential operators, f_{loc} and f_{ext} model forcings.
1074 ϕ is the vector of prognostic state variables. The models interact through a
1075 transition area Γ that, depending on the boundary conditions, may be re-
1076 stricted to a single interface γ .

1077 Let Δx_{loc} and Δx_{ext} (resp. Δt_{loc} and Δt_{ext}) be the grid (resp. time) steps on
1078 Ω_{loc} and Ω_{ext} . Today, the availability of global/regional operational or reanal-
1079 ysis products allows to consider the case where typical values of time/grid

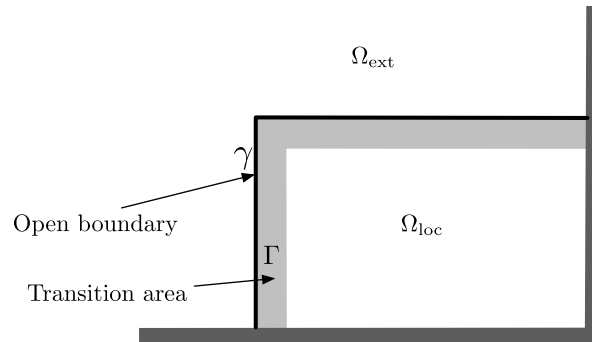


Figure 4: The local domain Ω_{loc} embedded in the exterior domain Ω_{ext} . Ω_{loc} has an artificial interface γ and possibly a transition area Γ on which boundary conditions are prescribed.

1080 steps obey:

$$\frac{\Delta x_{\text{ext}}}{\Delta x_{\text{loc}}} \approx \frac{\Delta t_{\text{ext}}}{\Delta t_{\text{loc}}} \approx 2 - 10.$$

1081 The model interactions across the interface γ and/or within the transition
 1082 area Γ are described in the next Sections.

1083 6.2. Open boundary conditions (OBC) and one-way interaction

1084 We start with a description of the two main classes of OBC methods:
 1085 relaxation methods which aim to relax the local solution towards the ex-
 1086 ternal solution within the transition area Γ and radiation methods which
 1087 propagate out the information to prevent waves reflection. Simple radiation
 1088 methods are appropriate only for a wave equation, the extension to general
 1089 hyperbolic systems using a characteristic variables approach is explained in
 1090 (6.2.2). Advanced open boundary conditions like Perfectly Matched Layer
 1091 (PML) and Absorbing Boundary Conditions (ABC) (see Nataf, 2013) will
 1092 not be discussed here since their derivations require very simplified problems
 1093 and they have still to be validated in realistic applications. In (6.2.4), we dis-
 1094 cuss the specificities of local mesh refinement when the local computational
 1095 grid is nested within a coarser resolution grid and also mention the impact

1096 of variabilities at interfaces. For a review of open boundary conditions, the
 1097 reader is referred to Palma and Matano (2000); Blayo and Debreu (2005).

1098 *6.2.1. Relaxation and radiation methods:*

1099 *Relaxation methods.* Basic Dirichlet (a.k.a. clamped) boundary conditions
 1100 do not perform well (except for certain basic equations): this abrupt forcing
 1101 generates inconsistencies and discontinuities near the interface γ . The flow
 1102 relaxation scheme (FRS) (Davies, 1976) relaxes the interior solution towards
 1103 external data in the transition area Γ near the boundary and can be written
 1104 under the following relaxation (or nudging) form (Martinsen and Engedahl,
 1105 1987) (considering ϕ as a scalar variable and omitting the model forcing):

$$\partial_t \phi_{\text{loc}} + L_{\text{loc}}(\phi_{\text{loc}}) = -\frac{1}{\tau}(\phi_{\text{loc}} - \phi_{\text{ext}}) \quad \text{in } \Omega_{\text{loc}}, \quad (53)$$

1106 The right hand side of (53) is the relaxation term. τ is a relaxation time
 1107 scale. $\lambda = \frac{1}{\tau}$ is a positive function, which decreases away from the lateral
 1108 boundary γ and vanishes outside of Γ . At the discrete level, the right hand
 1109 side of (53) can be solved implicitly to remove associated stability constraints.
 1110 It is difficult to prescribe the size of the transition area Γ and the variation
 1111 of λ within Γ , since they depend on the space and time scales of the phe-
 1112 nomena (Källberg, 1977). Typical profiles of λ are based on quadratically or
 1113 exponentially decreasing functions of the distance to the boundary γ .

1114 Due to the smallness of the coastal model domain, it may also happen
 1115 that the large scales of the solution are better reproduced in the external
 1116 domain Ω_{ext} . It is particularly the case when the external model makes use
 1117 of data assimilation techniques (reanalysis product or operational forecast).
 1118 In this situation, there is a potential benefit to relax the large scales of the
 1119 local solution to the ones computed by the external model while the small
 1120 scales features are still governed by the coastal model evolution. To this aim,
 1121 spectral nudging methods (Waldron et al., 1996) can be viewed as a FRS
 1122 scheme which acts on the whole local domain on specified (large) scales. It
 1123 can be written under the following form:

$$\partial_t \phi_{\text{loc}} + L_{\text{loc}}(\phi_{\text{loc}}) + \Lambda(\phi_{\text{loc}} - \phi_{\text{ext}}) = 0 \quad \text{in } \Omega_{\text{loc}}, \quad (54)$$

1124 where the operator Λ is now a low pass filter acting on the whole Ω_{loc} domain.
 1125 The expression of Λ may be based on Fourier transform of $(\phi_{\text{loc}}, \phi_{\text{ext}})$ (with
 1126 relaxation coefficients fixed in the Fourier space), on Gaussian correlation

1127 kernels and more simply on iterative Laplacian smoothing. When applied to
 1128 coastal modelling, the nudging term is usually reduced near the coast where
 1129 the external model may have a coarser representation of the coastline.

1130 Finally, most of the time, the FRS scheme is associated to a sponge
 1131 layer that damps the small scales near the boundary using increased viscos-
 1132 ity/diffusivity ν :

$$\partial_t \phi_{\text{loc}} + L_{\text{loc}}(\phi_{\text{loc}}) = -\frac{1}{\tau}(\phi_{\text{loc}} - \phi_{\text{ext}}) + \nu_{\Gamma} \Delta \phi_{\text{loc}} \quad \text{in } \Omega_{\text{loc}}. \quad (55)$$

1133 *Radiation methods.* In the case of outflow conditions, the FRS scheme will
 1134 only behave well (and in particular will prevent waves reflection) when the
 1135 external data is already an accurate representation of the solution. In other
 1136 cases, radiation methods can be used to propagate out the disturbances. The
 1137 basic radiation methods solve the Sommerfeld radiation condition (56) at the
 1138 interface,

$$\partial_t \phi_{\text{loc}} + c \partial_n \phi_{\text{loc}} = 0 \quad \text{on } \gamma, \quad (56)$$

1139 and corresponds to the transport of ϕ through γ at the phase speed projected
 1140 to the boundary, c (∂_n denotes a derivative perpendicular to and towards the
 1141 outside of the boundary). Obviously this boundary condition is only ex-
 1142 act for a wave propagation problem and when c is known. In practice, c
 1143 ($= -\partial_t \phi_{\text{loc}} (\partial_n \phi_{\text{loc}})^{-1}$) is estimated at the discrete level using internal values
 1144 (Orlanski, 1976), leading to different implementations, including, in two di-
 1145 mensions, variants taking into account tangential derivatives (Raymond and
 1146 Kuo, 1984). Besides the evaluation of the phase speed c , the relevancy of this
 1147 type of boundary condition for non-monochromatic and/or dispersive waves
 1148 is questionable.

1149 The radiation condition is valid only for outflow conditions (e.g. $c > 0$ at an
 1150 eastern boundary). In other cases, relaxation methods as described in the
 1151 previous paragraph are more appropriate. Radiation and relaxation methods
 1152 can be combined to give:

$$\partial_t \phi_{\text{loc}} + c \partial_n \phi_{\text{loc}} = -\frac{\phi_{\text{loc}} - \phi_{\text{ext}}}{\tau_{\gamma}} \quad \text{on } \gamma. \quad (57)$$

1153 where τ_{γ} , the relaxation time scale, has different values $\tau_{\text{in}}, \tau_{\text{out}}$ according to
 1154 inflow ($\tau_{\gamma} = \tau_{\text{in}}$) or outflow ($\tau_{\gamma} = \tau_{\text{out}}$) conditions (Marchesiello et al., 2001).
 1155 During inflow conditions c is set to zero and τ_{in} is small leading to a strong
 1156 relaxation towards external solution. τ_{out} is large but not infinity in order to

1157 prevent the internal solution to drift for external data. Note that even if (57)
 1158 is written at the interface γ , it is most of the time associated to a relaxation
 1159 term active on the whole transition area Γ . For consistency, the boundary
 1160 value of the relaxation time scale τ defined in (53) should be greater than
 1161 τ_{out} .

1162 6.2.2. Characteristic methods

1163 As mentioned previously, radiation methods are only valid when the tem-
 1164 poral evolution of the state variable is governed by a wave equation. They
 1165 can be extended to more general cases by looking at the hyperbolic parts
 1166 of the equations. By definition hyperbolic systems can be decomposed into
 1167 a series of wave propagation problems whose solutions are the characteristic
 1168 variables. The problem is then well posed if the incoming characteristics vari-
 1169 able are specified and the outgoing characteristic extrapolated from internal
 1170 values (Blayo and Debreu, 2005).

1171 Considering a one-dimensional version of the linearised barotropic equation
 1172 (45)

$$\partial_t \eta = -H \partial_x \bar{u}, \quad \partial_t \bar{u} = -g \partial_x \eta,$$

1173 the two characteristics are given by

$$w_{\pm} = \bar{u} \pm \sqrt{\frac{g}{H}} \eta$$

1174 and propagate with speeds $c_{\pm} = \pm \sqrt{gH}$ (i.e. $\partial_t w_{\pm} + c_{\pm} \partial_x w_{\pm} = 0$). At
 1175 open boundaries, the incoming characteristics are prescribed ($w_{\text{loc}} = w_{\text{ext}}$)
 1176 and the outgoing characteristic are computed from internal values. The com-
 1177 putation of outgoing characteristic variables at the boundary can be based
 1178 on simple extrapolation techniques or on the application of upwind biased
 1179 schemes. It is well known that the specification of the incoming characteris-
 1180 tics of the barotropic equations is equivalent to the Flather boundary condi-
 1181 tion (Flather, 1976) (which can also be obtained by a Sommerfeld radiation
 1182 condition for \bar{u} , with $c = \sqrt{gH}$, and a 1D version of the continuity equa-
 1183 tion). At an eastern boundary where $w_- = \bar{u} - \sqrt{\frac{g}{H}} \eta$ must be prescribed,
 1184 the Flather boundary condition reads

$$\bar{u} = \bar{u}_{\text{ext}} + \sqrt{\frac{g}{H}} (\eta - \eta_{\text{ext}}) \quad (58)$$

1185 and where η is given by another boundary condition (e.g. $\partial_x \eta = 0$).
 1186 The use of the full characteristic method gives instead:

$$\bar{u} = \frac{1}{2} (w_{+, \text{int}} + w_{-, \text{ext}}) = \frac{1}{2} (\bar{u}_{\text{ext}} + \bar{u}_{\text{int}}) + \frac{1}{2} \sqrt{\frac{g}{H}} (\eta_{\text{int}} - \eta_{\text{ext}}) \quad (59)$$

1187 and

$$\eta = \frac{1}{2} \sqrt{\frac{H}{g}} (w_{+, \text{int}} - w_{-, \text{ext}}) = \frac{1}{2} (\eta_{\text{ext}} + \eta_{\text{int}}) + \frac{1}{2} \sqrt{\frac{H}{g}} (\bar{u}_{\text{int}} - \bar{u}_{\text{ext}}), \quad (60)$$

1188 where $w_{+, \text{int}} = \bar{u}_{\text{int}} + \sqrt{\frac{g}{H}} \eta_{\text{int}}$ is computed from internal values. The Flather
 1189 type boundary condition (58), or some of its variants, is used in most of
 1190 the coastal ocean models where it is assumed that surface gravity waves are
 1191 indeed dominant for the specification of the boundary conditions. If \bar{u}_{ext}
 1192 is not known but only η_{ext} (e.g. tidal conditions), a reduced model (e.g.
 1193 geostrophic balance) may be used to deduce \bar{u}_{ext} .

1194 6.2.3. 3D models

1195 The 3D primitive equation models support the propagation of internal
 1196 gravity waves whose characteristics can be obtained through a vertical nor-
 1197 mal mode decomposition. Setting 3D boundary conditions on the original
 1198 state variables without taking into account these propagations renders the
 1199 problem ill-posed (Oliger and Sundström, 1978). A remedy can be to add
 1200 a small vertical viscosity in the hydrostatic balance equations (7) (Témam
 1201 and Tribbia, 2003). Characteristics-based methods can formally be extended
 1202 to 3D-based on a vertical mode decomposition (Jensen, 1998; Blayo and De-
 1203 breu, 2005) resulting into a series of shallow water models. However the
 1204 number of assumptions used in their derivations (in particular the linearisa-
 1205 tion around an horizontally constant background density field and a constant
 1206 background state velocity field, typically the barotropic solution) make them
 1207 difficult to apply in practice. In addition, the staggering of the grid variables
 1208 on an Arakawa C-grid add some difficulties to the discrete implementation
 1209 of a combination of variables at different grid locations, thus introducing a
 1210 number of additional assumptions. That is why, in 3D primitive equation
 1211 models, the preceding relaxation/radiation boundary conditions are usually
 1212 applied on each of the prognostic variables ($\eta, \bar{u}, \bar{v}, u, v, T, S$), with a Flather-
 1213 like boundary condition for the barotropic part.

1214 *6.2.4. Local mesh refinement (one-way nesting)*

1215 One-way nested models can use any of the preceding boundary condi-
1216 tions with parameters adjusted according to the space and time refinement
1217 factors which are here assumed to be relatively small. One-way nesting may
1218 be performed online (Penven et al., 2006) or offline (Mason et al., 2010). The
1219 key element for a choice between these two approaches is the spatio-temporal
1220 variability of the boundary conditions. When this variability is high, online
1221 nesting, with high frequency / high resolution exchanges between local and
1222 external domains, is more efficient. Indeed storage and performance issues
1223 limit the frequency/resolution of the outputs made during the coarse reso-
1224 lution run. However in an offline approach, the obvious advantage is that
1225 the area covered by the local (high resolution) domain does not have to be
1226 known in advance, i.e. before running the external (coarse resolution) model.

1227 *6.3. Two-way interaction*

1228 We consider now a two-way interaction between the external and local
1229 models. The external model feels the local model by a feedback of the local
1230 solution. We differentiate between traditional two-way nesting algorithms
1231 where the local domain corresponds to a local grid refinement of the external
1232 domain and more general two-way coupling algorithms.

1233 We will not detail here the interpolation/update operators between the two
1234 models. The reader is referred to Debreu and Blayo (2008) for their design,
1235 in particular in terms of scale selectivity and conservation.

1236 *6.3.1. Two-way nesting*

1237 Two-way nesting algorithms have been reviewed in Debreu and Blayo
1238 (2008). In this paragraph, we describe strongly coupled models which even-
1239 tually can be viewed as a single model with an abrupt change of resolution
1240 at the high/coarse resolution grids interface γ .

1241 *Grid interactions.* In two-way nesting applications, the feedback from the
1242 high to the coarse resolution grid prevents the two solutions to drift. In the
1243 limit of equal local and external grid resolutions ($L_{\text{ext}} = L_{\text{loc}}$) the original
1244 solution (without nesting) should be recovered. This implies a strong cri-
1245 terion on the forcing of the local model: the boundary conditions have to
1246 act on the difference between external and local solutions. We will call this
1247 a consistency condition. Typically, the sponge layer in (55) should now be
1248 written

$$\partial_t \phi_{\text{loc}} + \dots = \nu_{\Gamma} \Delta(\phi_{\text{loc}} - \phi_{\text{ext}}) \quad \text{in } \Omega_{\text{loc}}, \quad (61)$$

1249 and if radiation conditions are used, (57) should be replaced by:

$$\partial_t(\phi_{\text{loc}} - \phi_{\text{ext}}) + c \partial_n(\phi_{\text{loc}} - \phi_{\text{ext}}) = -\frac{\phi_{\text{loc}} - \phi_{\text{ext}}}{\tau}. \quad (62)$$

1250 In a sense, in these equations, the temporal and spatial scales of the external
1251 solutions are not assumed to be much more larger than those of the local
1252 domain so that the simplification occurring in (55) and (57) cannot be made.
1253 Condition (62) was used in Perkins et al. (1997).

1254 *Elliptic systems and/or time splitting.* The discrete versions of L_{ext} and L_{loc}
1255 may involve the solution of an elliptic system. This occurs for example when
1256 an implicit treatment of the surface gravity waves is applied, see Section
1257 (5.1.1), or if a nonhydrostatic kernel is involved (leading to the solution
1258 of a Poisson system), see Section 8.2. In that case, special care must be
1259 taken in order to get to correct solution (i.e. continuity of the solution and
1260 its derivatives). For being properly treated, the implicit solver has to be
1261 transformed into a multi-resolution solver which includes the grid interactions
1262 (e.g., paragraph 2.2.1 of Debreu and Blayo (2008) and Haley and Lermusiaux
1263 (2010); Cailleau et al. (2008)).

1264 Similarly, when an explicit mode splitting scheme is employed (see Section
1265 5.1), the models should be coupled at the barotropic time step instead of at
1266 the baroclinic time step (Debreu et al., 2012). This also allows to satisfy the
1267 consistency condition previously mentioned.

1268 *Vertical refinement.* Most of the current two-way nested models apply only
1269 horizontal mesh refinements. Local vertical refinements (e.g. increase of res-
1270 olution in surface and/or bottom boundary layers) are difficult to manage
1271 for several reasons. Vertical parameterizations (see Section 3.2.1) involve im-
1272 plicit solvers due to stability constraints and, so, as for horizontal implicit
1273 solvers (paragraph above) are more difficult to tackle on multiresolution grids.
1274 Coupling between barotropic and baroclinic modes (see Section 5.1) can also
1275 become cumbersome if only part of the water column is computed on the
1276 fine grid. Instead of a local vertical mesh refinement, a local change of verti-
1277 cal coordinate systems is achievable. In coastal applications, the capacity to
1278 change locally the vertical coordinate systems (4.2) can become crucial for
1279 some applications. Indeed, mesh refinement along coastal areas with very
1280 small water depths may require some local adaptation of the parameters of

1281 the vertical coordinate systems (parameters of the terrain-following coordi-
1282 nates, number of layers, ...). In that case, vertical remapping has to be
1283 applied between coarse and fine grids.

1284 *Time refinement.* In traditional applications, horizontal mesh refinement is
1285 most of the time coupled with time refinement in order to satisfy stability
1286 conditions. If the main stability constraint is given by external gravity waves
1287 propagation (cf 5.1), at a velocity of \sqrt{gH} , we may expect that, when refining
1288 the grid near the coast and so with smaller depths, the time step does not have
1289 to be reduced. This is certainly the case for some applications, but generally
1290 having the possibility to refine the time steps may become important when
1291 the actual time step is constrained by other phenomena (e.g. drying and
1292 flooding, advection ...).

1293 *6.3.2. Two-way coupling*

1294 Less strong local/external coupling may also be of interest, particularly
1295 when the space and time refinement factors are large and/or if the models
1296 L_{ext} and L_{loc} have different physics. In that case, two-way relaxation methods
1297 may also be of interest. The spectral nudging method introduced in Section
1298 6.2.1 can be extended to two-way interactions. The smooth semi-prognostic
1299 method (Sheng et al., 2005) is an example of such a technique. More gen-
1300 erally, grids interactions can be (weakly) incorporated in any assimilation
1301 scheme coupling at the same time the assimilation of observations and the
1302 grid interactions.

1303 *6.4. Discrete point of view*

1304 In addition to the preceding continuous formulations, a number of ques-
1305 tions arise when taking into account the model discretisations.

1306 *6.4.1. Implementation of boundary conditions*

1307 We already mentioned the discretisation of the Sommerfeld radiation con-
1308 dition, including the sensitivity to the computation of the normal wave speed
1309 in 2D. The discrete implementation of boundary conditions has to deal with
1310 the time stepping algorithm and the grid staggering. As an example, Mason
1311 et al. (2010) proposed a stable implementation of a 2D characteristic method
1312 for the barotropic equations on a staggered C -grid. This paper introduces a
1313 stable treatment of the outgoing characteristics (computation of \bar{u}_{int} and η_{int}
1314 in (59)).

1315 *6.4.2. Link with internal numerical schemes*

1316 More generally, the problem of open boundary conditions and model
1317 nesting is also fundamentally tied to the discrete internal schemes (e.g. im-
1318 plicit/explicit treatment, time integration scheme, discrete conservation prop-
1319 erties, diffusive terms). All these aspects interact with an efficient implemen-
1320 tation of the boundary conditions. The trivial example is the use of a first-
1321 order upwind biased scheme for a simple advection equation: the original
1322 equation $\partial_t\phi + c\partial_x\phi = 0$ is hyperbolic and thus requires only one boundary
1323 condition at inflow, otherwise over-specification occurs. However, the modi-
1324 fied equation (i.e. including spatial truncation errors) is of parabolic nature

1325 $\partial_t\phi + c\partial_x\phi = \mu\partial_{xx}\phi + \mathcal{O}(\Delta x)^2$, $\mu = c \frac{\Delta x}{2}$ and allows for the specification of
1326 boundary conditions both at inflow and outflow boundaries. Indeed, in prac-
1327 tice the numerical scheme will naturally take into account only external data
1328 at inflow. Similarly if a dispersive scheme is used to discretise the spatial
1329 derivative (e.g. second-order centered), radiation methods will not perform
1330 well even in the monochromatic wave case. This makes the derivation of a
1331 very general OBC difficult and may also explain why some boundary condi-
1332 tions work for some models and not for others.

1333 A promising approach concerning the derivation of boundary conditions is
1334 the summation-by-parts approach (Svärd and Nordström, 2014) that can
1335 make the link between internal schemes and boundary conditions (possibly
1336 weekly imposed) according to a discrete energy estimate.

1337 *Sanity control.* At the discrete level, some basic sanity controls can be made.
1338 This is particularly important for one- and/or two-way nesting. The consis-
1339 tency condition has been mentioned previously: assuming that the same
1340 numerical/physical choices are made for the local and external solution, a
1341 simulation with spatial and temporal refinement equal to one should lead
1342 to the same solution with or without nesting. This has several implications
1343 on the formulation of the boundary conditions, the choice of the number of
1344 ghost cells and the treatment of barotropic/baroclinic coupling.

1345 The second sanity control is to verify the constancy preservation (see Sec-
1346 tion 7.1): in absence of sinks and sources, if a tracer is globally initialised to
1347 a constant value, the tracer should remain constant on both grid and with
1348 the same value. This has again several implications on the way interpola-
1349 tion/update schemes are constructed and the consistency of barotropic and
1350 baroclinic exchanges.

1351 **7. Numerical treatment of single terms and processes**

1352 This section discusses discrete algorithms that are commonly used for
1353 the solution of the governing equations formulated in Sec. 3 and 4. Origini-
1354 nally, coastal ocean models were discretised using numerical methods loosely
1355 inherited from large scale ocean models, namely second-order in space and
1356 Leapfrog-in-time schemes (Blumberg and Mellor, 1987). However, over the
1357 years, the numerics of those models have evolved toward the use of more
1358 advanced discretisation techniques, more similar to techniques used in other
1359 fields of computational fluid dynamics, in order to accommodate to the spe-
1360 cific constraints of coastal applications. Indeed, as discussed in Sec. 2, coastal
1361 ocean dynamics is characterised by strong vertical and horizontal gradients,
1362 long waves, rapid variations on short time and spatial scales as well as large
1363 dissipation and velocities near the bottom which all require specific numeri-
1364 cal treatments. The diversity of methods in use in coastal models is large
1365 so that the discussion can only focus on techniques which are more widely
1366 used or are expected to become more widely used. Since the numerical re-
1367 quirements for each process can be rather different, this section considers
1368 separately sub-systems of the full system of primitive equations. However,
1369 it should not overshadow the fact that a numerical kernel must be designed
1370 as a whole, not just as an advection or a wave propagation equation since
1371 interferences between numerical methods used for different processes exist.

1372 There often exists some confusion to properly characterise the class of dis-
1373 cretisation techniques used in state-of-the-art oceanic coastal models. Since
1374 there are significant differences in truncation error between finite-difference
1375 and finite-volume advection-diffusion schemes (e.g. Leonard, 1995), clarifica-
1376 tions are needed. As far as the tracer conservation is concerned, it is obvious
1377 that they must be interpreted in a finite-volume sense, meaning that for a
1378 given tracer q the discrete quantity $q_{i,j,k}$ is the average over a control vol-
1379 ume $\mathcal{V}_{i,j,k}$ (Fig. 2). For the momentum equations, the generally adopted
1380 formulation is inherited from Lilly (1965) who introduced a discretisation
1381 approach which has the property to conserve energy in a discrete sense as
1382 long as second-order centered schemes are used. Momentum advection terms
1383 in Lilly (1965) can be viewed as a finite-volume discretisations provided that
1384 proper horizontal metric terms are added. However, not every term in the
1385 momentum equation can be cast in a flux divergence form (e.g. Coriolis term,
1386 curvilinear metric terms). For those terms momentum components should
1387 be interpreted in a finite-different sense. Note that the fact that tracer values

1388 are cell-averaged implies that the pressure deduced from the hydrostatic rela-
 1389 tion is a point-wise value located on cell interfaces in the vertical. Generally
 1390 speaking, discretisation techniques in most existing structured-grid oceanic
 1391 coastal models can be classified as finite volume discretisations. The arrange-
 1392 ment on the computational grid is shown in Fig. 2. We now give more details
 1393 on the specifics of different terms.

1394 *7.1. Tracer and momentum advection*

1395 We consider here the advection equation written in a conservative way
 1396 for a layer-averaged quantity q_k (q can either represent a tracer or horizontal
 1397 momentum components when a flux-form of nonlinear terms is used) along
 1398 with the continuity equation (29)

$$\begin{aligned} \partial_t(h_k q_k) + \partial_x(h_k u_k q_k) + \partial_y(h_k v_k q_k) + \delta_k(w^s q) &= 0, \\ \partial_t h_k + \partial_x(h_k u_k) + \partial_y(h_k v_k) + \delta_k(w^s) &= 0, \end{aligned} \tag{63}$$

1400 using the notations introduced in Sec. 4 and the definition of a vertical differ-
 1401 ence located at the centre of the cell k , $\delta_k(a) = a_{k+1/2} - a_{k-1/2}$ for any quantity
 1402 a . We retain the continuity equation here to emphasise that the advection
 1403 equation must be conservative while satisfying a constancy preservation prop-
 1404 erty (i.e. if q is initialised with a constant, it remains so). An overview of the
 1405 time and space discretisations of (63) used in large and mesoscales oceanic
 1406 models can be found in Lemarié et al. (2015). Broadly speaking, it is well
 1407 known that classical even-ordered linear advection schemes tend to produce
 1408 unphysical oscillations which can be controlled by an explicit scale-selective
 1409 dissipation whose coefficients A_M and A_c must be tuned to ensure no build-
 1410 up of grid scale noise. On the contrary, odd-ordered linear advection schemes
 1411 are inherently dissipative near the grid-scale (e.g. App. B in Soufflet et al.,
 1412 2016), but are not oscillation free with the exception of the first-order upwind
 1413 scheme which can not, however, be considered seriously due to its unaccept-
 1414 able artificial diffusion. The linear compact implicit schemes (Lele, 1992)
 1415 are a very attractive alternative but they require a matrix inversion which
 1416 makes them tractable for vertical advection only. Note that an important
 1417 constraint on the vertical advection is that the oceanic interior vertical mixing
 1418 is exceptionally weak so that upwind schemes in models with quasi-Eulerian
 1419 vertical coordinate or dissipative remapping schemes in models with an ALE
 1420 coordinate (see section 4.2) must be avoided.

1421 *7.1.1. Design of numerical models*

1422 In practice, several strategies coexist in the coastal community. A first
1423 choice is to consider simple second-order centered schemes supplemented by
1424 an explicit diffusion and a non-dissipative time-stepping algorithm in order
1425 to ensure energy consistency of the whole code at a discrete level (Marsaleix
1426 et al., 2008). A second choice is to rely exclusively on standard high-order
1427 upwind schemes in the horizontal direction and low-dispersive centered ad-
1428 vection schemes in the vertical (e.g. fourth-order compact schemes), without
1429 any explicit dissipation, combined with a high-order predictor-corrector time-
1430 stepping algorithm using a method of lines (e.g. Shchepetkin and McWilliams,
1431 2005). In this case, it is accepted that strong gradients will generate over-
1432 shoots and undershoots and that there is an uncontrolled sink of kinetic en-
1433 ergy and tracer variance in the model caused by dissipative truncation errors.
1434 This last point is, however, generally not worrisome as long as a first-order
1435 upwind scheme is avoided. As an alternative to the method of lines, where
1436 space and time discretisations are considered separately, a coupled space-time
1437 approach¹ could be used for advective terms (e.g. Hundsdorfer and Trompert,
1438 1994; Daru and Tenaud, 2004). This type of approach can be viewed as a
1439 conservative semi-Lagrangian approach where the characteristics are tracked
1440 in space-time. The resulting schemes are one-step schemes with interfacial
1441 fluxes depending on the local Courant number $\alpha^x = u_k \Delta t / \Delta x$. They have
1442 the property to be free of computational mode, exact for a Courant number
1443 $\alpha^x = 1$, and to be easily extended to arbitrary high-order of accuracy (e.g.
1444 Daru and Tenaud, 2004). Examples of such schemes are the first-order up-
1445 wind scheme, the Lax-Wendroff scheme or the QUICKEST scheme which are
1446 respectively first, second and third order accurate in space and time. What-
1447 ever the strategy used (uncoupled or coupled space and time), it is generally
1448 preferable to prevent spurious numerical oscillations by using non-oscillatory
1449 schemes which are more computationally demanding but provide a way to
1450 ensure nonlinear stability. Since non-oscillatory schemes are expected to be
1451 increasingly used to simulate coastal flows, we provide additional comments
1452 on this point to highlight the associated delicacies.

¹The coupled space and time approach is also known in the literature as flux-form semi-Lagrangian approach, as well as transient interpolation method, or direct space-time discretisation.

1453 *7.1.2. Nonlinear stability and flux correcting/limiting methods*

1454 Numerical methods with an order of accuracy larger than one are prone to
1455 numerical oscillations. A nonlinear stability criteria often considered is that
1456 the numerical solution must not oscillate without bounds. Using the notion
1457 of total variation (TV) as a measure of the overall amount of oscillations, nu-
1458 merical schemes have been constructed to ensure that the total variation is ei-
1459 ther bounded (TVB) or diminishing (TVD) (Harten, 1983; Shu, 1987). Since
1460 TVD schemes necessarily degenerate to first order accuracy near smooth ex-
1461 trema, they are prone to clipping errors manifested by the appearance of a
1462 flat plateau in the solution due to an excess of diffusion. To avoid this type of
1463 error, a less stringent constraint is the monotonicity-preservation (MP) which
1464 relaxes the TVD constraint near extrema (e.g. Suresh and Huynh, 1997; Daru
1465 and Tenaud, 2004). Flux correcting/limiting is generally used to impose the
1466 TVD, TVB or MP stability conditions (e.g. Durran, 2010). Historically,
1467 the flux limiting/correcting methods were derived in a coupled space and
1468 time framework using the second-order Lax-Wendroff scheme. They can be
1469 easily extended to higher-order accuracy using one-step coupled time-space
1470 approach of arbitrary high order (e.g. Daru and Tenaud, 2004). However
1471 if a method of lines is used the time and space dimensions are decoupled
1472 therefore the constraints on total variation must be imposed both in time
1473 and space. For this purpose, a family of Runge-Kutta (RK) schemes satis-
1474 fying the TVD property has been derived by Shu (1988) and Gottlieb and
1475 Shu (1998). These RK schemes are TVD over a range of time-steps which
1476 is generally smaller than the stability range given by the more traditional
1477 CFL-type condition. Note that a consequence of the TVD, TVB and MP
1478 stability constraints is a better control of numerical oscillations hence those
1479 constraints could be used not only for momentum advection as a way to limit
1480 spurious mixing by reducing the grid Reynolds number (Ilicak et al., 2012),
1481 but also for the advection of tracers and layer thickness subject to mono-
1482 tonicity or positivity constraints. There is an abundant literature on the
1483 comparison of different flux limiting/correcting strategies, see Mohammadi-
1484 Aragh et al. (2015) for a recent study in the oceanic modelling context. Note
1485 that in multi-dimensions, the TVD, TVB or MP properties are generally ap-
1486 plied independently in each spatial directions. It can be shown that in this
1487 case the resulting scheme does not strictly satisfy those properties anymore.
1488 Nonetheless this approach generally provides acceptable results.

1489 *7.1.3. Multidimensional aspects and stability constraints*

1490 The extension of one-dimensional advection schemes to multi-dimensions
1491 in the context of a method of lines is straight-forward since the necessary
1492 transverse terms are discretised in a transparent way. If a quasi-Eulerian
1493 vertical coordinate is used, the stability constraint in three dimensions reads

$$1494 \quad \alpha^x + \alpha^y + \beta\alpha^z \leq \alpha^* \quad (64)$$

1495 where α^* is the CFL stability constraint associated to the numerical schemes
1496 used for the time and space discretisations, and β a coefficient arising from
1497 the fact that different advection schemes with different stability criteria may
1498 be used in the horizontal and vertical directions. Typical values of α^* and β
1499 can be found in Lemarié et al. (2015). As far as the coupled space and time
1500 approach is concerned, a simple application of the one-dimensional fluxes in
1501 each spatial direction would result in a scheme that can be at most first-
1502 order accurate, whatever the order of accuracy of the 1D fluxes, and the
1503 scheme would be unconditionally unstable. To overcome this issue a direc-
1504 tional splitting can be used to introduce the necessary transverse terms in
1505 the discretisation. A simple method to introduce transverse terms while pre-
1506 serving constancy is the splitting of Bott (2010). With this type of approach
1507 the stability constraint is given by

$$\max \{ \alpha^x, \alpha^y, \alpha^z \} \leq 1$$

1508 which is less stringent than (64).

1509 For coastal applications, Shchepetkin (2015) has emphasised the severe
1510 stability constraint potentially imposed by vertical advection. Several ways
1511 can be used to mitigate this issue (i) use a semi-implicit advection scheme
1512 (ii) use a local time-step for vertical advective terms based on the maximum
1513 vertical Courant number in each water column (iii) use a quasi-Lagrangian
1514 vertical coordinate which is subject to a gentle Lipschitz stability condition
1515 rather than the usually severe CFL condition (e.g. White et al., 2009). This
1516 last remark applies to models using rezoning/remapping strategies because
1517 models using a transport algorithm instead of remapping (e.g. Hofmeister
1518 et al., 2010) will still be subject to a CFL type stability constraint.

1519 *7.2. Internal pressure gradient errors*

1520 Since in coastal ocean models the use of bottom-following coordinates is
1521 mandatory (see Sec. 2.1), the coordinate surfaces may intersect with isopyc-
1522 nal or geopotential surfaces at a relatively large angle when the bathymetry

1523 is steep. This makes it significantly harder to accurately compute the in-
 1524 ternal horizontal pressure gradient since the pressure is not known along
 1525 constant horizontal surfaces. Using the notations introduced in Sec. 4, for a
 1526 generalised vertical coordinate s , the x -component of the internal horizontal
 1527 pressure gradient (HPG) is expressed using the chain rule

$$1528 \quad \frac{1}{\rho_0} (\partial_x p)_z = \frac{1}{\rho_0} [(\partial_x p)_s - \partial_z p (\partial_x z)_s], \quad (65)$$

1529 where p is the hydrostatic pressure deduced from the hydrostatic relation (7).
 1530 The subscript s is denoting differentiation with respect to constant s . In an
 1531 arbitrary general coordinate the two terms in rhs are nontrivial, of opposite
 1532 sign and may be large compared to the order of magnitude of their difference,
 1533 except for two special cases: For isopycnal coordinates, the first term van-
 1534 ishes. The second term in the rhs is sometimes referred to as compensating
 1535 hydrostatic term which vanishes for geopotential coordinates ($s = z$). At a
 1536 discrete level, unbalanced truncation errors in the computation of the two
 1537 large terms in the rhs will interfere with each other and give rise to a possibly
 1538 large pressure-gradient error leading to hydrostatic inconsistency manifested
 1539 by unphysical spontaneous motions, even in the absence of lateral density
 1540 gradients (i.e., $\rho = \rho(z)$). A very large body of literature is dedicated to this
 1541 subject (e.g. Blumberg and Mellor, 1987; Mellor et al., 1994; McCalpin, 1994;
 1542 Burchard and Petersen, 1997; Lin, 1997; Shchepetkin and McWilliams, 2003;
 1543 Adcroft et al., 2008; Marsaleix et al., 2011; Berntsen, 2011) where different
 1544 strategies have been followed to reformulate (65) in a way more convenient
 1545 for the discretisation. Those strategies are generally motivated either by
 1546 achieving a high-order accuracy to cancel the two terms in (65) in the case
 1547 of a flat stratification (e.g. McCalpin, 1994; Shchepetkin and McWilliams,
 1548 2003) or by ensuring an energetic consistency (e.g. Marsaleix et al., 2008).
 1549 In this latter case, the aim is to make sure in a discrete sense that the change
 1550 of kinetic energy due to the work of pressure forces is balanced by the change
 1551 of potential energy due to buoyancy forces. This balance occurs only with a
 1552 linear equation of state and involves the discrete advection for density (e.g.
 1553 Shchepetkin and McWilliams, 2003, App. A).

1554 Mainly three strategies have been followed in practical applications to
 1555 reformulate and discretise (65). (i) A first strategy is to directly use the
 1556 hydrostatic assumption (6) to express p in terms of density integrals

$$1557 \quad \frac{1}{\rho_0} (\partial_x p)_z = \frac{g}{\rho_0} [(\partial_x I_\rho(z))_s + \rho (\partial_x z)_s], \quad I_\rho(z) = \int_z^\eta \rho(x, y, \xi) d\xi, \quad (66)$$

1558 assuming a zero atmospheric pressure gradient at the surface. When dis-
 1559 cretising this form of pressure gradient, averaging of $I_\rho(z)$ in the vertical and
 1560 ρ in the horizontal are needed since the only term computed at its natural
 1561 position is $(\partial_x z)_s$. According to Shchepetkin and McWilliams (2003) this
 1562 explains why this approach is often prone to large hydrostatic inconsisten-
 1563 cies. However, high-order schemes have been proposed in McCalpin (1994)
 1564 to compute the horizontal derivatives and horizontal averaging of ρ combined
 1565 with a spectral representation in the vertical. Note that high-order methods
 1566 in the vertical should be used with care in case of strongly stratified flows
 1567 because density is generally not smooth on the grid scale, especially with
 1568 coarse vertical resolution. (ii) a second and intuitive approach consists in
 1569 computing the pressure (i.e. $I_\rho(z)$) and then to vertically interpolate the
 1570 result at an horizontal surface of reference before differentiating (e.g. Lin,
 1571 1997; White et al., 2009). This is the preferred option in atmospheric mod-
 1572 els. In Lin (1997) a flux-form finite-volume approach based on this concept
 1573 is adopted. (iii) the preferred approach for most oceanic models is to use
 1574 a *density-Jacobian* discretisation. As done in (8) and (9), by combining the
 1575 Leibniz rule and the hydrostatic relation we easily obtain that

$$\frac{1}{\rho_0} (\partial_x p)_z = g \frac{\rho(\eta)}{\rho_0} \partial_x \eta - \int_z^\eta \underbrace{[(\partial_x b)_s - \partial_{z'} b (\partial_x z')_s]}_{\mathcal{J}_{x,z'}(b,z')} dz' \quad (67)$$

1576 where the buoyancy b is defined in Sec. 3. Compared to the straight-forward
 1577 approach (66) differentiation comes first and integration then. The density-
 1578 Jacobian formulation clearly shows that if $s = \rho$ only one term is nonzero and
 1579 the pressure gradient term can be computed accurately provided that proper
 1580 care is taken to the equation of state (Adcroft et al., 2008). The Jacobian
 1581 in (67) must be computed at cell corners, if we refer to Fig. 5 a standard
 1582 second-order discretisation reads

$$(\mathcal{J}_{x,z})_{i+1/2,k+1/2} = \frac{1}{2\Delta x} \{ (1+r_x)b_{i+1,k+1} + (1-r_x)b_{i+1,k} \\
 - (1-r_x)b_{i,k+1} - (1+r_x)b_{i,k} \} \quad (68)$$

1583
 1584 with $r_x = -\frac{z_{i+1,k+1/2} - z_{i,k+1/2}}{z_{i+1/2,k+1} - z_{i+1/2,k}}$ the grid slope. This discretisation of the Jaco-
 1585 bian has been widely used in coastal models for years. It can be shown that
 1586 the standard second-order Jacobian discretisation corresponds to a discrete

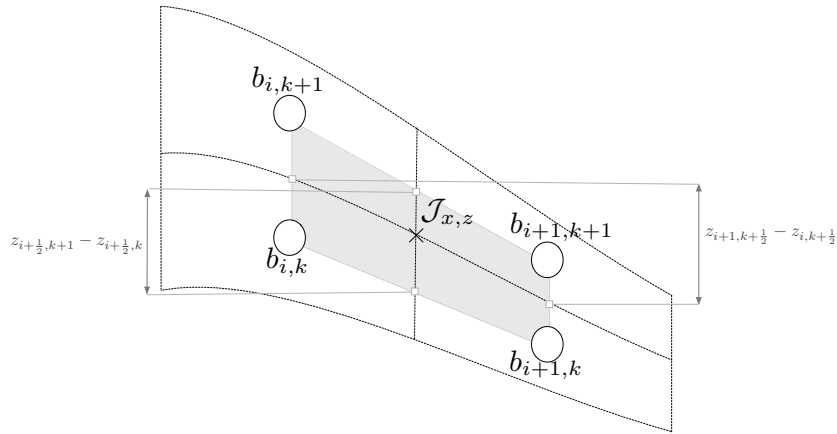


Figure 5: Elementary computational stencil of the standard second-order density Jacobian $\mathcal{J}_{x,s}$. The distances involved in the computation of the grid slope r_x are reported.

1587 form of Green's theorem. Indeed, (68) can be written as the sum of four line
 1588 integrals discretised using a simple trapezoidal rule. In an attempt to fur-
 1589 ther reduce the pressure gradient errors, Shchepetkin and McWilliams (2003)
 1590 have introduced a high-order (cubic) discretisation for those line integrals.
 1591 In their work, care has been taken to the robustness of the scheme even in
 1592 case of non-smooth density fields. The resultant scheme turned out to be a
 1593 significant step forward compared to existing approaches. Note that besides
 1594 the imbalance in the truncation errors in (65) there is an other source of pres-
 1595 sure gradient error stemming from the use of a nonlinear equation of state
 1596 including compressibility of seawater (Dukowicz, 2001). Ways to remove this
 1597 source of error by rearranging the terms in the equation of state are presented
 1598 in Shchepetkin and McWilliams (2003), Adcroft et al. (2008) or Marsaleix
 1599 et al. (2011). This latter source of error is sometimes overlooked, however it
 1600 must be stressed that the careless inclusion of compressibility terms into the
 1601 equation of state would have significant dynamic consequences.

1602 The value of the parameter r_x in (68) is a good qualitative indicator of dis-
 1603 cretisation errors. For $r_x = 0$ the grid is flat and the pressure gradient term
 1604 reduces to a single term while for $|r_x| = 1$ there is a 45 degrees slope between
 1605 the grid and the horizontal direction, and (68) reduces to a simple differenti-
 1606 ation of two terms in the diagonal. More generally, for $|r_x| \leq 1$ we expect the

1607 discretisation to be fairly accurate since it is based on vertical interpolations,
1608 this is the so-called "hydrostatic consistency" situation (Fig. 5). Values of
1609 $|r_x|$ greater than 1 generally lead to a degradation of the accuracy due to
1610 the need of vertical extrapolation to compute the pressure gradient term.
1611 This corresponds to a situation of "hydrostatic inconsistency", see Haney
1612 (1991). A strong requirement to avoid the emergence of spurious motions
1613 is thus to keep the value of r_x at a reasonable level. To do so several ways
1614 are commonly used concurrently, *(i)* bathymetry smoothing (e.g. Martinho
1615 and Batteen, 2006) is systematically used in terrain-following coordinates to
1616 limit the maximum slopes *(ii)* the function responsible for the vertical place-
1617 ment of grid points is designed in such a way to minimise the departure of
1618 the vertical coordinate isosurfaces from the horizontal direction (e.g. Schär
1619 et al., 2002; Shchepetkin and McWilliams, 2009; Berntsen, 2011; Lemarié
1620 et al., 2012b) *(iii)* a quasi-Lagrangian vertical coordinate whose layer distri-
1621 bution in the rezoning step can be chosen to reduce grid slopes or to follow
1622 isopycnals (e.g. Burchard and Petersen, 1997; White et al., 2009; Hofmeis-
1623 ter et al., 2010). Note that trying to confine the maximum grid slopes at
1624 the bottom to quickly obtain nearly flat coordinate isosurfaces when going
1625 toward the surface must be done with care in the sense that large pressure
1626 gradient errors at depth will affect the circulation in the upper layers anyway
1627 through baroclinic-barotropic coupling. Besides the approaches discussed so
1628 far, we could imagine alternative strategies. For example, the coordinate
1629 system could be determined using only the low-frequency variations in the
1630 bathymetry and high frequencies could be handled using an immersed bound-
1631 ary method (e.g. Lundquist et al., 2010). Other alternatives could be the use
1632 of well-balanced discretisations (Botta et al., 2004) or to express horizon-
1633 tal momentum using the covariant velocity components instead of the usual
1634 contravariant components (Weller and Shahrokhi, 2014). Eventually, as em-
1635 phasised by Mellor et al. (1994), the interaction between pressure gradient
1636 and other terms in the equations should be further clarified, especially the
1637 interaction with active tracers advection. More specifically, the interplay
1638 between numerically-induced mixing of active tracers and HPG errors is ex-
1639 pected to play a crucial role in the time-evolution of circulation errors (e.g.
1640 Lemarié et al., 2012b, Sec. 6.2). However, the importance of HPG errors in
1641 simulations of coastal currents is difficult to evaluate in practical applications.
1642 The competing effects of the model dynamics, its sensitivity to the horizon-
1643 tal/vertical grid resolution and discrete numerical algorithms, are tricky to
1644 untangle.

1645 *7.3. Inertia-gravity waves*

1646 Most of the work on the discretisation of inertia-gravity waves was mainly
 1647 concerned with finding the most appropriate variable arrangement among
 1648 the Arakawa grids A to E by looking at discrete dispersion relations (e.g.
 1649 Mesinger and Arakawa, 1976). Here we restrict ourselves to the C-grid ar-
 1650 rangement which is the preferred option in coastal models since the Rossby
 1651 radius of deformation is generally properly resolved, with the exception of
 1652 fjord-type systems such as the Baltic Sea, where very high resolution $< 1km$
 1653 is required (Holtermann et al., 2014). Typical space-time discretisation tech-
 1654 niques can be found in Beckers and Deleersnijder (1993) or Lemarié et al.
 1655 (2015) and are summarised below.

1656 *7.3.1. Inertial oscillations*

1657 In the absence of other terms but Coriolis terms in (30) and (31) we
 1658 obtain the equations of free motion on a rotating plane

$$1659 \quad \partial_t(h_k u_k) = fh_k v_k; \quad \partial_t(h_k v_k) = -fh_k u_k. \quad (69)$$

1660 A characteristic of the Coriolis acceleration is that it is directed perpendic-
 1661 ular to the velocity direction. Hence, it does not play any role in the kinetic
 1662 energy budget, which forms an important constraint for the discretisation
 1663 (e.g. Arakawa and Lamb, 1977). In (69), the quantity $fh_k v_k$ must be given
 1664 at u -points and $fh_k u_k$ at v -points. If (69) is semi-discretised in space, this
 1665 constraint is trivially satisfied locally on an Arakawa B-grid, since u and
 1666 v are collocated, but can only be satisfied globally on an Arakawa C-grid.
 1667 Considering that the Coriolis frequency f is cell centered, the following dis-
 1668 cretisation of the rhs in (69)

$$1669 \quad (fh_k v_k)_{i+1/2,j} = \overline{f_{i,j} h_{i,j,k} \bar{v}_k^v}, \quad (fh_k u_k)_{i,j+1/2} = \overline{f_{i,j} h_{i,j,k} \bar{u}_k^y}, \quad (70)$$

1670 where $\bar{\cdot}^m$ is an averaging operator in the direction m ($m = x, y$), ensures that
 1671 all the terms associated to the Coriolis force cancel when a kinetic energy
 1672 equation is derived from (30) and (31) (Sec. III.C in Arakawa and Lamb,
 1673 1977). In (70), the horizontal variations of the curvature metric terms have
 1674 been ignored for clarity. An alternative energetically-consistent discretisation
 1675 providing a different logic for the cancellation of the terms when the kinetic
 1676 energy budget is formed at the discrete level has been introduced in Espelid
 1677 et al. (2000) and reads

$$1678 \quad (fh_k v_k)_{i+1/2,j} = f_{i+1/2,j} \overline{(h_k v_k)_{i+1/2,j}^w}; \quad (fh_k u_k)_{i,j+1/2} = f_{i,j+1/2} \overline{(h_k u_k)_{i,j+1/2}^w}, \quad (71)$$

1679 where $\overline{\cdot}^w$ is a weighted average defined as

$$1680 \quad \overline{(h_k v_k)}_{i+1/2,j}^w = \frac{w_{i+1/2,j,k}}{4} \sum_{n=0}^{n=1} \sum_{m=0}^{m=1} \frac{(hv)_{i+n,j-m+1/2,k}}{w_{i+n,j-m+1/2,k}}; \quad w_{i+1/2,j,k} = \sqrt{\frac{gh_{i+1/2,j,k}}{|f_{i+1/2,j}|}}$$

1681 for each layer k , same rationale applies to $\overline{(h_k u_k)}_{i,j+1/2}^w$. Compared to (70),
 1682 this formulation requires the Coriolis parameter to be defined at u and v
 1683 points and allows more freedom in the way to define the thickness layer h_k
 1684 at cell interfaces.

1685 When the time dimension is discretised, the energy conservation prop-
 1686 erty is less straight-forward to ensure. First, a simple forward Euler step
 1687 to integrate (69) would be unconditionally unstable. The use of a (semi)-
 1688 implicit scheme would remove stability constraints. This approach is essen-
 1689 tially adopted in models which treat the gravity waves in a semi-implicit way
 1690 (e.g. Walters et al., 2009). In general, for coastal applications, the baroclinic
 1691 time-step is much smaller than the inertial period meaning that the Coriolis
 1692 term is not expected to impose any limitation on the time-step. For this
 1693 reason explicit schemes are generally preferred. To circumvent the stabil-
 1694 ity issues of the Euler forward step, a Forward-Backward in Time (FBT)
 1695 approach is often used (Bleck and Smith, 1990)

$$1696 \quad \begin{aligned} (h_k u_k)_{i+1/2,j}^{n+1} &= (h_k u_k)_{i+1/2,j}^n + \Delta t (f h_k v_k)_{i+1/2,j}^{n+s} \\ (h_k v_k)_{i+1/2,j}^{n+1} &= (h_k v_k)_{i+1/2,j}^n - \Delta t (f h_k u_k)_{i,j+1/2}^{n+1-s}, \end{aligned} \quad (72)$$

1697 and is stable for $f\Delta t \leq 2$. In (72), s is either 0 if n is even or 1 otherwise.
 1698 The major drawbacks of this approach are that it requires to switch at each
 1699 time-step the order of integration of the u and v components and it is not
 1700 energetically-consistent even if the spatial discretisation is. Other popular
 1701 explicit schemes to integrate (69) include the third-order Adams-Bashforth
 1702 scheme (stable for $f\Delta t \leq 0.72$) and the leapfrog scheme (stable for $f\Delta t \leq 1$)
 1703 which both globally ensure that there is no false generation of kinetic energy
 1704 since u and v are considered at the same moment in time.

1705 7.3.2. Internal gravity waves

1706 Elements about the temporal discretization of external gravity waves are
 1707 introduced in Sec. 5.1 so that we focus here on internal gravity waves. The

1708 numerical integration of those waves is generally studied on the following
 1709 one-dimensional subsystem

$$\begin{aligned}
 \partial_t p_q + \rho_0 c_q^2 \partial_x u_q &= 0 \\
 \rho_0 \partial_t u_q + \partial_x p_q &= 0,
 \end{aligned}
 \tag{73}$$

1711 for a given vertical mode q ($q = 0$ corresponds to the barotropic mode) with
 1712 c_q the gravity wave speed associated with q^{th} vertical mode. The details to
 1713 derive (73) from the full three-dimensional equations can be found, e.g., in
 1714 Lemarié et al. (2015). In (73), the term $\partial_x u_q$ in the first equation can be
 1715 traced back to the horizontal divergence in the continuity equation and the
 1716 term $\partial_x p_q$ in the second equation to the horizontal pressure gradient term in
 1717 the primitive equations. The stability constraint imposed by internal gravity
 1718 waves reads

$$\Delta t \sqrt{c_1^2 \left(\frac{1}{\Delta x^2} + \frac{1}{\Delta y^2} \right)} \leq \alpha_{\text{igw}}^*$$

1720 where α_{igw}^* is the CFL stability criterion depending on space and time dis-
 1721 cretization used for internal waves and c_1 the speed of the fastest internal
 1722 wave. Typical values for α_{igw}^* can be found in Lemarié et al. (2015) and
 1723 Tab. 1. Following Hallberg (1997) and Shchepetkin and McWilliams (2008),
 1724 a general family of two-level schemes for the time integration of (73) in a
 1725 forward manner is

$$\begin{aligned}
 p_q^* &= p_q^n - c_q^2 \Delta t \partial_x (\rho_0 u_q^n) \\
 \rho_0 u_q^* &= \rho_0 u_q^n - \Delta t \partial_x (\vartheta p_q^* + (1 - \vartheta) p_q^n) \\
 p_q^{n+1} &= p_q^n - c_q^2 \Delta t \partial_x (\varsigma \rho_0 u_q^* + (1 - \varsigma) \rho_0 u_q^n) \\
 \rho_0 u_q^{n+1} &= \rho_0 u_q^n - \Delta t \partial_x \left((1 - \varphi) [(1 - \varepsilon) p_q^{n+1} + \varepsilon p_q^*] + \varphi p_q^n \right)
 \end{aligned}
 \tag{74}$$

1727 where the parameters ϑ , ς , ε and φ can be chosen to improve both accu-
 1728 racy and stability. As reported in Tab. 1, the general discretization (74)
 1729 encompasses several well-known schemes presented in the literature. Among
 1730 the various alternatives, by far the simpler strategy is the so-called forward-
 1731 backward approach (e.g. Mesinger and Arakawa, 1976). Other alternatives
 1732 include the time staggering of tracers and momentum (e.g. Backhaus, 1985)
 1733 or the use of a larger stencil in time (Brown and Campana, 1978; Shchepetkin
 1734 and McWilliams, 2005). Of interest for the coastal modeling community,
 1735 Rueda et al. (2007) showed that the original implementation of the Casulli

	Forward-Backward	Casulli and Cattani (1994)	Rueda et al. (2007)	Shchepetkin and McWilliams (2008)
ϑ	-	-	1/6	13/24
ς	0	0	1/2	1/4
φ	0	1/2	1/2	1/4
ε	0	0	0	5/18
α_{igw}^*	1	unstable	1	$\sqrt{3}$
Order of accuracy	2 nd	1 st	3 rd	3 rd

Table 1: Parameter values (ϑ , ς , ε , φ) in the general two-level forward-time integration scheme (74) corresponding to different alternatives existing in the literature. The associated stability constraint α_{igw}^* and order of accuracy are also given. For simplicity the parameters reported for the Shchepetkin and McWilliams (2008) scheme have been slightly modified compared to the original paper without compromising its properties.

1736 and Cattani (1994) time-integration scheme with a semi-implicit treatment
1737 of the external gravity waves is baroclinically unstable for the integration
1738 of internal gravity waves unless a backward Euler scheme is used for the
1739 external mode. As far as the spatial discretisation is concerned, the over-
1740 whelming majority of oceanic models consider simple second-order schemes
1741 to compute $\partial_x u_q$ (i.e. the continuity equation) and $\partial_x p_q$ (i.e. the horizontal
1742 pressure gradient). However studies by Blayo (2000) and Demange et al.
1743 (2014) emphasised that higher-order approximations of both the pressure
1744 gradient term and the horizontal divergence in the continuity equation allow
1745 a significantly better representation of internal waves propagation, compared
1746 to standard algorithmic choices.

1747 7.4. Orientation of diffusion tensor and numerically-induced mixing

1748 In (8), (9), (15), and (17), the horizontal turbulent fluxes are oriented in
1749 a direction (\tilde{x}, \tilde{y}) to be defined. In the case of a stratified flow, if the verti-
1750 cal coordinate $s \neq \rho$ it is well known that maintaining the diffusion tensor
1751 along the coordinate lines can be responsible for non-physical mixing of water
1752 masses and associated spurious baroclinic currents (e.g. Barnier et al., 1998).
1753 It is thus relatively common for non-isopycnic models to implement a rota-
1754 tion of the diffusion tensor in a direction non-aligned with the computational
1755 grid (e.g. Stelling and Van Kester, 1994; Griffies et al., 1998). However, the

1756 implementation of such a rotation tensor turned out to be very delicate no-
1757 tably to avoid unphysical undershooting and overshooting and to maintain
1758 reasonable accuracy in case of large slopes, similarly to the HPG calculations
1759 (Beckers et al., 1998, 2000; Lemarié et al., 2012a). Since for a generalized
1760 coordinate it is expected that the slope between the isopycnal direction and
1761 the direction of the computational grid is larger than for a classical z coord-
1762 inate, a good compromise is generally to rotate the explicit diffusion in the
1763 geopotential direction rather than the physically correct isopycnal direction.
1764 This allows to avoid delicacies associated with the computation of isopycnal
1765 slopes in unstratified regions and at the intersection with the surface and the
1766 bottom.

1767 A non negligible amount of non-physical mixing of water masses can also
1768 be due to the advection operator. Indeed, as mentioned earlier, oceanic
1769 coastal models generally rely either on high-order linear upwind schemes or
1770 on flux correcting/limiting approaches to discretise horizontal advection. The
1771 associated truncation errors are dissipative. Much effort have been recently
1772 directed toward the quantification and/or modification of physical orienta-
1773 tion of this mixing of numerical nature (e.g. Burchard and Rennau, 2008;
1774 Marchesiello et al., 2009; Ilicak et al., 2012; Klingbeil et al., 2014). For ex-
1775 ample, Marchesiello et al. (2009) showed that the dissipative truncation error
1776 associated to a third-order upwind scheme in a terrain-following coordinate
1777 model was greatly exceeding the small level of physically acceptable mixing
1778 observed in the oceanic interior. The physical results proved to be greatly
1779 improved by splitting the third-order upwind scheme between a centered and
1780 a diffusive part and when the diffusive part is rotated in the isopycnal direc-
1781 tion (Marchesiello et al., 2009; Lemarié et al., 2012b). This approach, which
1782 is viable only for linear advection schemes, required a thorough analysis of
1783 the biharmonic isopycnal mixing operator to obtain a stable and sufficiently
1784 accurate discretisation for large slopes (Lemarié et al., 2012a). However, this
1785 methodology has some limitations: the rotated operator is derived under the
1786 small slope approximation which may no longer be valid in coastal applica-
1787 tions (Lemarié et al., 2012b, Sec. 2.4.2) and it is unclear how the diffusion
1788 operator behaves in case of fast temporal variations of isopycnals. An alter-
1789 native approach to have more control on the orientation of mixing for coastal
1790 applications is the use of quasi-Lagrangian approach (e.g. Hofmeister et al.,
1791 2010; Leclair and Madec, 2011). Besides the orientation of the diffusion ten-
1792 sor, Ilicak et al. (2012) emphasised that spurious diapycnal mixing can be
1793 aggravated if the grid Reynolds number is too large (i.e. if the velocity field

1794 is not smooth on the grid scale). Useful diagnostics to help characterising the
 1795 amount and/or orientation of spurious mixing can be found in Ilicak et al.
 1796 (2012) and Klingbeil et al. (2014). Note that even if much of the attention
 1797 is on the advection operator, a non-negligible amount of numerical mixing
 1798 could also be associated to other terms in the equations (Soufflet et al., 2016).

1799 7.5. Bottom friction

1800 Due to the relatively thick bottom boundary layers in the coastal ocean,
 1801 see (1), an accurate discretisation of bottom friction is required. The no-
 1802 slip bottom boundary condition for u and v (12) is typically not directly
 1803 discretised, because a vertical resolution on scales of millimetres would be
 1804 required to obtain sufficient accuracy. Instead, it is assumed that the velocity
 1805 profiles in the lowest grid box of an ocean model follow the law of the wall:

$$1806 \quad [u(z'), v(z')] = \frac{[u_*^b, v_*^b]}{\kappa} \ln \left(\frac{z' + z_0^b}{z_0^b} \right), \quad (75)$$

1807 with the bottom roughness length, z_0^b , the bottom friction velocity vector,
 1808 (u_*^b, v_*^b) and the distance from the wall, $z' = z + H$. With (75), the discrete
 1809 bottom boundary condition has the form of a quadratic friction law

$$1810 \quad \frac{\tau_{[x,y]}^b(h, u, v)}{\rho_0} = \left(\frac{\kappa}{\ln \left(\frac{h/2 + z_0^b}{z_0^b} \right)} \right)^2 \cdot [u, v] (u^2 + v^2)^{1/2} \quad (76)$$

$$= c_d \cdot [u, v] (u^2 + v^2)^{1/2}.$$

1811 In (76),

$$1812 \quad \tau_{[x,y]}^b = \rho_0 [u_*^b, v_*^b] \left((u_*^b)^2 + (v_*^b)^2 \right)^{1/2} \quad (77)$$

1813 is the bed stress vector, c_d is the non-dimensional bottom drag coefficient,
 1814 h is the thickness of the lowest grid box, and (u, v) is the velocity vector in
 1815 the lowest grid box. Note that for the limit of $h \rightarrow 0$ we obtain $c_d \rightarrow \infty$ and
 1816 thus retain the original no-slip condition (12). The numerically calculated
 1817 bed stress vector calculated in (76) is then used in the bottom boundary
 1818 condition (13). In situations when the near-bottom velocity profile deviates
 1819 strongly from the law of the wall, e.g. when stratification due to high sedi-
 1820 ment concentrations or a wave-enhanced bottom boundary layer (or both) are

1821 present, the vertical resolution needs to be sufficiently high. One other pos-
 1822 sibility would be to parameterise such unresolved processes (Burchard et al.
 1823 (2008); Warner et al. (2008)). Specific care needs to be taken for the bottom
 1824 (and surface) boundary conditions when turbulence closure models are used.
 1825 As shown by Burchard and Petersen (1999) and Burchard et al. (2005b), flux
 1826 boundary conditions for turbulent quantities provide much higher accuracy
 1827 in reproducing the law of the wall than Dirichlet boundary conditions.

1828 7.6. Numerical treatment of turbulence closure equations

1829 The discretisation of turbulence closure budget equations requires speci-
 1830 fic care, since turbulence quantities are often non-negative scalars such as
 1831 the turbulent kinetic energy (TKE) k or its dissipation rate ε . Furthermore,
 1832 these quantities often cover several orders of magnitude across fairly short
 1833 time and spatial scales such as in oscillating tidal flow. The problem of a
 1834 straight forward, explicit-in-time discretisation of the TKE equation is best
 1835 demonstrated for the idealised case of freely decaying homogeneous turbu-
 1836 lence. In this case the TKE budget equation (24) simplifies to the following
 1837 form:

$$1838 \quad \partial_t k = -\varepsilon. \quad (78)$$

1839 An explicit discretisation of (78) would be

$$1840 \quad \frac{k^{n+1} - k^n}{\Delta t} = -\varepsilon^n \quad \Rightarrow \quad k^{n+1} = k^n - \Delta t \varepsilon^n, \quad (79)$$

1841 where n denotes a variable on the old time level and $n + 1$ denotes a variable
 1842 on the new time level. With (79) the time-step criterion for positivity of k^{n+1}
 1843 is $\Delta t < \varepsilon^n / k^n$, which for example in tidal flow might require very small time
 1844 steps during slack tide, when production is small and dissipation is high. A
 1845 solution to this problem has been proposed by Patankar (1980):

$$1846 \quad \begin{aligned} \frac{k^{n+1} - k^n}{\Delta t} &= -\varepsilon^n \frac{k^{n+1}}{k^n} = -c_\varepsilon \frac{k^{n+1} (k^n)^{1/2}}{l^n} \\ \Rightarrow k^{n+1} &= \frac{k^n}{1 + \Delta t \frac{\varepsilon^n}{k^n}} = \frac{k^n}{1 + \Delta t c_\varepsilon \frac{(k^n)^{1/2}}{l^n}}, \end{aligned} \quad (80)$$

1847 which gives unconditionally positive results for k^{n+1} . Note that the second
 1848 equalities in equations (80) are derived by using the cascading relation (26).

1849 This so-called Patankar trick is used in almost all discretisations of turbulence
1850 closure budget equations, including those for other parameters such as the
1851 dissipation rate ε and the turbulence frequency ω , see Deleersnijder et al.
1852 (1997) and Burchard et al. (2005b) for details. The Patankar trick may also
1853 be applied to sink terms in biogeochemical models to guarantee positivity,
1854 but to obtain conservation of state variables, source terms must be treated
1855 accordingly (Burchard et al. (2005a)).

1856 Another issue of the numerical treatment of turbulence closure models is
1857 the energy-consistency between mean flow and turbulence. Physically, the
1858 kinetic energy extracted from the mean flow due to vertical stress divergence
1859 is a source of turbulent kinetic energy transferred as shear production P . The
1860 same applies to the exchange of energy between mean potential energy and
1861 turbulence kinetic energy which is transferred as buoyancy production B .
1862 Burchard (2002b) shows how a consistent energy exchange can be obtained
1863 also on the numerical level.

1864 8. Existing coastal ocean community models

1865 Previous sections have discussed the various choices that have to be made
1866 when designing a numerical model with a focus on coastal applications. The
1867 present section gives an overview of the specifics of some existing hydro-
1868 static and non-hydrostatic structured-grid models to illustrate the diversity
1869 of methods in use in coastal models and their evolution over the years. We
1870 have strived here to present a fair description of past and ongoing develop-
1871 ments, however the reader must be warned that omissions and inaccuracies
1872 in the model description are inherent to this type of exercise.

1873 8.1. Hydrostatic structured-grid models

1874 In this subsection examples of structured-grid oceanic models used in
1875 practice to tackle research or engineering applications related to coastal en-
1876 vironments are given, see Tab. 2 for a list of the most popular models histor-
1877 ically used in this context. In this list we can find models originally designed
1878 for shallow seas applications (e.g. BOM, COHERENS, GETM, HAMSOM,
1879 Mars3D, MOHID), as well as mesoscale oceanic models, like NCOM, POL-
1880 COMS, POM or ROMS, adapted to handle nearshore and coastal scales (e.g.
1881 Oey, 2005; Uchiyama et al., 2010; Warner et al., 2013). More recently, global
1882 climate models (e.g. NEMO, Hycom) are also sometimes used to study shelf
1883 processes provided some adjustments in their numerical formulation (e.g.

1884 Leclair and Madec, 2011; Lahaye et al., 2011). Finally, models specifically
1885 designed for commercial/engineering applications (e.g. Delft3D, ECOM-si,
1886 MIKE 3, TRIM3D) can also be used for real case studies (e.g. Cheng et al.,
1887 1993). As summarised in Tab. 3, the choice of discrete algorithms in oceanic
1888 models bear the imprints of their original target application and development
1889 time. In the 90's the situation was very clear: climate models were generally
1890 discretised on a B-grid using a geopotential coordinate under the rigid-lid
1891 assumption and leapfrog (LF) time-stepping (Griffies, 2004) while mesoscale
1892 models, largely inspired by POM, made use of a C-grid, a terrain-following
1893 coordinate and an explicit free surface. At that time coastal and engineering
1894 models were predominantly C-grid models based on a semi-implicit free sur-
1895 face and baroclinic forward in time methods influenced by Backhaus (1985)
1896 and Casulli and Cheng (1992). Nowadays, the distinction between the differ-
1897 ent class of models is less clear because newly developed models are generally
1898 designed to handle a larger range of spatio-temporal scales permitted by the
1899 advances in computational power and the maturity of nesting strategies (see
1900 Sec. 6). In early 2000's, the emergence of models like ROMS, GETM or
1901 Hycom came with a thorough rethinking of several model components like
1902 time-stepping algorithms (Shchepetkin and McWilliams, 2005), vertical coor-
1903 dinate (Bleck, 2002; Burchard and Beckers, 2004), turbulent closure schemes
1904 (Umlauf and Burchard, 2003), or open boundary conditions (Marchesiello
1905 et al., 2001) which increased further the diversity of models. Tab. 3 reflects
1906 the variety of models and modelling techniques that are presently used. How-
1907 ever some general trends can be distinguished :

- 1908 • Models originally developed with coastal applications in mind are char-
1909 acterized by 2-level (one-step) time-stepping with a coupled space and
1910 time treatment of advective terms. This choice combines simplicity and
1911 ease to implement monotonicity-preserving advection.

- 1912 • The majority of models based on a coupled space and time approach
1913 favour the superbee slope limiter to impose the TVD property. This
1914 choice corresponds to the upper boundary of the TVD region and leads
1915 to the least numerical diffusion among the existing slope limiters (e.g.
1916 Cushman-Roisin and Beckers, 2011). However, this limiter tends to
1917 erroneously amplify the gradients. According to Durran (2010), the
1918 monotonicized centered limiter is expected to provide superior results in
1919 terms of accuracy. Other flux-limiter methods currently used for prac-
1920 tical applications is the ultimate quickest scheme (or equivalently the

1921 so-called P2-PDM scheme). Note that the WENO or FCT approaches
1922 are still relatively marginally used.

1923 • As motivated in Sec. 3.2.1, the overwhelming majority of coastal mod-
1924 els rely on TKE-based vertical closure models. A dynamic equation for
1925 TKE is solved either in combination with a diagnostic mixing length
1926 or with a second dynamic equation for a length related quantity.

1927 • The recently developed models are almost exclusively based on an ex-
1928 plicit external mode computation which allows more accuracy in the
1929 computation of fast barotropic waves and is expected to provide en-
1930 hanced scalability and performance on parallel computers.

1931 • The vertical coordinate system is one of the aspect that focuses the
1932 most attention nowadays. The general trend is to allow more flexibility
1933 in the definition of the coordinate within the Arbitrary Lagrangian-
1934 Eulerian framework.

1935 8.2. *Non-hydrostatic models*

1936 Within the last decade several existing coastal ocean models were ex-
1937 tended to abandon the hydrostatic pressure assumption (POM: Kanarska
1938 and Maderich (2003), BOM: Heggelund et al. (2004), ROMS: Kanarska et al.
1939 (2007), Symphonie: Auclair et al. (2011), GETM: Klingbeil and Burchard
1940 (2013)). Scaling analysis shows that the nonhydrostatic pressure contribu-
1941 tion, formally defined by

$$1942 \quad \partial_z p_{\text{nh}} = -(\partial_t w + \partial_x(uw) + \partial_y(vw) + \partial_z(ww) - f_h u - F_z), \quad (81)$$

1944 cannot be neglected when approaching sufficiently high spatial resolutions
1945 that promote processes with significant vertical accelerations (Marshall et al.,
1946 1997; Klingbeil and Burchard, 2013). Practical examples on coastal ocean
1947 scales are flows above irregular topography, high-frequency internal gravity
1948 waves or gravity plumes. In order to simulate these processes in a physically
1949 correct way, the vertical momentum balance must not be degenerated to (7)
1950 anymore.

1951 For solving the full set of incompressible Navier-Stokes equations algo-
1952 rithms were implemented on top of the hydrostatic model kernels that do
1953 not require a complete rewrite of the existing kernels. These were usually
1954 based on either the classical projection method (Chorin, 1968; Témam, 1969)

Model	Acronym	website
BOM	Bergen Ocean Model	http://www.mi.uib.no/BOM/
COHERENS	COupled Hydrodynamical Ecological model for REgioNal Shelf seas	http://odnature.naturalsciences.be/coherens/
Delft-3D	Deltares flow	http://oss.deltares.nl/web/delft3d
ECOM-si	Estuarine, Coastal and Ocean Model (semi-implicit)	http://woodshole.er.usgs.gov/operations/modeling/ecomsi.html
GETM	General Estuarine Transport Model	http://www.getm.eu/
HAMSOM	Hamburg Shelf Ocean Model	https://wiki.zmaw.de/ifm/T0/Hamsom/modelhistory
ROMS	Regional Oceanic Modeling System	
↔ Rutgers		https://www.myroms.org/
↔ UCLA		http://research.atmos.ucla.edu/cesr/ROMS_page.html
↔ AGRIF		http://www.romsagrif.org/
Mars3D	Model for Applications at Regional Scale	http://wwz.ifremer.fr/mars3d/
MIKE 3	Danish Hydraulic Institute	https://www.mikepoweredbydhi.com/
MOHID	MOdelo HIDrodinâmico	http://www.mohid.com/
NCOM	Navy Coastal Ocean Model	http://www.dtic.mil/dtic/tr/fulltext/u2/a508063.pdf
POLCOMS	Proudman Oceanographic Laboratory Coastal Ocean Modelling System	http://cobs.noc.ac.uk/modl/polcoms/
POM	Princeton Ocean Model	http://www.ccpo.odu.edu/POMWEB/
Symphonie	Sirocco Ocean Model	http://sirocco.omp.obs-mip.fr/ocean_models/S-model
TRIM-3D	Tidal Residual, Intertidal Mudflat	
Hycom	HYbrid Coordinate Ocean Model	https://hycom.org/
NEMO	Nucleus for the European Modeling of the Ocean	http://www.nemo-ocean.eu/

Table 2: Summary of most significant oceanic models historically used for applications to three-dimensional coastal studies. The ROMS code has three variants referred to as ROMS-Rutgers, ROMS-UCLA, and ROMS-Agrif (see Shchepetkin and McWilliams, 2009, for more details). Hycom and NEMO are examples for large scale models which are also applied to the coastal ocean.

	Introd. ref.	Horz grid	Mode splitting	Internal Time-stepping	External Time-stepping	Mom. advec.	Tracer advec.	Vertical discret.	Turb. closure
BOM	Svendsen et al. (1996)	C	SPE	LF-AM3	LF-TR	TVD Superbee	TVD Superbee	s	MY2.5
COHERENS	Luyten et al. (1999)	C	SPI/SPE	2-level	-	TVD Superbee	TVD Superbee	s	$k-\epsilon$
Delft-3D	Gerritsen et al. (2004)	C	SPI	ADI	ADI	UP3	UP3 w/ Forester fltr	z & s	$k-\epsilon$
ECOM-si	Blumberg (1992)	C	SPI	2-level	θ -scheme	C2	C2	s	MY2.5
GETM	Burchard and Bolding (2002)	C	SPE	2-level	FB	TVD	TVD	adapt.	GOTM
HAMSOM	Backhaus (1985)	C	SPI	2-level	θ -scheme	upstream	upstream	σ	$k-\epsilon$
ROMS (Rutgers)	Haidvogel et al. (2000)	C	SPE	LF-TR	LF-AM3	UP3	MPDATA	s	GLS
ROMS (UCLA)	Shepovkin and McWilliams (2005)	C	SPE	LF-AM3	Gen FB	UP3	UP3	s	KPP
ROMS (Agrif)	Penven et al. (2006)	C	SPE	LF-AM3	Gen FB	UP3	WENO5Z	s	KPP
Mars3D	Lazure and Salomon (1991)	C	SPI	2-level	ADI	QK3	QK3	s	GLS
MIKE 3	Pietrzak et al. (2002)	C	SPI	2-level	ADI	Ultimate QK3	Ultimate QK3	s	$k-\epsilon$
MOHID	Martins et al. (2001)	C	SPI	2-level	ADI	upstream	TVD Superbee	s	GOTM
NCOM	Martin (2000)	C	SPI	LF	θ -scheme	SUP3	FCT(UP3)	hyb z/s	MY2.5
POLCOMS	Holt and James (2001)	B	SPE	2-level	FB	PPM w/ limiters	PPM w/ limiters	σ	MY2.5
POM	Blumberg and Mellor (1978)	C	SPE	LF	LF	C2	MPDATA	s	MY2.5
Symphonic	Johns et al. (1992) Marsaleix et al. (1998)	C	SPE	LF	LF	C4	SUP3	s	TKE
TRIM-3D	Cheng et al. (1993)	C	SPI	2-level	θ -scheme	SL	TVD Van-Leer	-	GLS
Hycom	Bleck (2002)	C	SPE	LF	LF	Enstrophy-conserving	FCT(C2)	hyb $z/s/\rho$	KPP
NEMO	Madec et al. (1991)	C	SPE	LF	LF	SUP3	FCT(C2)	z & s	GLS

Table 3: Properties of some structured-grid coastal ocean models (note that the models might have many more choices than those listed here). Acronyms represent the following: FB=Forward-Backward, Gen = generalised, ADI = Alternating Direction Implicit, SPE=Split-Explicit, SPI=Split-Implicit, (S)UP3= (Split) third-order UPwind, QK3=third-order quickest, LF=Leapfrog, PPM=Piecewise Parabolic Method, TVD=Total Variation Diminishing, C2=second-order centered, C4=fourth-order centered, TR=trapezoidal, AM3=third-order Adams-Moulton interpolation, MPDATA=Multidimensional Positive Definite Advection Transport Algorithm.

1955 or the pressure correction method (van Kan, 1986). Both methods require
1956 the solution of a Poisson equation for either the nonhydrostatic pressure
1957 (Kanarska and Maderich, 2003; Heggelund et al., 2004) or its correction (Ka-
1958 narska et al., 2007; Auclair et al., 2011), which should be derived by inserting
1959 the discrete momentum equations into the discrete incompressibility condi-
1960 tion to force a divergence-free final velocity field. The specific characteristics
1961 of coastal ocean models demand for some adaptations and care, e.g. for the
1962 consistent coupling of the free surface to the corrected nonhydrostatic veloc-
1963 ities or the numerical treatment of the additional diagonals in the coefficient
1964 matrix that is neither symmetric nor positive-definite in general. Strategies
1965 to avoid the additional diagonals, only caused by the cross-terms of the ver-
1966 tical coordinate transformation, were presented by Heggelund et al. (2004)
1967 and Berntsen and Furnes (2005). Following Berntsen and Furnes (2005),
1968 Keilegavlen and Berntsen (2009) demonstrated that simulations with the
1969 nonhydrostatic pressure defined directly in σ -coordinates showed no signifi-
1970 cant deviations to results obtained with the pressure defined in z -coordinates.
1971 An alternative algorithm for weakly nonhydrostatic regimes (e.g. internal lee
1972 waves) that avoids the Poisson equation was presented by Klingbeil and Bur-
1973 chard (2013). They treat the nonhydrostatic pressure as the hydrostatic one,
1974 i.e. diagnose the time-lagged right-hand side of (81), integrate it vertically
1975 and insert it into the horizontal momentum equations.

1976 9. Future perspectives

1977 The present review of the numerics of structured-grid coastal ocean mod-
1978 els gives an overview of the numerical methods available for todays coastal
1979 ocean models. There is no single model which combines all those methods.
1980 Thus, by just recombining existing methods, todays model platforms may be
1981 further improved.

1982 But what are the future challenges in coastal ocean modelling? There are
1983 various trends which will drive further developments. One driver is certainly
1984 the ever ongoing growth of computational resources allowing for higher spa-
1985 tial resolution, better process representations, integration into regional Earth
1986 system models of growing complexity, application of more elaborate data as-
1987 similation schemes, and use of large ensemble simulations with high numbers
1988 of individual model simulations for better representation of model statistics.

1989 *Non-hydrostatic and Boussinesq assumption*

1990 The possible higher spatial resolution will in many coastal ocean scenarios
1991 allow for resolving non-hydrostatic processes. In cases where the horizontal
1992 resolution becomes substantially smaller than the water depth, hydrostatic
1993 models would lose their predictability when for example relatively short
1994 internal waves still propagate at their hydrostatic phase speed. Therefore,
1995 one challenge to the developers of coastal ocean models is to allow for efficient
1996 non-hydrostatic pressure calculation in situations where needed. As discussed
1997 in section 8.2, there are only a few of such examples among the structured-
1998 grid models. The challenge would therefore be that models automatically
1999 analyse whether in some regions the non-hydrostatic pressure contribution is
2000 relevant, and if so, the non-hydrostatic dynamics should be applied. On other
2001 (e.g., shallower) parts of the model domain it might be ignored. It should
2002 however be kept in mind that diagnosed non-hydrostatic pressure might also
2003 be a numerical artefact (Vitousek and Fringer, 2011).

2004 Another possibility to consistently add non-hydrostatic effects, while avoid-
2005 ing the costly direct solution of a 3D Poisson equation for the pressure, is to
2006 relax both the hydrostatic and Boussinesq assumptions (Auclair et al., 2016).
2007 Since relaxing the Boussinesq assumption reintroduces the acoustic waves, an
2008 acoustic mode must be considered on top of the internal and external modes.
2009 This three-mode approach has the advantage to be completely explicit (i.e.
2010 local in space) and thus to have very good properties in terms of scalabil-
2011 ity. However, it raises new challenges to derive consistent open boundary
2012 conditions to couple models based on different modeling assumptions.

2013 *Physics-dynamics coupling*

2014 The development of numerical models generally dissociates the dynamical
2015 kernel, which handles the resolved scales, from the "physics", that account
2016 for under-resolved processes. However, both components are strongly cou-
2017 pled since there is constantly a transfer of information back and forth from
2018 the dynamics to the physics so that the dynamical core must not violate
2019 physical principles. Energy-consistency is certainly one important example
2020 of such coupling. As discussed in section 7.1, most advection schemes are
2021 not variance conserving, which means for the momentum budget violation of
2022 kinetic energy conservation. The rate of numerical dissipation can be diag-
2023 nosed (e.g. Klingbeil et al., 2014) and it can be shown that more complex
2024 advection schemes limit the numerical dissipation (Mohammadi-Aragh et al.,
2025 2015). Another source of energy-conservation violation is due to the exchange

2026 between mean kinetic energy and potential energy. This exchange is repre-
2027 sented by the pressure-gradient term in the momentum equations and the
2028 advection terms of the potential temperature and salinity equations. Since
2029 those terms are discretised completely independently, energy-consistency is
2030 not given. Another issue is the energy consistency between loss of mean
2031 kinetic energy due to vertical stress divergence and production of turbu-
2032 lent kinetic energy (see section 7.6 and Burchard, 2002b). Generally better
2033 energy-consistency may also be achieved by more suitable choices for verti-
2034 cal coordinates. As discussed in section 4.2, generalised vertical coordinates
2035 give a high degree of freedom to construct an optimised vertical grid lay-
2036 out. This flexibility needs to be better exploited in the future to improve the
2037 performance of coastal ocean models.

2038 It should be briefly mentioned that also the physics of coastal ocean mod-
2039 els (as well as for large scale ocean models) is generally not energy-consistent,
2040 since e.g. the energy lost by horizontal stress divergence is not reintroduced
2041 into any other energy compartment of the model. This is an important issue
2042 which could however not be further discussed in this numerical review (see
2043 e.g., the discussion by Eden et al., 2014).

2044 *Multi-resolution strategies*

2045 One other aspect of ongoing discussions in the coastal ocean developers
2046 community is the optimal layout for horizontal grids. In both, structured-
2047 grid and unstructured-grid models, substantial progress has been made in
2048 the past. While unstructured-grid models have the better ability to solve
2049 multi-scale problems, the numerical cost per nominal grid point is up to one
2050 order of magnitude larger than for structured-grid models. It does there-
2051 fore depend on the kind of problem to decide which type of model is better
2052 suited. For complex domains such as lagoon systems or estuarine networks,
2053 unstructured-grid models are the better choice while for classical coastal or
2054 shelf sea scenarios structured-grid models are more efficient. Structured-grid
2055 models have gained flexibility due to more flexible grids (such as curvilinear
2056 grids, see section 4.3 or two-way nesting, see section 6.3). Flexible multi-level
2057 nesting strategies reducing the number of masked grid points (land points) in
2058 the model domain might in the future help to better tackle multi-scale prob-
2059 lems using structured grids. And there are efforts to increase the efficiency
2060 of unstructured-grid models. Both types of models - structured-grid models
2061 with flexible nesting and unstructured-grid models - might in the future sup-
2062 port horizontal mesh-adaptivity to resolve moving or intermittent dynamic

2063 features (as for example done in larger scale models to follow hurricanes). It
2064 depends on the success of such developments which type of model is gaining
2065 more ground in the future of coastal ocean modelling.

2066 *Coupling with other earth system compartments*

2067 Finally, stand-alone hydrodynamic coastal ocean models will always have
2068 a limited area of application. All such models are developed to also function
2069 as hydrodynamic core of coupled model systems. Most common is the
2070 coupling to biogeochemical models, where the hydrodynamic model provides
2071 advective and turbulent transports as well as the light regime and many
2072 other potential functional links between hydrodynamics and biogeochemistry.
2073 Without accurate physical and numerical representation of the hydrodynamics
2074 (e.g., in terms of the mixed-layer depth), biogeochemical models will have
2075 no predictability. Links between hydrodynamics and biogeochemistry may
2076 be complex. One tool to flexibly provide such a link is FABM (Framework
2077 of Biogeochemical Models, Bruggeman and Bolding (2014)).

2078 Coupling to several other Earth system compartments is common, such as
2079 to statistical surface wave models, sea ice models, atmospheric models, benthic
2080 models, and hydrological models. Several comprehensive system models
2081 exist, such as COAWST (Warner et al., 2008), interactively coupling hydro-
2082 dynamics (from ROMS) with surface waves, atmosphere, biogeochemistry,
2083 sediment transport and benthos to study complex coastal ocean scenarios
2084 in hindcast and sensitivity mode, or NEMO-Nordic (Gröger et al., 2015),
2085 coupling hydrodynamics (from NEMO) with atmosphere, sea ice, biogeo-
2086 chemistry, and hydrology for the purpose of regional climate downscaling
2087 and sensitivity scenarios. It is obvious that all coupling interfaces to other
2088 compartments require hydrodynamic process adaptations on the side of the
2089 hydrodynamic module, and that those need to be numerically discretised
2090 with care. It is expected that in the future, such complex coupled model
2091 systems will be much more widely used, such that quite some pressure to
2092 further develop hydrodynamic model will be generated.

2093 Despite the substantial growth of computational resources, regional cli-
2094 mate system models with run-times of typically more than a century and
2095 which maybe executed as large ensemble runs with many individual simula-
2096 tions will require high accuracy at relatively low resolution. Therefore the
2097 development of efficient and accurate numerical schemes at low resolution
2098 will be an important task also for the future.

2099 **Acknowledgements:** This paper is a contribution to the project M5
2100 (Reducing spurious diapycnal mixing in ocean models) of the Collaborative
2101 Research Centre TRR 181 on Energy Transfer in Atmosphere and Ocean
2102 funded by the German Research Foundation. Further support has been
2103 granted by the project MOSSCO (Modular System for Shelves and Coasts)
2104 funded by the German Federal Ministry of Research and Education (BMBF)
2105 under the project identification number FKZ 03F0667B. F. Lemarié and
2106 L. Debreu acknowledge the support of the french national research agency
2107 (ANR) through contracts ANR-14-CE23-0010 (HEAT) and ANR-16-CE01-
2108 0007 (COCOA). We are grateful to Robert Hallberg (Princeton) for dis-
2109 cussing principles of turbulence closure schemes for global ocean models with
2110 us.

2111 **References**

- 2112 Adcroft, A., Hallberg, R., Harrison, M., 2008. A finite volume discretization
2113 of the pressure gradient force using analytic integration. *Ocean Modell.* 22,
2114 106–113.
- 2115 Adcroft, A., Hill, C., Marshall, J., 1997. Representation of topography by
2116 shaved cells in a height coordinate ocean model. *Mon. Wea. Rev.* 125,
2117 2293–2315.
- 2118 Adcroft, A. J., Campin, J.-M., 2004. Rescaled height coordinates for accu-
2119 rate representation of free-surface flows in ocean circulation models. *Ocean*
2120 *Modell.* 7, 269–284.
- 2121 Adcroft, A. J., Hallberg, R. W., 2006. On methods for solving the oceanic
2122 equations of motion in generalized vertical coordinates. *Ocean Modell.* 11,
2123 224–233.
- 2124 Arakawa, A., Lamb, V. R., 1977. Computational design of the basic dynam-
2125 ical processes of the UCLA General Circulation Model. *Meth. Comput.*
2126 *Phys.* 17, 174–267.
- 2127 Auclair, F., Bordoix, L., Dossmann, Y., Duhaut, T., Paci, A., Ulses, C.,
2128 Nguyen, C., 2016. A non-hydrostatic non-Boussinesq algorithm for free-
2129 surface ocean modelling. *Ocean Modell.*In revision.
- 2130 Auclair, F., Estournel, C., Floor, J. W., Herrmann, M. J., Nguyen, C.,
2131 Marsaleix, P., 2011. A non-hydrostatic algorithm for free-surface ocean
2132 modelling. *Ocean Modelling* 36, 49–70.
- 2133 Backhaus, J. O., 1976. Zur Hydrodynamik im Flachwassergebiet. Ein nu-
2134 merisches modell. *Dt. Hydrogr. Z.* 29, 222–238.
- 2135 Backhaus, J. O., 1985. A three-dimensional model for the simulation of shelf
2136 sea dynamics. *Dt. Hydrogr. Z.* 38, 165–187.
- 2137 Barnier, B., Marchesiello, P., Miranda, A. P. D., Molines, J.-M., Coulibaly,
2138 M., 1998. A sigma-coordinate primitive equation model for studying the
2139 circulation in the south atlantic. part i: Model configuration with error
2140 estimates. *Deep-Sea Res.* 45, 543–572.

- 2141 Beckers, J.-M., Burchard, H., Campin, J.-M., Deleersnijder, E., Mathieu,
2142 P.-P., 1998. Another reason why simple discretizations of rotated diffu-
2143 sion operators cause problems in ocean models. Comments on the paper
2144 *isoneutral diffusion in a z-coordinate ocean model* by Griffies et al. J. Phys.
2145 Oceanogr. 28, 1552–1559.
- 2146 Beckers, J.-M., Burchard, H., Deleersnijder, E., Mathieu, P.-P., 2000. On the
2147 numerical discretization of rotated diffusion operators in ocean models.
2148 Mon. Wea. Rev. 128, 2711–2733.
- 2149 Beckers, J.-M., Deleersnijder, E., 1993. Stability of a FBTCs scheme applied
2150 to the propagation of shallow-water inertia-gravity waves on various space
2151 grids. J. Comp. Phys. 108, 95–104.
- 2152 Beckmann, A., Döscher, R., 1997. A method for improved representation of
2153 dense water spreading over topography in geopotential-coordinate models.
2154 J. Phys. Oceanogr. 27, 581–591.
- 2155 Berntsen, J., 2011. A perfectly balanced method for estimating the internal
2156 pressure gradients in σ -coordinate ocean models. Ocean Modell. 38, 85–95.
- 2157 Berntsen, J., Furnes, G., 2005. Internal pressure errors in sigma-coordinate
2158 ocean models – sensitivity of the growth of the flow to the time stepping
2159 method and possible non-hydrostatic effects. Continental Shelf Research
2160 25, 829–848.
- 2161 Beron-Vera, F., Ochoa, J., Ripa, P., 1999. A note on boundary conditions
2162 for salt and freshwater balances. Ocean Modell. 1, 111–118.
- 2163 Blaas, M., Dong, C., Marchesiello, P., McWilliams, J. C., Stolzenbach, K. D.,
2164 2007. Sediment-transport modeling on southern californian shelves: A
2165 roms case study. Cont. Shelf Res. 27, 832–853.
- 2166 Blayo, E., 2000. Compact finite difference schemes for ocean models: 1. ocean
2167 waves. J. Comp. Phys. 164, 241–257.
- 2168 Blayo, E., Debreu, L., 2005. Revisiting open boundary conditions from the
2169 point of view of characteristic variables. Ocean Modell. 9, 231–252.
- 2170 Bleck, R., 2002. An oceanic general circulation model framed in hybrid
2171 isopycnic-Cartesian coordinates. Ocean Modell. 4, 55–88.

- 2172 Bleck, R., Smith, L. T., 1990. A wind-driven isopycnic coordinate model
2173 of the north and equatorial atlantic ocean: 1. model development and
2174 supporting experiments. *J. Geophys. Res.* 95, 3273–3285.
- 2175 Blumberg, A. F., 1992. A primer for ecom-si. Tech. rep., HydroQual, Inc.
- 2176 Blumberg, A. F., Mellor, G. L., 1978. A coastal ocean numerical model. In:
2177 Sündermann, J., Holz, K.-P. (Eds.), *Mathematical Modelling of Estuarine*
2178 *Physics*. Springer-Verlag, New York, pp. 203–214.
- 2179 Blumberg, A. F., Mellor, G. L., 1987. A description of a coastal ocean cir-
2180 culation model. In: Heaps, N. S. (Ed.), *Three dimensional ocean models*.
2181 American Geophysical Union, Washington, D.C., pp. 1–16.
- 2182 Bolding, K., Burchard, H., Pohlmann, T., Stips, A., 2002. Turbulent mixing
2183 in the Northern North Sea: a numerical model study. *Cont. Shelf Res.* 22,
2184 2707–2724.
- 2185 Bott, A., 2010. Improving the time-splitting errors of one-dimensional advec-
2186 tion schemes in multidimensional applications. *Atmos. Res.* 97, 619–631.
- 2187 Botta, N., Klein, R., Langenberg, S., Lützenkirchen, S., 2004. Well balanced
2188 finite volume methods for nearly hydrostatic flows. *J. Comp. Phys.* 196,
2189 539–565.
- 2190 Brown, J. A., Campana, K. A., 1978. An economical time-differencing system
2191 for numerical weather prediction. *Mon. Wea. Rev.* 106, 1125–1136.
- 2192 Bruggeman, J., Bolding, K., 2014. A general framework for aquatic biogeo-
2193 chemical models. *Environmental Modelling & Software* 61, 249–265.
- 2194 Bryan, K., 1969. A numerical method for the study of the circulation of the
2195 world ocean. *J. Comp. Phys.* 4, 347–376.
- 2196 Burchard, H., 2001. Simulating the wave-enhanced layer under breaking sur-
2197 face waves with two-equation turbulence models. *J. Phys. Oceanogr.* 31,
2198 3133–3145.
- 2199 Burchard, H., 2002a. Applied turbulence modelling in marine waters. Vol.
2200 100 of *Lecture Notes in Earth Sciences*. Springer, Berlin, Heidelberg, New
2201 York.

- 2202 Burchard, H., 2002b. Energy-conserving discretisation of turbulent shear and
2203 buoyancy production. *Ocean Modell.* 4, 347–361.
- 2204 Burchard, H., Baumert, H., 1995. On the performance of a mixed-layer model
2205 based on the k - ϵ turbulence closure. *J. Geophys. Res.* 100, 8523–8540.
- 2206 Burchard, H., Baumert, H., 1998. The formation of estuarine turbidity max-
2207 ima due to density effects in the salt wedge. A hydrodynamic process study.
2208 *J. Phys. Oceanogr.* 28, 309–321.
- 2209 Burchard, H., Beckers, J.-M., 2004. Non-uniform adaptive vertical grids in
2210 one-dimensional numerical ocean models. *Ocean Modell.* 6, 51–81.
- 2211 Burchard, H., Bolding, K., 2002. GETM – a general estuarine transport
2212 model. Scientific documentation. Tech. rep., European Commission.
- 2213 Burchard, H., Bolding, K., Villarreal, M. R., 2004. Three-dimensional mod-
2214 elling of estuarine turbidity maxima in a tidal estuary. *Ocean Dyn.* 54,
2215 250–265.
- 2216 Burchard, H., Craig, P. D., Gemmrich, J. R., van Haren, H., Mathieu, P.-
2217 P., Meier, H. E. M., Nimmo Smith, W. A. M., Prandke, H., Rippeth,
2218 T. P., Skillingstad, E. D., Smyth, W. D., Welsh, D. J. S., Wijesekera,
2219 H. W., 2008. Observational and numerical modelling methods for quanti-
2220 fying coastal ocean turbulence and mixing. *Progr. Oceanogr.* 76, 399–442.
- 2221 Burchard, H., Deleersnijder, E., Meister, A., 2005a. Application of Modified
2222 Patankar schemes to stiff biogeochemical models for the water column.
2223 *Ocean Dyn.* 55, 326–337.
- 2224 Burchard, H., Deleersnijder, E., Stoyan, G., 2005b. Some numerical as-
2225 pects of turbulence-closure models. In: Baumert, H. Z., Simpson, J. H.,
2226 Sündermann, J. (Eds.), *Marine Turbulence: Theories, Observations and*
2227 *Models*. Cambridge University Press, Cambridge, Cambridge, pp. 197–206.
- 2228 Burchard, H., Petersen, O., 1997. Hybridization between σ - and z -co-
2229 ordinates for improving the internal pressure gradient calculation in marine
2230 models with steep bottom slopes. *Int. J. Numer. Meth. Fl.* 25, 1003–1023.
- 2231 Burchard, H., Petersen, O., 1999. Models of turbulence in the marine en-
2232 vironment – A comparative study of two-equation turbulence models. *J.*
2233 *Mar. Syst.* 21, 29–53.

- 2234 Burchard, H., Petersen, O., Rippeth, T. P., 1998. Comparing the perfor-
2235 mance of the Mellor-Yamada and the k - ε two-equation turbulence models.
2236 J. Geophys. Res. 103, 10543–10554.
- 2237 Burchard, H., Rennau, H., 2008. Comparative quantification of physically
2238 and numerically induced mixing in ocean models. Ocean Modell. 20, 293–
2239 311.
- 2240 Cailleau, S., Fedorenko, V., Barnier, B., Blayo, E., Debreu, L., 2008. Com-
2241 parison of different numerical methods used to handle the open boundary
2242 of a regional ocean circulation model of the bay of biscay. Ocean Modell.
2243 25, 1–16.
- 2244 Canuto, V. M., Howard, A., Cheng, Y., Dubovikov, M. S., 2001. Ocean
2245 turbulence. Part I: One-point closure model. Momentum and heat vertical
2246 diffusivities. J. Phys. Oceanogr. 31, 1413–1426.
- 2247 Casulli, V., Cattani, E., 1994. Stability, accuracy and efficiency of a semi-
2248 implicit method for three-dimensional shallow water flow. Computers
2249 Math. Appl. 27, 99–112.
- 2250 Casulli, V., Cheng, R. T., 1992. Semi-implicit finite difference methods for
2251 three-dimensional shallow water flow. Int. J. Numer. Meth. Fluids 15, 629–
2252 648.
- 2253 Cheng, R. T., Casulli, V., Gartner, J. W., 1993. Tidal, Residual, Intertidal
2254 Mudflat (TRIM) model and its applications to San Francisco Bay, Califor-
2255 nia. Estuar., Coast. Shelf S. 36, 235–280.
- 2256 Chorin, A. J., 1968. Numerical Solution of the Navier-Stokes Equations.
2257 Mathematics of Computation 22, 745–762.
- 2258 Craig, P. D., 1989. A model for diurnally forced vertical current structure
2259 near 30° latitude. Cont. Shelf Res. 9, 965–980.
- 2260 Cushman-Roisin, B., Beckers, J.-M., 2011. Introduction to geophysical fluid
2261 dynamics: physical and numerical aspects. Vol. 101. Academic Press.
- 2262 Danabasoglu, G., Yeager, S. G., Bailey, D., Behrens, E., Bentsen, M., Bi, D.,
2263 Biastoch, A., Böning, C., Bozec, A., Canuto, V. M., et al., 2014. North
2264 Atlantic simulations in coordinated ocean-ice reference experiments phase
2265 II (CORE-II). Part I: mean states. Ocean Modell. 73, 76–107.

- 2266 Daru, V., Tenaud, C., 2004. High order one-step monotonicity-preserving
2267 schemes for unsteady compressible flow calculations. *J. Comp. Phys.* 193,
2268 563–594.
- 2269 Davies, H. C., 1976. A lateral boundary formulation for multi-level prediction
2270 models. *Q. J. R. Meteorolog. S.* 102, 405–418.
- 2271 Debreu, L., Blayo, E., 2008. Two-way embedding algorithms: a review.
2272 *Ocean Dyn.* 58, 415–428.
- 2273 Debreu, L., Marchesiello, P., Penven, P., Cambon, G., 2012. Two-way nesting
2274 in split-explicit ocean models: Algorithms, implementation and validation.
2275 *Ocean Modell.* 49–50, 1–21.
- 2276 Defne, Z., Ganju, N. K., 2015. Quantifying the residence time and flushing
2277 characteristics of a shallow, back-barrier estuary: application of hydrody-
2278 namic and particle tracking models. *Estuaries and Coasts* 38, 1719–1734.
- 2279 Deleersnijder, E., 1993. Numerical mass conservation in a free-surface sigma
2280 coordinate marine model with mode splitting. *Journal of Marine Systems*
2281 4, 365–370.
- 2282 Deleersnijder, E., Beckers, J.-M., 1992. On the use of the σ -coordinate system
2283 in regions of large bathymetric variations. *J. Mar. Syst.* 3, 381–390.
- 2284 Deleersnijder, E., Beckers, J.-M., Campin, J.-M., El Mohajir, M., Fichefet,
2285 T., Luyten, P., 1997. Some mathematical problems associated with the
2286 development and use of marine models. In: Diaz, J. I. (Ed.), *The mathe-*
2287 *matics of models for climatology and environment*. Vol. 48 of NATO ASI
2288 Series. Springer, Berlin, Heidelberg, pp. 41–86.
- 2289 Delhez, E. J. M., Grégoire, M., Nihoul, J. C. J., Beckers, J.-M., 1999. Dissec-
2290 tion of the GHER turbulence closure scheme. *J. Mar. Syst.* 21, 379–397.
- 2291 Demange, J., Debreu, L., Marchesiello, P., Lemarié, F., Blayo, E., Sep.
2292 2014. Numerical representation of internal waves propagation. Research
2293 report, INRIA, available online at [http://hal.inria.fr/hal-01063417/](http://hal.inria.fr/hal-01063417/PDF/RR-8590.pdf)
2294 [PDF/RR-8590.pdf](http://hal.inria.fr/hal-01063417/PDF/RR-8590.pdf).
- 2295 Dukowicz, J. K., 2001. Reduction of density and pressure gradient errors in
2296 ocean simulations. *J. Phys. Oceanogr.* 31, 1915–1921.

- 2297 Durrán, D. R., 2010. Numerical Methods for Fluid Dynamics With Applica-
2298 tions to Geophysics, 2nd Edition. Springer.
- 2299 Durrán, D. R., 2013. Numerical methods for wave equations in geophysical
2300 fluid dynamics. Vol. 32. Springer Science & Business Media.
- 2301 Durski, S. M., Glenn, S. M., Haidvogel, D. B., 2004. Vertical mixing schemes
2302 in the coastal ocean: Comparison of the level 2.5 Mellor-Yamada scheme
2303 with an enhanced version of the K profile parameterisation. *J. Geophys.*
2304 *Res.* 109, C01015, doi:10.1029/2002JC001702.
- 2305 Eden, C., Czeschel, L., Olbers, D., 2014. Toward energetically consistent
2306 ocean models. *J. Phys. Oceanogr.* 44, 3160–3184.
- 2307 Eden, C., Greatbatch, R. J., 2008. Towards a mesoscale eddy closure. *Ocean*
2308 *Modell.* 20, 223–239.
- 2309 Espelid, T. O., Berntsen, J., Barthel, K., 2000. Conservation of energy for
2310 schemes applied to the propagation of shallow-water inertia-gravity waves
2311 in regions with varying depth. *Int. J. for Numer. Meth. Eng.* 49, 1521–1545.
- 2312 Ezer, T., Mellor, G. L., 2004. A generalised coordinate ocean model and a
2313 comparison of the bottom boundary layer dynamics in terrain-following
2314 and in z -level grids. *Ocean Modell.* 6, 379–403.
- 2315 Fairall, C. W., Bradley, E. F., Rogers, D. P., Edson, J. B., Young, G. S.,
2316 1996. Bulk parameterization of air-sea fluxes for Tropical Ocean-Global
2317 Atmosphere Coupled-Ocean Atmosphere Response Experiment. *J. Geo-*
2318 *phys. Res.* 101, 3747–3764.
- 2319 Flather, R., 1976. A tidal model of the north-west european continental shelf.
2320 *Memoires de la Societe Royale des Sciences de Liege* 6, 141–164.
- 2321 Flather, R. A., Heaps, N. S., 1975. Tidal computations for Morecambe Bay.
2322 *Geophys. J. Roy. Astron. Soc.* 42, 489–517.
- 2323 Gaspar, P., Gregoris, Y., Lefevre, J., 1990. A simple eddy kinetic energy
2324 model for simulations of the oceanic vertical mixing: Tests at station Papa
2325 and long-term upper ocean study site. *J. Geophys. Res.* 95, 16179–16193.
- 2326 Gent, P. R., McWilliams, J. C., 1990. Isopycnal mixing in ocean circulation
2327 models. *J. Phys. Oceanogr.* 20, 150–155.

- 2328 Gerdes, R., 1993. A primitive equation ocean circulation model using a gen-
2329 eral vertical coordinate transformation. 1. Description and testing of the
2330 model. *J. Geophys. Res.* 98, 14683–14701.
- 2331 Gerritsen, H., De Goede, E., Genseberger, M., Uittenbogaard, R., 2004.
2332 Validation document Delft3D-FLOW. Tech. rep., WL Delft Hydraulics.
- 2333 Gottlieb, S., Shu, C.-W., Jan. 1998. Total variation diminishing runge-kutta
2334 schemes. *Math. Comput.* 67, 73–85.
- 2335 Gräwe, U., Flöser, G., Gerkema, T., Duran-Matute, M., Badewien, T.,
2336 Schulz, E., Burchard, H., 2016. A numerical model for the entire Wad-
2337 den Sea: skill assessment and analysis of hydrodynamics. *J. Geophys. Res.*
2338 121, 5231–5251.
- 2339 Gräwe, U., Holtermann, P., Klingbeil, K., Burchard, H., 2015. Advantages of
2340 vertically adaptive coordinates in numerical models of stratified shelf seas.
2341 *Ocean Modell.* 92, 56–68.
- 2342 Griffies, S., Adcroft, A., 2008. Formulating the equations of ocean models.
2343 In: Hecht, M., Hasumi, H. (Eds.), *Ocean Modeling in an Eddy Regime*.
2344 Vol. 177 of *Geophysical Monograph Series*. American Geophysical Union,
2345 Washington, D.C., pp. 281–317.
- 2346 Griffies, S. M., 2004. *Fundamentals of ocean climate models*. Vol. 518. Prince-
2347 ton University Press.
- 2348 Griffies, S. M., 2007. *Elements of mom4p1*. Tech. rep., NOAA/GFDL, version
2349 prepared on September 27, 2007.
- 2350 Griffies, S. M., Gnanadesikan, A., Pacanowski, R. C., Larichev, V. D.,
2351 Dukowicz, J. K., Smith, R. D., 1998. Isonutral diffusion in a z -coordinate
2352 ocean model. *J. Phys. Oceanogr.* 28, 805–830.
- 2353 Gröger, M., Dieterich, C., Meier, M. H., Schimanke, S., 2015. Thermal air-
2354 sea coupling in hindcast simulations for the North Sea and Baltic Sea on
2355 the NW European shelf. *Tellus A* 67.
- 2356 Haidvogel, D. B., Arango, H. G., Hedstrom, K., Beckmann, A., Malanotte-
2357 Rizzoli, P., Shchepetkin, A. F., 2000. Model evaluation experiments in
2358 the north atlantic basin: simulations in nonlinear terrain-following coordi-
2359 nates. *Dynam. Atmos. Ocean* 32, 239–281.

- 2360 Haidvogel, D. B., Wilkin, J. L., Young, R., 1991. A semi-spectral primitive
2361 equation ocean circulation model using vertical sigma and orthogonal
2362 curvilinear horizontal coordinates. *J. Comput. Phys.* 94, 151–185.
- 2363 Haley, P. J., Lermusiaux, P. F. J., 2010. Multiscale two-way embedding
2364 schemes for free-surface primitive equations in the “multidisciplinary simulation,
2365 estimation and assimilation system”. *Ocean Dyn.* 60, 1497–1537.
- 2366 Hallberg, R., 1997. Stable split time stepping schemes for large-scale ocean
2367 modeling. *J. Comput. Phys.* 135, 54–65.
- 2368 Haney, R. L., 1991. On the pressure gradient force over steep topography in
2369 sigma coordinate ocean models. *J. Phys. Oceanogr.* 21, 610–619.
- 2370 Harcourt, R. R., 2014. A second-moment closure model of Langmuir Turbu-
2371 lence. *J. Phys. Oceanogr.* 43, 673–697.
- 2372 Harten, A., 1983. High resolution schemes for hyperbolic conservation laws.
2373 *J. Comput. Phys.* 49, 357–393.
- 2374 Heggelund, Y., Vikebø, F., Berntsen, J., Furnes, G., 2004. Hydrostatic and
2375 non-hydrostatic studies of gravitational adjustment over a slope. *Continental Shelf Research* 24,
2376 2133–2148.
- 2377 Hirt, C. W., Amsden, A. A., Cook, J. L., 1974. An Arbitrary Lagrangian-
2378 Eulerian Computing Method for All Flow Speeds. *J. Comput. Phys.* 14,
2379 227–253.
- 2380 Hofmeister, R., Burchard, H., Beckers, J.-M., 2010. Non-uniform adaptive
2381 vertical grids for 3d numerical ocean models. *Ocean Modell.* 33, 70–86.
- 2382 Holt, J., Harle, J., Proctor, R., Michel, S., Ashworth, M., Batstone, C.,
2383 Allen, I., Holmes, R., Smyth, T., Haines, K., Bretherton, D., Smith, G.,
2384 2009. Modelling the global coastal ocean. *Philosophical Transactions of the Royal Society of London A: Mathematical, Physical and Engineering Sciences* 367, 939–951.
- 2387 Holt, J. T., James, I. D., 2001. An s coordinate density evolving model of
2388 the northwest european continental shelf: 1. model description and density
2389 structure. *J. Geophys. Res.* 106, 14015–14034.

- 2390 Holt, J. T., James, I. D., 2006. An assessment of the fine-scale eddies in a
2391 high-resolution model of the shelf seas west of Great Britain. *Ocean Modell.*
2392 13, 271–291.
- 2393 Holtermann, P., Burchard, H., Gräwe, U., Klingbeil, K., Umlauf, L., 2014.
2394 Deep-water dynamics and boundary mixing in a non-tidal stratified basin.
2395 A modeling study of Baltic Sea. *J. Geophys. Res.* 119.
- 2396 Hundsdorfer, W., Trompert, R. A., Feb. 1994. Method of lines and direct
2397 discretization: A comparison for linear advection. *Appl. Numer. Math.* 13,
2398 469–490.
- 2399 Ilicak, M., Adcroft, A. J., Griffies, S. M., Hallberg, R. W., 2012. Spurious
2400 dianeutral mixing and the role of momentum closure. *Ocean Modell.* 45-46,
2401 37–58.
- 2402 IOC, SCOR and IAPSO, 2010. The international thermodynamic equation of
2403 seawater - 2010: Calculation and use of thermodynamic properties. Tech.
2404 rep., Intergovernmental Oceanographic Commission, UNESCO.
- 2405 Jackson, L., Hallberg, R., Legg, S., 2008. A parameterization of shear-driven
2406 turbulence for ocean climate models. *J. Phys. Oceanogr.* 38, 1033–1053.
- 2407 Jensen, T. G., 10 1998. Open boundary conditions in stratified ocean models.
2408 *J. Mar. S.* 16, 297–322.
- 2409 Johns, B., Marsaleix, P., Estournel, C., Vhil, R., 1992. On the wind-driven
2410 coastal upwelling in the gulf of lions. *J. Mar. S.* 3, 309–320.
- 2411 Jungclaus, J. H., Backhaus, J. O., 1994. Application of a transient reduced
2412 gravity plume model to the denmark strait overflow. *J. Geophys. Res.* 99,
2413 12375–12396.
- 2414 Källberg, P., February 1977. Test of a lateral boundary relaxation scheme in
2415 a barotropic model. Internal report, ECMWF Research Department.
- 2416 Kanarska, Y., Maderich, V., 2003. A non-hydrostatic numerical model for
2417 calculating free-surface stratified flows. *Ocean Dynamics* 53, 176–185.
- 2418 Kanarska, Y., Shchepetkin, A., McWilliams, J., 2007. Algorithm for non-
2419 hydrostatic dynamics in the Regional Oceanic Modeling System. *Ocean*
2420 *Modell.* 18, 143–174.

- 2421 Kantha, L. H., Clayson, C. A., 2000a. Numerical models of oceans and
2422 oceanic processes. Vol. 66 of International Geophysics Series. Academic
2423 Press.
- 2424 Kantha, L. H., Clayson, C. A., 2000b. Small-scale processes in geophysical
2425 fluid flows. Vol. 67 of International Geophysics Series. Academic Press.
- 2426 Kasahara, A., 1974. Various Vertical Coordinate Systems Used For Numerical
2427 Weather Prediction. *Mon. Wea. Rev.* 102, 509–522.
- 2428 Keilegavlen, E., Berntsen, J., 2009. Non-hydrostatic pressure in σ -coordinate
2429 ocean models. *Ocean Modelling* 28, 240–249.
- 2430 Klingbeil, K., Burchard, H., 2013. Implementation of a direct nonhydrostatic
2431 pressure gradient discretisation into a layered ocean model. *Ocean Modell.*
2432 65, 64–77.
- 2433 Klingbeil, K., Mohammadi-Aragh, M., Gräwe, U., Burchard, H., 2014. Quan-
2434 tification of spurious dissipation and mixing - discrete variance decay in a
2435 finite-volume framework. *Ocean Modell.* 81, 49–64.
- 2436 Knight, P. J., Howarth, M. J., Rippeth, T. P., 2002. Inertial currents in the
2437 Northern North Sea. *J. Sea Res.* 47, 269–284.
- 2438 Kondo, J., 1975. Air-sea bulk transfer coefficients in diabatic conditions.
2439 *Bound. Layer Meteor.* 9, 91–112.
- 2440 Lahaye, S., Gouillon, F., Baraille, R., Pichon, A., Pineau-Guillou, L., Morel,
2441 Y., 2011. A numerical scheme for modeling tidal wetting and drying. *J.*
2442 *Geophys. Res.* 116, c03028.
- 2443 Large, W. G., McWilliams, J. C., Doney, S. C., 1994. Oceanic vertical mixing:
2444 a review and a model with nonlocal boundary layer parameterisation. *Rev.*
2445 *Geophys.* 32, 363–403.
- 2446 Lazure, P., Salomon, J.-C., 1991. Coupled 2-d and 3-d modeling of coastal
2447 hydrodynamics. *Oceanol. Acta* 14, 173–180.
- 2448 Leclair, M., Madec, G., 2011. \tilde{z} -coordinate, an arbitrary lagrangian-eulerian
2449 coordinate separating high and low frequency motions. *Ocean Modell.* 37,
2450 139–152.

- 2451 Lele, S. K., 1992. Compact finite difference schemes with spectral-like reso-
2452 lution. *J. Comp. Phys.* 103, 16–42.
- 2453 Lemarié, F., Debreu, L., Madec, G., Demange, J., Molines, J., Honnorat,
2454 M., 2015. Stability constraints for oceanic numerical models: implications
2455 for the formulation of time and space discretizations. *Ocean Modell.* 92,
2456 124–148.
- 2457 Lemarié, F., Debreu, L., Shchepetkin, A., McWilliams, J., 2012a. On the
2458 stability and accuracy of the harmonic and biharmonic isoneutral mixing
2459 operators in ocean models. *Ocean Modell.* 52-53, 9–35.
- 2460 Lemarié, F., Kurian, J., Shchepetkin, A. F., Molemaker, M. J., Colas, F.,
2461 McWilliams, J. C., 2012b. Are There Inescapable Issues Prohibiting the
2462 use of Terrain-Following Coordinates in Climate Models ? *Ocean Modell.*
2463 42, 57–79.
- 2464 Leonard, B., 1995. Order of accuracy of QUICK and related convection-
2465 diffusion schemes. *Appl. Math. Model.* 19, 640–653.
- 2466 Lilly, D. K., 1965. On the computational stability of numerical solutions
2467 of time-dependent non-linear geophysical fluid dynamics problems. *Mon.*
2468 *Wea. Rev.* 93, 11–25.
- 2469 Lin, S.-J., 1997. A finite-volume integration method for computing pressure
2470 gradient force in general vertical coordinates. *Quart. J. Roy. Meteorol. Soc.*
2471 123, 1749–1762.
- 2472 Lundquist, K. A., Chow, F. K., Lundquist, J. K., 2010. An immersed bound-
2473 ary method for the weather research and forecasting model. *Mon. Wea.*
2474 *Rev.* 138, 796–817.
- 2475 Luyten, P., Jones, J., Proctor, R., Tabor, A., Tett, P., Wild-Allen, K., 1999.
2476 Coherens - a coupled hydrodynamical-ecological model for regional and
2477 shelf seas: User documentation. Tech. rep., MUMM Report, Management
2478 Unit of the Mathematical Models of the north Sea.
- 2479 MacCready, P., Geyer, W. R., 2010. Advances in estuarine physics. *Annu.*
2480 *Rev. Fluid Mech.* 2, 35–58.

- 2481 Madala, R. V., Piacsek, S. A., 1977. A semi-implicit numerical model for
2482 baroclinic oceans. *J. Comp. Phys.* 23, 167–178.
- 2483 Madec, G., Delecluse, P., Crepon, M., Chartier, M., 1991. A three-
2484 dimensional numerical study of deep-water formation in the northwestern
2485 mediterranean sea. *J. Phys. Oceanogr.* 21, 1349–1371.
- 2486 Marchesiello, P., Debreu, L., Couvelard, X., 2009. Spurious diapycnal mixing
2487 in terrain-following coordinate models: The problem and a solution. *Ocean*
2488 *Modell.* 26, 159–169.
- 2489 Marchesiello, P., McWilliams, J. C., Shchepetkin, A., 2001. Open bound-
2490 ary conditions for long-term integration of regional oceanic models. *Ocean*
2491 *Modell.* 3, 1–20.
- 2492 Marsaleix, P., Auclair, F., Estournel, C., Nguyen, C., Ulses, C., 2011. An
2493 accurate implementation of the compressibility terms in the equation of
2494 state in a low order pressure gradient scheme for sigma coordinate ocean
2495 models. *Ocean Modell.* 40, 1–13.
- 2496 Marsaleix, P., Auclair, F., Floor, J. W., Herrmann, M. J., Estournel, C.,
2497 Pairaud, I., Ulses, C., 2008. Energy conservation issues in sigma-coordinate
2498 free-surface ocean models. *Ocean Modell.* 20, 61–89.
- 2499 Marsaleix, P., Estournel, C., Kondrachoff, V., Vehil, R., Jan. 1998. A numer-
2500 ical study of the formation of the Rhône River plume. *J. Marine Syst.* 14,
2501 99–115.
- 2502 Marshall, J., Hill, C., Perelman, L., Adcroft, A. J., 1997. Hydrostatic, quasi-
2503 hydrostatic, and nonhydrostatic ocean modeling. *Journal of Geophysical*
2504 *Research* 102 (C3), 5733–5752.
- 2505 Martin, P. J., 1985. Simulation of the mixed layer at OWS November and
2506 Papa with several models. *J. Geophys. Res.* 90, 903–916.
- 2507 Martin, P. J., 2000. Description of the navy coastal ocean model version 1.0.
2508 Tech. rep., NRL Report.
- 2509 Martinho, A. S., Batteen, M. L., 2006. On reducing the slope parameter in
2510 terrain-following numerical ocean models. *Ocean Modell.* 13, 166–175.

- 2511 Martins, F., Leitão, P., Silva, A., Neves, R., 2001. 3D modeling in the Sado
2512 estuary using a new generic vertical discretization approach. *Oceanologica*
2513 *Acta* 24, S51–S62.
- 2514 Martinsen, E. A., Engedahl, H., 1987. Implementation and testing of a lateral
2515 boundary scheme as an open boundary condition in a barotropic ocean
2516 model. *Coast. Eng.* 11, 603–627.
- 2517 Mason, E., Molemaker, J., Shchepetkin, A. F., Colas, F., McWilliams, J. C.,
2518 Sangrà, P., 2010. Procedures for offline grid nesting in regional ocean mod-
2519 els. *Ocean Modell.* 35, 1–15.
- 2520 Mathis, M., Elizalde, A., Mikolajewicz, U., Pohlmann, T., 2015. Variability
2521 patterns of the general circulation and sea water temperature in the North
2522 Sea. *Progr. Oceanogr.* 135, 91–112.
- 2523 McCalpin, J. D., 1994. A comparison of second-order and fourth-order pres-
2524 sure gradient algorithms in a σ -coordinate ocean model. *Int. J. Numer.*
2525 *Meth. Fl.* 18, 361–383.
- 2526 Mellor, G. L., 2002. Oscillating bottom boundary layers. *J. Phys. Oceanogr.*
2527 32, 3075–3088.
- 2528 Mellor, G. L., Blumberg, A. F., 1985. Modeling vertical and horizontal diffu-
2529 sivities with the sigma coordinate system. *Mon. Wea. Rev.* 113, 1379–1383.
- 2530 Mellor, G. L., Ezer, T., Oey, L.-Y., 1994. The pressure gradient conundrum of
2531 sigma coordinate ocean models. *J. Atmos. Ocean. Technol.* 11, 1126–1134.
- 2532 Mellor, G. L., Yamada, T., 1982. Development of a turbulence closure model
2533 for geophysical fluid problems. *Rev. Geophys.* 20, 851–875.
- 2534 Mesinger, F., Arakawa, A., 1976. Numerical Methods used in atmospheric
2535 models, vol. 1. Tech. rep., World Meteor. Org., gARP Publ. Ser. 17.
- 2536 Mohammadi-Aragh, M., Klingbeil, K., Brüggemann, N., Eden, C., Burchard,
2537 H., 2015. The impact of advection schemes on restratification due to lateral
2538 shear and baroclinic instabilities. *Ocean Modell.* 94, 112–127.
- 2539 Nataf, F., 2013. Absorbing boundary conditions and perfectly matched lay-
2540 ers in wave propagation problems. *Direct and Inverse problems in Wave*
2541 *Propagation and Applications* 14, 219–231.

- 2542 Nihoul, J. C., Waleffe, F., Djenidi, S., 1986. A 3d-numerical model of the
2543 northern bering sea. *Environmental Software* 1, 76–81.
- 2544 Oey, L.-Y., 2005. A wetting and drying scheme for POM. *Ocean Modell.* 9,
2545 133–150.
- 2546 Olbers, D., Willebrand, J., Eden, C., 2012. *Ocean dynamics*. Springer-Verlag
2547 Berlin Heidelberg.
- 2548 Oliger, J., Sundström, A., 1978. Theoretical and practical aspects of some
2549 initial boundary value problems in fluid dynamics. *SIAM J. Appl. Math.*
2550 35, 419–446.
- 2551 Orlandi, I., 1976. A simple boundary condition for unbounded hyperbolic
2552 flows. *J. Comput. Phys.* 21, 251–269.
- 2553 Oschlies, A., 2002. Improved representation of upper ocean dynamics and
2554 mixed layer depths in a model of the North Atlantic on switching from
2555 eddy-permitting to eddy-resolving grid resolution. *J. Phys. Oceanogr.* 32,
2556 2277–2298.
- 2557 Palma, E. D., Matano, R. P., 2000. On the implementation of open boundary
2558 conditions for a general circulation model: The three-dimensional case. *J.*
2559 *Geophys. Res.* 105, 8605–8627.
- 2560 Patankar, S. V., 1980. *Numerical Heat Transfer and Fluid Flow*. McGraw-
2561 Hill, New York.
- 2562 Paulson, C. A., Simpson, J. J., 1977. Irradiance measurements in the upper
2563 ocean. *J. Phys. Oceanogr.* 7, 952–956.
- 2564 Peaceman, D. W., Rachford, Jr., H. H., 1955. The numerical solution of
2565 parabolic and elliptic differential equations. *SIAM Journal* 3, 28–41.
- 2566 Penven, P., Debreu, L., Marchesiello, P., McWilliams, J. C., 2006. Evaluation
2567 and application of the roms 1-way embedding procedure to the central
2568 california upwelling system. *Ocean Modell.* 12, 157–187.
- 2569 Perkins, A. L., Smedstad, L. F., Blake, D. W., Heburn, G. W., Wallcraft,
2570 A. J., 1997. A new nested boundary condition for a primitive equation
2571 ocean model. *J. Geophys. Res.* 102, 3483–3500.

- 2572 Pietrzak, J., Jakobson, J. B., Burchard, H., Vested, H. J., Petersen, O., 2002.
2573 A three-dimensional hydrostatic model for coastal and ocean modelling us-
2574 ing a generalised topography following co-ordinate system. *Ocean Modell.*
2575 4, 173–205.
- 2576 Raymond, W. H., Kuo, H. L., 1984. A radiation boundary condition for
2577 multi-dimensional flows. *Q.J.R. Meteorol. Soc.* 110, 535–551.
- 2578 Rippeth, T. P., Fisher, N., Simpson, J. H., 2001. The semi-diurnal cycle of
2579 turbulent dissipation in the presence of tidal straining. *J. Phys. Oceanogr.*
2580 31, 2458–2471.
- 2581 Rodi, W., 1987. Examples of calculation methods for flow and mixing in
2582 stratified flows. *J. Geophys. Res.* 92, 5305–5328.
- 2583 Roquet, F., Madec, G., McDougall, T. J., Barker, P. M., 2015. Accurate
2584 polynomial expressions for the density and specific volume of seawater
2585 using the TEOS-10 standard. *Ocean Modell.*, 29–43.
- 2586 Rueda, F. J., Sanmiguel-Rojas, E., Hodges, B. R., 2007. Baroclinic stabil-
2587 ity for a family of two-level, semi-implicit numerical methods for the 3d
2588 shallow water equations. *Int. J. Numer. Meth. Fluids* 54, 237–268.
- 2589 Schär, C., Leuenberger, D., Fuhrer, O., Lüthi, D., Girard, C., 2002. A new
2590 terrain-following vertical coordinate formulation for atmospheric predic-
2591 tion models. *Mon. Wea. Rev.* 130, 2459–2480.
- 2592 Shchepetkin, A. F., 2015. An adaptive, courant-number-dependent implicit
2593 scheme for vertical advection in oceanic modeling. *Ocean Modell.* 91, 38–
2594 69.
- 2595 Shchepetkin, A. F., McWilliams, J. C., 2003. A method for computing hor-
2596 izontal pressure-gradient force in an oceanic model with a non-aligned
2597 vertical coordinate. *J. Geophys. Res.* 108 (C3), 3090–3124.
- 2598 Shchepetkin, A. F., McWilliams, J. C., 2005. The Regional Oceanic Model-
2599 ing System: A split-explicit, free-surface, topography-following-coordinate
2600 ocean model. *Ocean Modell.* 9, 347–404.

- 2601 Shchepetkin, A. F., McWilliams, J. C., 2008. Computational kernel algo-
2602 rithms for fine-scale, multiprocess, longtime oceanic simulations. In: Ciar-
2603 let, P. G. (Ed.), Computational methods for the atmosphere and the oceans
2604 Special Volume. Vol. XIV of Handbook of numerical analysis. Elsevier, pp.
2605 121–183.
- 2606 Shchepetkin, A. F., McWilliams, J. C., 2009. Correction and commentary for
2607 "ocean forecasting in terrain-following coordinates: Formulation and skill
2608 assessment of the regional ocean modeling system" by Haidvogel et al., J.
2609 Comp. Phys. 227, pp. 3595-3624. J. Comput. Phys. 228, 8985–9000.
- 2610 Sheng, J., Greatbatch, R. J., Zhai, X., Tang, L., 2005. A new two-way nest-
2611 ing technique for ocean modeling based on the smoothed semi-prognostic
2612 method. Ocean Dyn. 55, 162–177.
- 2613 Shu, C. W., 1987. TVB uniformly high-order accurate schemes for conserva-
2614 tion laws. Math. Comput. 49, 105–121.
- 2615 Shu, C.-W., Nov. 1988. Total-variation-diminishing time discretizations.
2616 SIAM J. Sci. Stat. Comput. 9, 1073–1084.
- 2617 Simpson, J. H., Brown, J., Matthews, J., Allen, G., 1990. Tidal straining,
2618 density currents, and stirring in the control of estuarine stratification. Es-
2619 tuaries 13, 125–132.
- 2620 Smagorinsky, J., 1963. General circulation experiments with the primitive
2621 equations. Mon. Wea. Rev. 91, 99–164.
- 2622 Smyth, W. D., Skyllingstad, E. D., Crawford, G. B., Wijesekera, H., 2002.
2623 Nonlocal fluxes and stokes drift effects in the K -profile parameterization.
2624 Ocean Dyn. 52, 104–115.
- 2625 Song, Y., Haidvogel, D. B., 1994. A semi-implicit ocean circulation model us-
2626 ing a generalised topography-following coordinate. J. Comput. Phys. 115,
2627 228–244.
- 2628 Soufflet, Y., Marchesiello, P., Lemarié, F., Jouanno, J., Capet, X., Debreu,
2629 L., Benshila, R., 2016. On effective resolution in ocean models. Ocean
2630 Modell. 98, 36–50.

- 2631 Starr, V. P., 1945. A quasi-lagrangian system of hydrodynamical equations.
2632 *Journal of Meteorology* 2, 227–237.
- 2633 Stelling, G. S., Duinmeijer, S. P. A., 2003. A staggered conservative scheme
2634 for every Froude number in rapidly varied shallow water flows. *Int. J.*
2635 *Numer. Meth. Fluids* 43, 1329–1354.
- 2636 Stelling, G. S., Van Kester, J. A. T. M., 1994. On the approximation of hor-
2637 izontal gradients in sigma co-ordinates for bathymetry with steep bottom
2638 slopes. *Int. J. Numer. Methods Fluids* 18, 915–935.
- 2639 Suresh, A., Huynh, H., 1997. Accurate monotonicity-preserving schemes with
2640 runge-kutta time stepping. *J. Comp. Phys.* 136, 83–99.
- 2641 Svård, M., Nordström, J., 2014. Review of summation-by-parts schemes for
2642 initial–boundary-value problems. *J. Comp. Phys.* 268, 17–38.
- 2643 Svendsen, E., Berntsen, J., Skogen, M., dlandsvik, B., Martinsen, E., 1996.
2644 Joint numerical sea modelling model simulation of the skagerrak circulation
2645 and hydrography during skagex. *J. Marine Syst.* 8, 219–236.
- 2646 Témam, R., 1969. Sur l’Approximation de la Solution de Équations de
2647 Navier-Stokes par la Méthode de Pas Fractionnaires (II). *Arch. Rational*
2648 *Mech. Anal.* 32, 377–385.
- 2649 Témam, R., Tribbia, J., 2003. Open boundary conditions for the primitive
2650 and boussinesq equations. *J. Atmos. Sci.* 60, 2647–2660.
- 2651 Uchiyama, Y., McWilliams, J. C., Shchepetkin, A. F., 2010. Wave-current
2652 interaction in an oceanic circulation model with a vortex-force formalism:
2653 Application to the surf zone. *Ocean Modell.* 34, 16–35.
- 2654 Umlauf, L., Burchard, H., 2003. A generic length-scale equation for geophys-
2655 ical turbulence models. *J. Mar. Res.* 61, 235–265.
- 2656 Umlauf, L., Burchard, H., 2005. Second-order turbulence models for geo-
2657 physical boundary layers. A review of recent work. *Cont. Shelf Res.* 25,
2658 795–827.
- 2659 Umlauf, L., Burchard, H., Hutter, K., 2003. Extending the k - ω turbulence
2660 model towards oceanic applications. *Ocean Modell.* 5, 195–218.

- 2661 van Haren, H., Maas, L., Zimmerman, J. T. F., Malschaert, H. R. H., 1999.
2662 Strong inertial currents and marginal internal wave stability in the central
2663 North Sea. *Geophys. Res. Lett.* 26, 2993–2996.
- 2664 van Kan, J., 1986. A second-order accurate pressure correction scheme for
2665 viscous incompressible flow. *Journal of Science and Statistical Computa-*
2666 *tion* 7, 870–891.
- 2667 van Leer, B., 1979. Toward the ultimate conservative difference scheme. V: A
2668 second order sequel to Godunov’s method. *J. Comput. Phys.* 32, 101–136.
- 2669 Vitousek, S., Fringer, O., 2011. Physical vs numerical dispersion in nonhy-
2670 drostatic ocean modeling. *Ocean Modell.* 40, 72–86.
- 2671 Waldron, K. M., Paegle, J., Horel, J. D., 1996. Sensitivity of a spectrally
2672 filtered and nudged limited-area model to outer model options. *Mon. Wea.*
2673 *Rev.* 124, 529–547.
- 2674 Walters, R. A., Lane, E. M., Hanert, E., 2009. Useful time-stepping methods
2675 for the Coriolis term in a shallow water model. *Ocean Modell.* 28, 66–74.
- 2676 Wang, S., Dieterich, C., Döscher, R., Höglund, A., Hordoir, R., Meier, H.
2677 E. M., Samuelsson, P., Schimanke, S., 2015. Development and evaluation
2678 of a new regional coupled atmosphere-ocean model in the North Sea and
2679 Baltic Sea. *Tellus A* 67, 10.3402/tellusa.v67.24284.
- 2680 Warner, J. C., Defne, Z., Haas, K., Arango, H. G., 2013. A wetting and
2681 drying scheme for ROMS. *Computers & Geosci.* 58, 54–61.
- 2682 Warner, J. C., Sherwood, C. R., Arango, H. G., Signell, R. P., 2005. Per-
2683 formance of four turbulence closure models implemented using a generic
2684 length scale method. *Ocean Modell.* 8, 81–113.
- 2685 Warner, J. C., Sherwood, C. R., Signell, R. P., Harris, C. K., Arango, H. G.,
2686 2008. Development of a three-dimensional, regional, coupled wave, current,
2687 and sediment-transport model. *Computers & Geosci.* 34, 1284–1306.
- 2688 Weller, H., Shahrokhi, A., 2014. Curl-free pressure gradients over orogra-
2689 phy in a solution of the fully compressible euler equations with implicit
2690 treatment of acoustic and gravity waves. *Mon. Wea. Rev.* 142, 4439–4457.

- 2691 White, L., Adcroft, A., Hallberg, R., 2009. High-order regridding-remapping
2692 schemes for continuous isopycnal and generalized coordinates in ocean
2693 models. *J. Comput. Phys.* 228, 8665–8692.
- 2694 White, L., Adcroft, A. J., 2008. A high-order finite volume remapping scheme
2695 for nonuniform grids: The piecewise quartic method (PQM). *J. Comput.*
2696 *Phys.* 227, 7394–7422.
- 2697 Wilcox, D. C., 1998. *Turbulence Modeling for CFD*, 2nd Edition. DCW In-
2698 dustries.
- 2699 Zijlema, M., Stelling, G., Smit, P., 2011. Swash: An operational public do-
2700 main code for simulating wave fields and rapidly varied flows in coastal
2701 waters. *Coast. Eng.* 58, 992–1012.